Deciphering cytoskeletal junctional interactions during blood vessel morphogenesis *in vivo*:

Introduction of novel genetic tools for mosaic analysis of Cdh5/VE-cadherin regulation and function

&

Phenotypic analysis of RadilB function in sprouting angiogenesis

Inauguraldissertation

zur

Erlangung der Würde eines Doktors der

Philosophie vorgelegt der

Philosophische-Naturwissenschaftlichen

Fakultät der Universität Basel

von

Niels Schellinx

aus Maastricht, Niederlande

Basel, 2018

Genehmigt von der Philosophisch-Naturwissenschaftlichen

Fakultät auf Antrag von

Prof. Dr. Markus Affolter

Prof. Dr. Claudia Lengerke

Basel, den 16. Oktober 2018

Prof. Dr. Martin Spiess

Dekan

Table of contents

List of abbreviations

CCM1	Cerebral Cavernous Malformations 1 (Krit1)
CD	Cluster of Differentiation
Cdc42	Cell division cycle 42
Cdh5	Cadherin 5 (vascular endothelial cadherin)
cDNA	complementary Deoxyribonucleic Acid
Cf	confer (compare)
Cre	Causes recombination
DA	Dorsal Aorta
DLAV	Dorsal Longitudinal Anastomotic Vessel
Dll4	Delta ligand-like 4
Dpf	Days post fertilisation
DOG	2-Deoxy-D-galactose
EC	Endothelial cell
Epac1	Exchange protein directly activated by CAMP 1
Esam	Endothelial cell-selective adhesion molecule
Flk1	Fetal liver kinase 1 (Vegfr2, KDR)
Flt1	Fms-related tyrosine kinase 1 (Vegfr1)
FRET	Förster resonance energy transfer
GalK	Galactokinase
GAP	GTPase Activating Protein
GEF	Guanine nucleotide Exchange Factor
GFP	Green Fluorescent Protein
GTP	Guanosine-5'-triphosphate
Heg1	Heart development protein with EGF-like domains 1 (Heart of Glass)
Hpf	Hours post fertilisation

HUVEC	Human Umbilical Vein Endothelial Cell
ISV	Intersegmental Vessel
JAM	Junctional Adherens Molecule
JBL	Junction-based Lamellipodium
KDR	Kinase Insert Domain Receptor (Vegfr2, Flt1)
Krit1	Krev Interaction Trapped 1 (CCM1)
LoxP	Locus of crossing over (x) from coliphage Pl
mClavGR2	monomeric Clavularia-derived green-to-red photoconvertible 2
NC	Neural Crest
Nls	Nuclear localisation signal
NMHCIIA	Non-Muscle Myosin Heavy Chain IIA
ORF	Open Reading Frame
PECAM1	Platelet and Endothelial Cell Adhesion Molecule 1
PCV	Post Cardinal Vein
Rac1	Ras-related C3 botulinum toxin substrate 1
Radil	Ras-associating and dilute domain-containing protein
Rain	Ras interacting (Rasip1)
Rasip1	Ras interacting protein 1 (Rain)
RFP	Red Fluorescent Protein
RhoA	Ras homolog family member A
ROCK	Rho-associated Coiled-coil containing protein Kinase
sFlt1	soluble Fms-related tyrosine kinase 1 (soluble Vegfr1)
SURE	Stop Unwanted Recombination Events
VE-cadherin	Vascular Endothelial cadherin (Cdh5)
Vegf	Vascular endothelial growth factor
Vegfr2	Vascular endothelial growth factor receptor 2 (Flt1, KDR)
ZO-1	Zonula Occludens 1

Abstract

VE-cadherin/Cdh5 is a prominent adhesion protein located in endothelial adherens junctions. Amongst its many functions, Cdh5 is important for cell shape changes to generate multicellular vascular tubes. Analysis of cytoskeletal organisation and dynamics has led to a model, in which bipolar actin polymerisation drives junctional elongation between endothelial cells (ECs) via Cdh5. I now want to analyse the Cdh5 based cell interactions, which drive tube formation, more closely, by generating mosaic angiogenic sprouts in zebrafish that contain cells with different Cdh5 levels. Therefore, I generated as my main project an inducible Cdh5 loss of function allele, using Bacterial Artificial Chromosome (BAC) recombineering technology. Hereto, the exon 2 of a BAC containing the *cdh5* gene was replaced by the Cdh5 open reading frame flanked by *loxP* sites, coupled to *tagRFP* to visualise its expression. Its subsequent introduction into the zebrafish genome led to expression of *tagRFP* at adherens junctions. Via expression of inducible Cre-recombinase (heat-shock or tamoxifen induced), this line will enable us to examine Cdh5 function at different time points during vascular development.

In order to examine to what extend individual neighbouring ECs contribute to the formation of adherens junctions, I additionally generated as a photo-convertible fluorescence-tagged Cdh5, using BAC recombineering technology. Hereto, the sequence encoding for mClavGR2 was introduced between the p120-catenin and β-catenin binding sites of the translated Cdh5 protein. Micro-injection of this BAC resulted in junctional *mClavGR2* expression in green, which was able to convert into red light emission. Via photo-conversion of single cells, this tool will allow the visualisation of Cdh5 derived from two different cells within the same adherens junction by emission of two different light rays (green and red). These tools will contribute to elucidate more about the dynamic endothelial cell behaviours underlying sprouting angiogenesis.

Rap1 is a small GTPase and member of the Ras superfamily and predominantly involved in cell adhesion and junction. Ras-interacting protein 1 (Rasip1) is a Rap1 effector protein, highly expressed in endothelial cells and controlling the activity of RhoA, Rac1 and Cdc42, all important to Cdh5 remodelling and organisation. Its absence impairs proper Cdh5 localisation and lumen formation in blood vessels in mice and zebrafish. Research on cell culture showed that Rasip1 is not the only Rap1 effector, but cooperates with Ras-associating and dilute domain-containing protein (Radil). Contrary to the other Rap1-specific effectors, Radil's mechanism of action is still unknown, although it shares three of its four protein domains with Rasip1. In this side project, genomic analysis showed three Radil paralogues (RadilA, -B and -C) in the zebrafish genome, of which two are not annotated. *In situ* hybridisation for each Radil paralogue showed that RadilB was endothelial specifically expressed. RadilB KO fish developed crooked and dilated blood vessels, and show intermittent lumen collapse during vessel growth. Further analysis on growing intersegmental vessels (ISVs) in the absence of RadilB showed that the intermittent lumen collapse only takes place in arterial ISVs that convert to venous ISVs and simultaneously divide. In contrary to wild type, a shunt of blood flow from the dorsal aorta into the post cardinal vein sometimes appears during this transformational phase. Meanwhile, ISVs in RadilB knockout fish underwent less cell divisions and showed aberrant Cdh5 localisation. The closely-related endothelial specific proteins Rasip1 and RadilB form two important targets for research that will elucidate more about Cdh5 organisation controlled by small GTPases and consequently about Cdh5 remodelling-based EC behaviours.

Chapter I

Introduction

1.1 Blood vessel formation

An efficient transport and exchange of fluids, gasses, nutrients and blood cells requires extensive networks of blood and lymphatic vessels. The lumen of both systems is lined by endothelial cells (ECs). Blood vessels transport blood throughout the entire body, whereas lymphatic vessels transport extravasated fluid from the tissues back to the blood vessels. There are three major classes of blood vessels: arteries, capillaries and veins. Arteries are surrounded by multiple layers of smooth muscle cells and transport blood away from the heart. The endothelial walls of capillaries consist only of one cell layer, which allows exchange of gasses, nutrients and waste compounds with the surrounding tissue. Veins are valve containing vessels that transport the blood towards the heart. Mural cells comprise vascular smooth muscle cells and pericytes that are both involved in formation and maintenance of normal vasculature. Pericytes cover ECs and establish direct cell-cell contact with ECs, whereas vascular smooth muscle cells cover arteries and, too lesser extent, veins, to enable regulation of the calibre of the blood vessels (Adams and Alitalo, 2007). Development of these transport networks arises from three processes: vasculogenesis, angiogenesis and lymphangiogenesis. The cardiovascular system is the first functional organ that develops during embryogenesis.

1.1.1. Vasculogenesis

Vasculogenesis is the *de novo* formation of blood vessels from progenitor cells, called angioblasts. The first endothelial cells in zebrafish arise in two stripes in the posterior lateral mesoderm at around 13 hours post fertilisation (hpf). These endothelial precursor cells, known as haemangioblasts, migrate at 17hpf towards the embryonic midline where they coalesce into a vascular cord: the dorsal aorta (DA), the first tube with arterial cell fate (Torres-Vázquez et al., 2003; Jin et al., 2005). Shortly afterwards at 20hpf, the DA gives rise to the formation of the postcardinal vein (PCV) by ventral sprouting (Herbert et al., 2009). Most other blood vessels of the organism, however, will be formed by angiogenesis.

1.1.2. Angiogenesis

Angiogenesis is the extension of blood vessels from pre-existing vascular structures. In general, three main processes are involved: cell sprouting, anastomosis and lumen formation.

1.1.2.1. Cell sprouting: tip cell selection and outgrowth

When the supply of nutrients and oxygen from the existing vessels cannot satisfy the demands within a tissue, the tissue will send out signals to stimulate formation of new blood vessels (Germain et al., 2010). Vascular endothelial growth factor (Vegf) is an important angiogenesis promoting signal that activates the endothelium, resulting in the selection of a tip cell. Although the Vegf receptors of all endothelial cells exposed to Vegf are activated, only a limited number

of cells will be selected to become a tip cell (Gerhardt et al., 2003). A Vegf/Notch dependent regulatory mechanism within the endothelium ensures the selection of a tip cell by blocking the neighbouring cells from developing into tip cells (Geudens and Gerhardt, 2011). VegfA/Vegfr2 signalling results in enrichment of the Notch ligand delta like ligand 4 (Dll4) and its presentation on the membrane of the EC directed towards its neighbouring cells. The subsequent activation of Notch by Dll4 in the neighbouring cells, will suppress the expression of Vegf receptor 2 (Vegfr2, alternative names: Flk1 and Kdr), Dll4 and platelet-derived growth factor B (PDGFB), and promote the expression of soluble Vegf receptors (sFlt1). These changes in protein production will make the cell less sensitive to Vegf and decrease their ability to activate Notch in their neighbouring cells (Gerhardt et al., 2003). Consequently, the endothelial cell producing most Dll4 will grow out as the tip followed by its neighbours as stalk cells (Figure I-IA). In addition, sFlt1 has been found to be important for local sprout outgrowth guidance (Chappell et al., 2009).

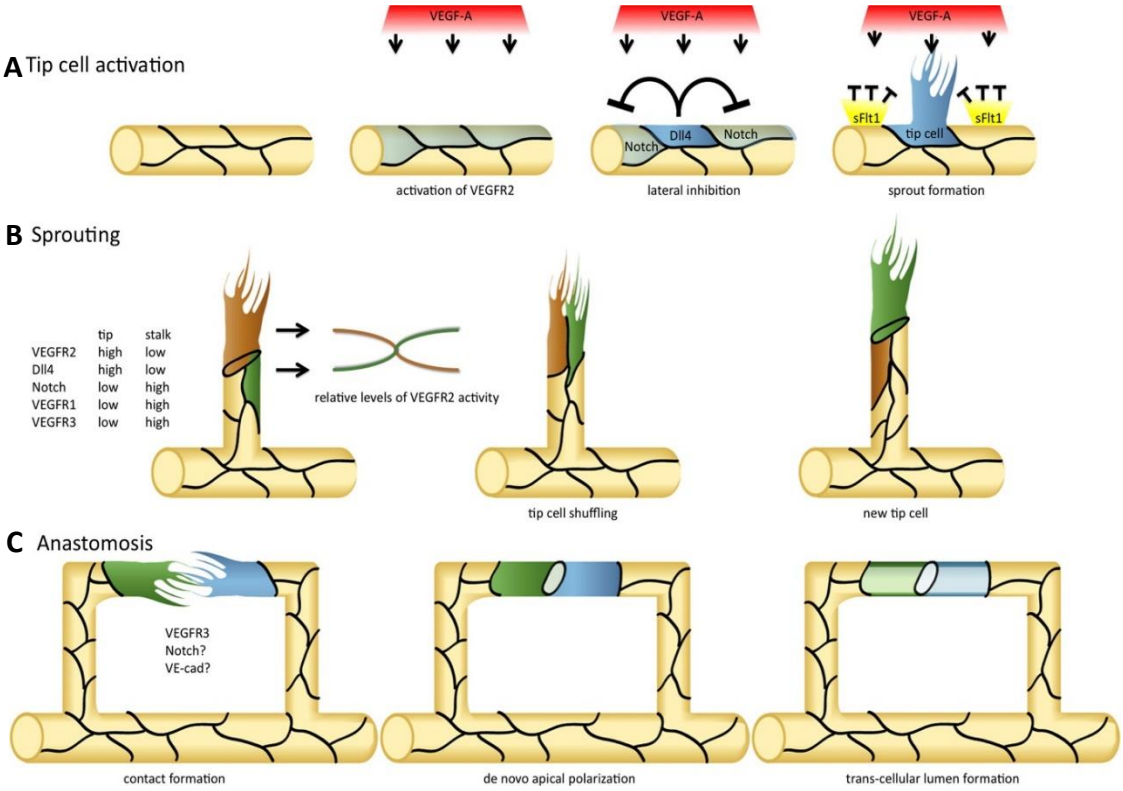

Figure I-I. Induction of sprouting. (**A**) Single endothelial cells will be selected as tip cell after activation by Vegf. Presentation of Dll4 to the neighbouring cells will suppress the expression of genes that make them less sensitive to Vegf stimulation. The selected tip cell spearheads the emerging sprout, using its filopodia to scan the environment for attractive and repulsive cues. The neighbouring cells will become the stalk or follower cells that elongate the sprout. (**B**) Outgrowth of a blood vessel sprout. Due to difference in the attractive and repellent cues, differences in sprout cell stimulation leads to tip cell competition. In some cases, the position of the tip cell can be taken over by another stalk cell. (**C)** Tip cells contact each other via their filopodia and establish a junctional ring. The cell membrane within this ring becomes apically polarized and forms a luminal pocket from which the lumen can be pushed through. Taken from Siekmann et al., 2013.

Tip cell selection is followed by sprout guidance and outgrowth. The selected tip cell has to change its characteristics drastically to acquire an invasive and motile behaviour, including by the formation of filopodia. The tip cell migrates towards the VEGF gradient, followed by its neighbouring cells, which act as proliferating cells, known as stalk cells (Adams and Alitalo, 2007). The outgrowth direction of the sprout is additionally guided by attractive and repulsive cues including netrins, class 3 semaphorins and SLIT proteins (Eichmann et al., 2005). In addition, Semaphorin-Plexin signalling ensures the proper endothelial abundance of sflt1, thereby repressing angiogenic potential of the growing sprout to ensure proper guidance (Zygmunt et al., 2011). A growing vascular sprout produces PDGFB that promotes the recruitment of supporting pericytes to ensure that the endothelium of the growing vessel stabilises sufficiently (Ando et al., 2016). The tip and stalk cell phenotype appeared to be plastic; stalk cells can overtake tip cells and former tip cells can migrate back to the base of the sprout (Figure I-IB). This kind of cell shuffling is transient and cyclic, as Notch signalling re-establishes a mixed pattern of cells with high and low receptor levels (Jakobsson et al., 2010).

1.1.2.2. Anastomosis and subsequent cell divisions

During the next step of angiogenesis, sprout fusion and lumen formation have to occur. When the filopodia of two tip cells encounter each other, strong adhesive interaction and EC-EC junctional contacts have to be established in order to accomplish fusion of the two sprouts, known as anastomosis (Adams and Alitalo, 2007). From the moment the filopodia of two tip cells contact each other, junctional proteins, including Cdh5 and ZO1, are deposited upon the contact sites (Figure I-IC) and grow into a junctional ring. Within this junctional ring, podocalyxin, a sialoglycoprotein, gets localised in order to polarise the tip cells by forming an apical membrane. The activity of filopodia reduces and the surface of the apical membrane in the junctional ring increases. Subsequently, the elongation of the ring allows transcellular lumen to push through, thereby establishing a new, perfused blood vessel connection. Finally, cell rearrangement by cell splitting allows the initial unicellular tube to remodel into a more durable multicellular tube (Lenard et al., 2013). The process of anastomosis is summarised in figure I-II.

The lack of Cdh5 does not prevent anastomosis, therefore other adhesion molecules cooperate in establishing junctions. Esam (Endothelial cell-selective adhesion molecule) is a JAM (cf. section 1.2) whose presence is restricted to endothelium. Aggregation assays have shown that Esam can generate efficient cell contacts, but its knock-out in mice and zebrafish does not lead to vascular defects (Hirata et al., 2001; Ishida et al., 2003). However, the combination of *esam* and *cdh5* mutant alleles aggravates the single Cdh5 mutant phenotype, including the maintenance of filopodial contacts prior to anastomosis as well as the subsequent assembly of ECs into an organised endothelium, suggesting that both proteins are redundant during blood vessel morphogenesis (Sauteur et al., 2017).

During spout outgrowth and after anastomosis, individual endothelial cells undergo division in order to overcome the distances between new established vessel connections. During cell division, ECs within a growing vessel undergo mitotic rounding, followed by symmetrically

cell furrowing and pinching of the cell body at the plane of division. During the division of unicellular cells, the lumen collapses in the plane of mitosis and reopens whenever the division process has been accomplished. Mitosis within multicellular tubes, however, does not lead to a lumen collapse (Aydogan et al., 2015).

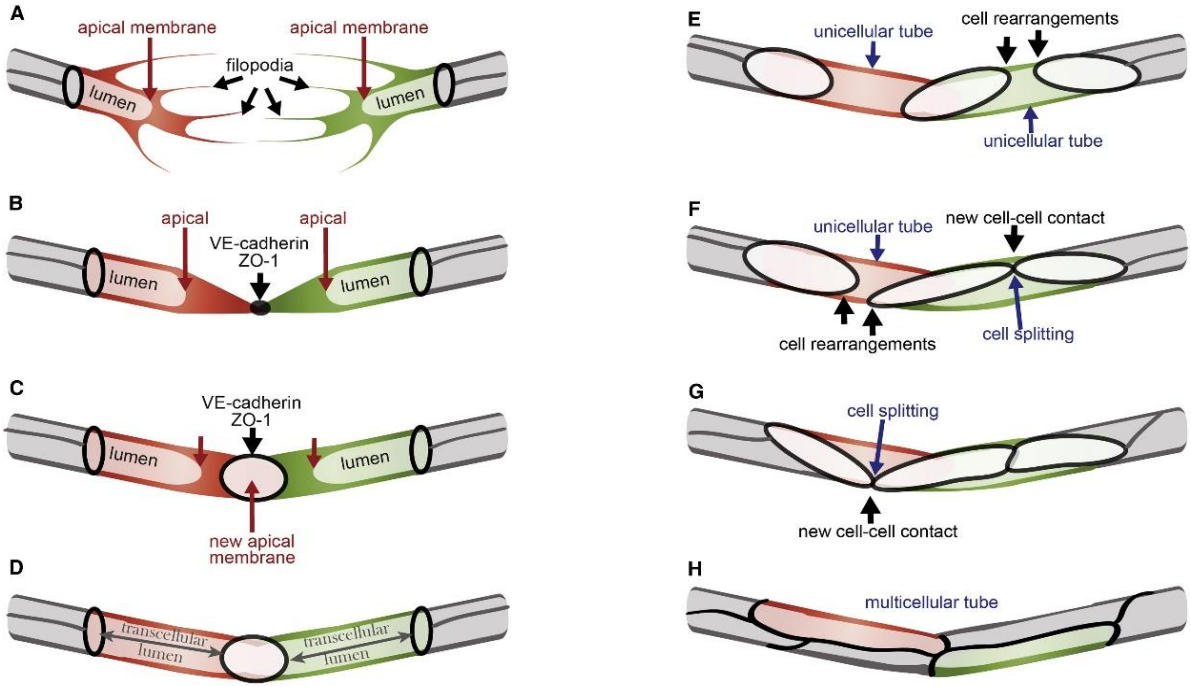

Figure I-II. Overview of blood vessel anastomosis. At the contact site of filopodia from two different sprouts, junctional proteins are deposited, which stabilises the contact site and grow out into a junctional ring. The surface of the functional ring gets polarised by the apical protein podocalyxin and its enlargement allows push though of the lumen between both cells. Cellular rearrangements changes the newly formed vessel from a unicellular into a multicellular configuration. Taken from Lenard et al., 2013.

1.1.2.3. Lumen formation

Upon anastomosis, the tip cells lose their tip cell features, including their filopodia. Subsequently, a lumen within the sprout forms to allow blood flow. Lumen formation can occur by different mechanisms, such as intracellular vacuole coalescence, where ECs form intracellular vacuoles that fuse with each other generating a lumen. But also intracellular vacuole exocytosis can facilitate lumen formation, as well as luminal repulsion, where CD34-sialomucins is localised to the cell-cell contact site and its negative charge induces electrostatic repulsion of the opposing EC surfaces (Ellertsdóttir et al., 2010; Strilić et al., 2010). After perfusion is established and ECs are matured, a new blood vessel is formed that improves oxygen delivery and consequently reduces pro-angiogenic signals from the tissue.

The two main mechanisms for lumen formation in zebrafish are cord hollowing and membrane invagination. Lumen formation by cord hollowing is driven by cell rearrangements in which cell contacts between at least three ECs generate two junctional rings that convert towards each other. In this case, both luminal pockets are brought towards each other and fuse into a lumen. By this mechanism, tubes become multicellular, but blood flow is not required (Figure I-IIIA). The majority of the vessels, however, form their lumen via membrane invagination for which less migration of the ECs is required, nor is the presence of continuous junctions demanded. In this case, the lumen extends through a single cell between two separate sites of contact. Blood pressure pushes the apical membrane through the cell body creating a unicellular tube with a transcellular lumen (Figure I-IIIB) (Herwig et al., 2011). Research on the formation of the common cardinal veins revealed a third mechanism of lumen formation, called lumen ensheathment. During this process, endothelial cells delaminate and align along an existing luminal space, extend via migration and eventually enclose the lumen (Helker et al., 2013).

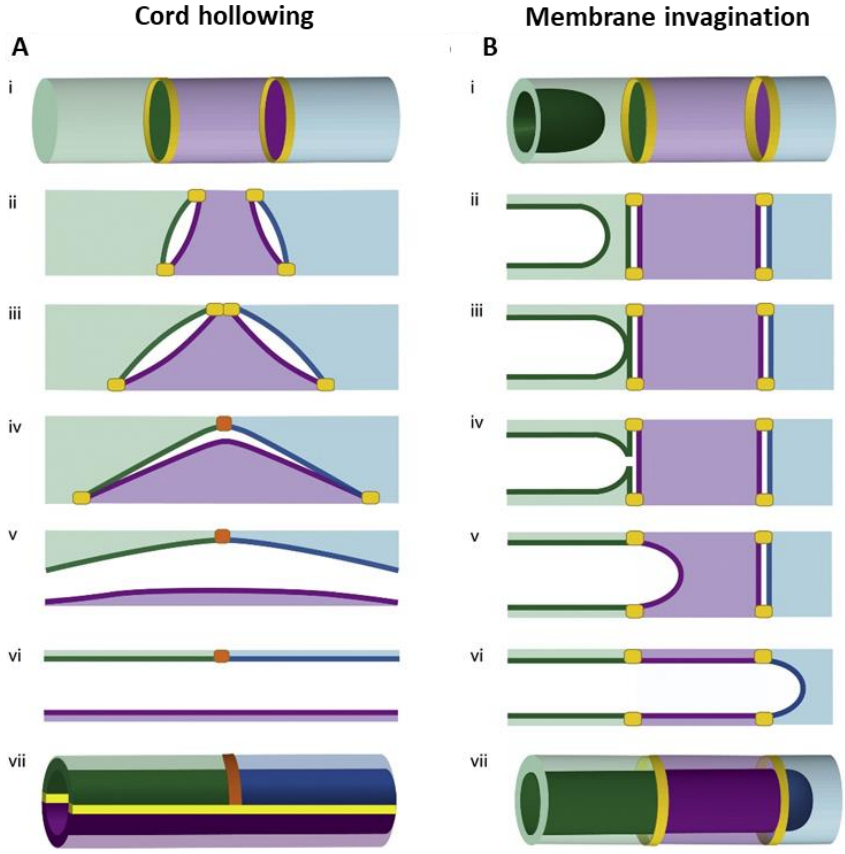

Figure I-III. Lumen formation by cord hollowing and membrane invagination. (**A**) During cord hollowing, two junctional rings convert towards each other by cellular rearrangement, leading to the fusion of both luminal pockets into a lumen in a multicellular tube. (**B**) During membrane invagination, the lumen extends through a single cell between two separate sites of contact, whereupon blood flow pushes the apical membrane through the cell body creating a unicellular lumenised tube. Taken from Herwig et al., 2011.

1.1.2.4. Secondary sprouting in the zebrafish trunk

For most analyses on sprouting angiogenesis and maturation, the development of the intersegmental vessels (ISVs) within the zebrafish trunk are used as a model, because of their metameric organisation and relatively simple anatomy (Ellertsdóttir et al., 2010). As most other forming blood vessels, they sprout, anastomose and form their lumen as describes so far. In more detail, ISVs derive from arterial precursors within the dorsal aorta and sprout dorsally around the neural tube and the notochord. At the dorsal side, they anastomose with their neighbouring sprouted ISVs thereby forming the dorsal longitudinal anastomotic vessel (DLAV) at around 30hpf (Figure I-IVA) (Isogai et al., 2003).

Venous ISVs and the intersegmental lymphatics, however, are formed by a process called secondary sprouting. At around 32hpf, bipotential Prox1-positive precursors within the PCV divide and develop either a venous or a lymphatic fate. Their identities are established asymmetrically in daughter cells where the up-regulation of *prox1* gives rise to a lymphatic cell, whereas down-regulation of *prox1* preserves the venous identity (Koltowska et al., 2015). Around 36hpf, both precursors sprout along the ISVs to form either lymphatic ISVs or anastomose around 50hpf with the existing arterial ISV respectively, thereby in the latter case changing the initial artery into a vein (Isogai et al., 2003). Simultaneously, the lymphatic sprouts continue migrating along the arterial ISVs and subsequently along the DLAV. At around 5dpf the lymphatic sprouts anastomose forming the thoracic duct (Hogan et al., 2009).

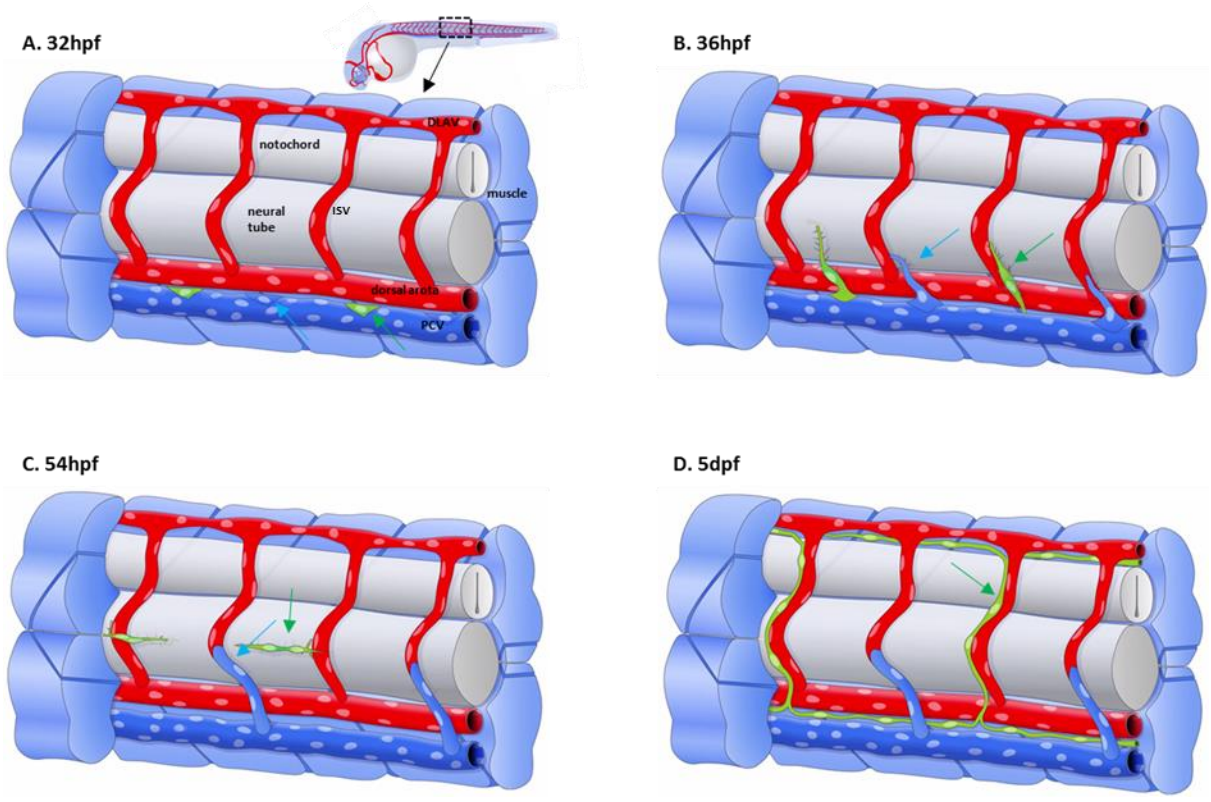

Figure I-IV. Secondary sprouting in the zebrafish trunk to develop intersegmental veins and lymphatics. (**A**) At around 32hpf, bipotential precursors within the PCV divide and develop either a venous (blue arrow) or a lymphatic fate (green arrow). **(B**) Around 36hpf, both precursors sprout along the ISVs, indicated as secondary sprouting (**C**) At 50hpf, the venous secondary sprout (blue) anastomoses with the existing arterial ISV (red) thereby changing the initial artery into a vein. (**D**) The

lymphatic sprouts continue to migrate along the arterial ISVs and subsequently along the DLAV. At around 5dpf the lymphatic sprouts anastomose. DLAV dorsal longitudinal anastomosing vessel, ISV intersegmental vessel, PCV post cardinal vein. Adapted from Hogan and Schulte-Merker, 2017.

1.2 Endothelial cell junctions

Most blood vessels develop by sprouting from pre-existing blood vessels in a process called angiogenesis (cf. 1.1.2.). During angiogenesis, endothelial cells need to reconcile two opposing challenges: during sprouting, anastomosis and lumen formation the cells have to be motile to change location, mutual position and cell shape whilst maintaining the permeability barrier and vascular integrity of the blood vessel. To this purpose, endothelial cells have several classes of cell-cell junctions at their disposal, from which adherens junctions and tight junctions are the most important ones. These junctions consist of adhesion mediating proteins, including vascular endothelial cadherin (Cdh5) forming adherens junctions, and claudins, occludins, junctional adhesion molecules (JAMs), endothelial selective adhesion molecule (ESAM) and nectins composing tight junctions. Further transmembrane proteins include amongst others PECAM-1 and CD146 (Szymborska and Gerhardt, 2018). In general, adherens junctions initiate and maintain cell-cell contacts whereas tight junctions regulate the passage of ions and solutes between cells (Bazzoni and Dejana, 2004).

In vitro studies have shown that Cdh5 plays an important role in various aspects related to endothelial cell biology, including regulation of EC adhesion, motility, shape, intracellular signalling and sensation of mechanical forces (Conway et al., 2013; Dejana and Vestweber, 2013). However, the *in vivo* roles of Cdh5 enabling ECs to form stable blood vessels are less understood.

1.2.1. The structure of vascular endothelial cadherin

Amongst the several classes of cadherins, Cdh5 is restricted to endothelial cells. Cdh5 is a single-pass transmembrane protein, which mediates homophilic, calcium-dependent adhesion. The extracellular domain of Cdh5 contains five cadherin repeats and the intracellular domain attaches the cadherin to the cytoskeleton, but also interacts with other cytoplasmic proteins (Figure I-V). Cadherin repeats can bind in cis and in trans to a neighbouring cadherin based on the calcium-dependent homophilic interaction of a conserved tryptophan residue at their amino-terminal end. Adhesion between cells are established by promotion of the homophilic interactions that form a pericellular zipper-like structure along the cell border (Bazzoni and Dejana, 2004).

The intracellular domain contains binding sites for proteins that regulate intracellular signalling (cf. section 1.3.1. on Rasip1) and two catenin-binding sites. One of these catenin-binding domains binds β-catenin at the distal C-terminus of Cdh5 and the other domain closer to the transcellular domain binds p120-catenin (Figure I-V). β-Catenin is also present in its free form in the cytoplasm and nucleus and can bind TCF/LEF transcription factor regulating cell proliferation (Klaus and Birchmeier, 2008). Multiple phosphorylation events regulate β-catenin's binding to Cdh5, where it serves as a scaffold recruiting cytoskeletal-associated proteins and α-catenin (Mateer et al., 2004). α-Catenin links the actin cytoskeleton to the adherens junction by binding on one hand to Cdh5-bound β-catenin and simultaneously to actin filaments in a 1:1:1:1 complex (Rimm et al., 1995). Plakoglobin (γ-catenin) has a similar

function as its homologue β-catenin and can also bind α-catenin. p120-Catenin stabilises Cdh5 by its electrostatic and hydrophobic properties. In addition, its binding masks residues implicated in chlathrin-mediated endocytosis and ubiquitination (Ishiyama et al., 2010).

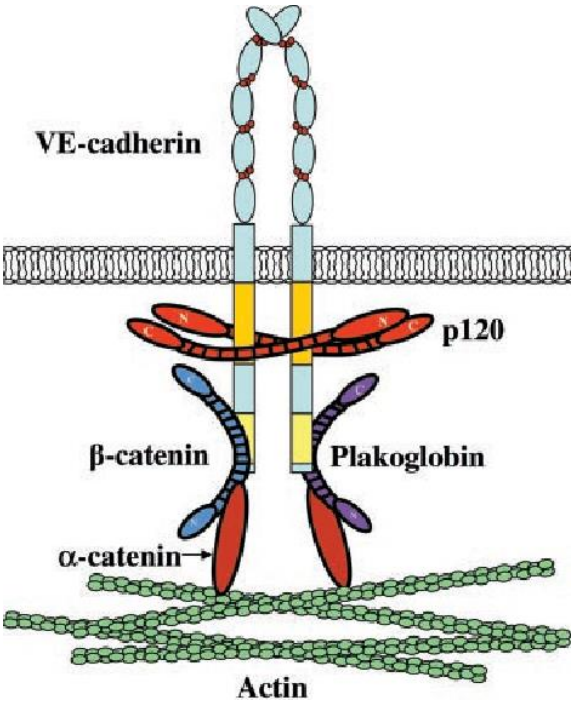

Figure I-V. Schematic representation of Cdh5 and its interaction with the cytoskeleton. Trans binding of the extracellular cadherin repeats provides adhesion between the Cdh5-based adherens junctions of neighbouring cells. In addition, Cdh5 connects as a scaffold to the actin cytoskeleton of neighbouring cells by binding actin via α-catenin and β-catenin or plakoglobin to the intracellular domain of Cdh5. p120-Catenin stabilises Cdh5. Taken from Vincent et al., 2004.

1.2.2. Mechano-transduction by Cdh5

Endothelial cells are constantly exposed to changes in mechanical forces, including forces from pulsatile blood flow, vessel wall contractions and trafficking of immune cells. ECs are perfectly capable of adapting to these force changes whilst maintaining the vascular barrier function and integrity. Cdh5-based adherens junctions increase junction size without a loss of tension when a mechanical pulling force is exerted (Liu et al., 2010). *In vitro* switching between stable (linear) junctions and remodelling (perpendicular) junctions induced by pulling forces on the Cdh5 is controlled by small GTPases that modulate cytoskeletal dynamics. As an example, Rac1 induces release of Cdh5 tension by supporting junctional stabilisation (Timmerman et al., 2015). On the contrary, activation of Rho increases acto-myosin contractility and promotes that way the formation of remodelling junctions (Liu et al., 2010).

Cell culture experiments showed that F-actin connection to α-catenin can also be stabilised by the recruitment of vinculin to the adherens junction, which binds to α-catenin whenever acto-myosin contractile forces are sensed and prevents junctions from opening too far (Le Duc et al., 2010). Meanwhile, actin remodelling proteins including zyxin, VASP and TES are recruited to the actin fibre under tension (Figure I-VI) (Dorland and Huveneers, 2017). EPLIN is only observed in vinculin-free adherens junctions, which suggest its involvement in force-dependent regulation of Cdh5 opposite to vinculin (Taguchi et al., 2011). Junctional remodelling enables the endothelial cells to adapt to changing forces, induced e.g. by thrombin, Vegf or histamine stimuli, in order to maintain the vascular barrier of the blood vessel and individual cell integrity.

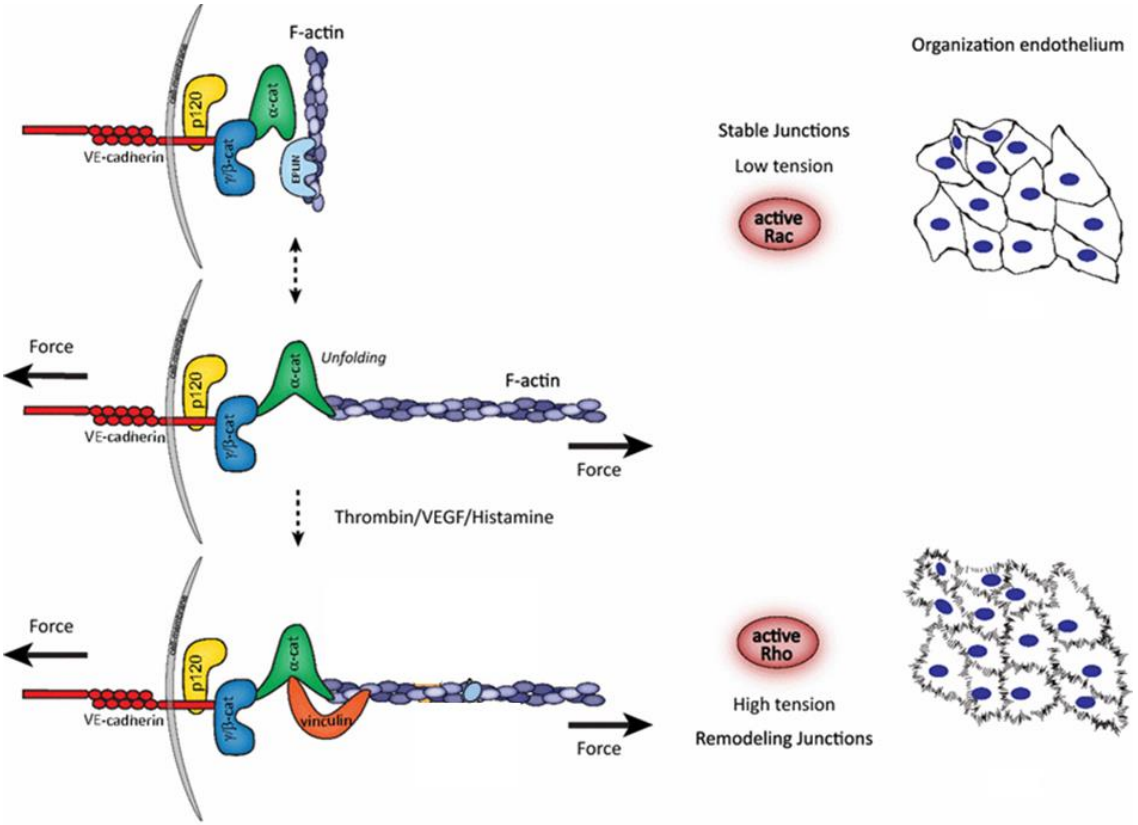

Figure I-VI. Mechano-transduction events during remodelling of endothelial adherens junctions. In absence of force on Cdh5, the small GTPase Rac1 is active and controls the linear configuration of adherens junctions. At the moment mechanical force on the F-actin-Cdh5 complex is exerted, recruitment of vinculin and actin remodelling proteins takes place, induced by thrombin/Vegf/histamine signalling. Meanwhile Rho gets activated and induces the remodelling of the adherens junctions in perpendicular configuration. Both events stabilising the F-actin-Cdh5 connection and ensures endothelial cell barrier function and integrity. Taken from Dorland and Huveneers, 2017.

In order to explore tensile changes exerted on Cdh5 in zebrafish, a Cdh5 tension sensor construct has been designed and initially introduced into VE-cadherin mutant HUVECs (Conway et al., 2013). To investigate tensional forces on Cdh5 *in vivo*, the same tension sensor module has been cloned into the zebrafish Cdh5 cDNA. In this bacterial artificial chromosome

(BAC) construct, a donor fluorescent protein Teal and an acceptor protein Venus, separated by a TV40 stretchable peptide, were introduced in the Cdh5 intracellular domain between the p120 and β-catenin binding sites (Figure I-VII). Proximity of both proteins could be measured by Förster resonance energy transfer (FRET), indicating whether Cdh5 is under tension or not. Introduction of the Cdh5-tension-sensor containing BAC into Cdh5 mutants could rescue the phenotype and compensate the loss of endogenous Cdh5 at wild type levels. This tool showed release of actomyosin contraction by ROCK inhibition, maturation of the dorsal aorta and a decrease of calcium signalling decreases Cdh5 tension. Interestingly, acute loss of blood pressure did not alter the tension on Cdh5 (Lagendijk et al., 2017).

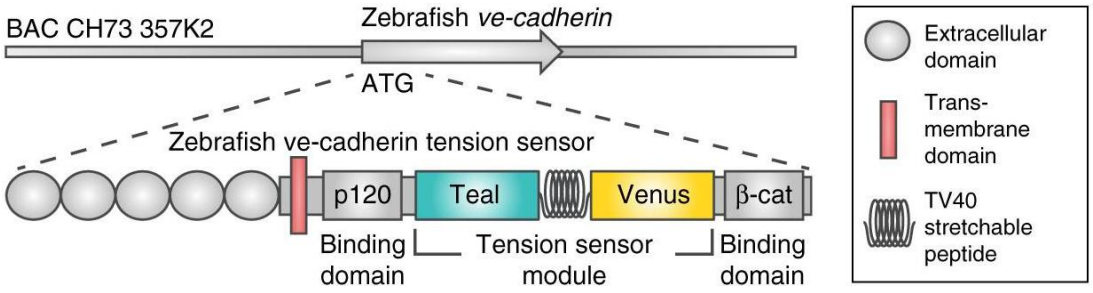

Figure I-VII. Design of the Chd5 tension-sensor line. Between the p120 and β-catenin binding sites**,** a donor fluorescent protein Teal and an acceptor protein Venus separated by a TV40 stretchable peptide were introduced by BAC recombineering. The distance between both fluorophores can be measured by FRET, which serves as read-out for tension upon Cdh5. Taken from Lagendijk et al., 2017.

1.2.3. Junctional remodelling in angiogenesis

In order to enable cell rearrangement and cell shape changes necessary for the formation of stable blood vessels, dynamic regulation of junctional actin is required. Absence of Cdh5 in Cdh5 null-mutants led to continuous sprouting activity upon tip cell contact, thereby impeding anastomosis (Lenard et al., 2013). In the zebrafish trunk, the formation of a tip cell as well as its outgrowth were not perturbed, however, tip cells failed to organise themselves into the DLAV. Moreover, the formed ISVs comprised of unicellular tubes with discontinues tight junctions and lumens. Neither junctional elongation, nor remodelling into multicellular tubes took place within Cdh5-deprived ISVs. (Sauteur et al., 2014). These observations showed that Cdh5 is required for cell rearrangement necessary to obtain multicellular tubes. Perturbation of the Cdh5-actin link by either inhibiting F-actin polymerisation or knock-out of β-catenin led also to defects in lumen formation and maintenance, stressing the importance of Cdh5 as an actin-cytoskeleton anchor (Cattelino et al., 2003; Sauteur et al., 2014). These findings led to a model in which the transmission of a deforming force by Cdh5 in stalk cells promote cell elongation. To this purpose, junctions need to be elongated, which is driven by actin polymerisation that uses Cdh5 as an anchor point (Figure I-VIII).

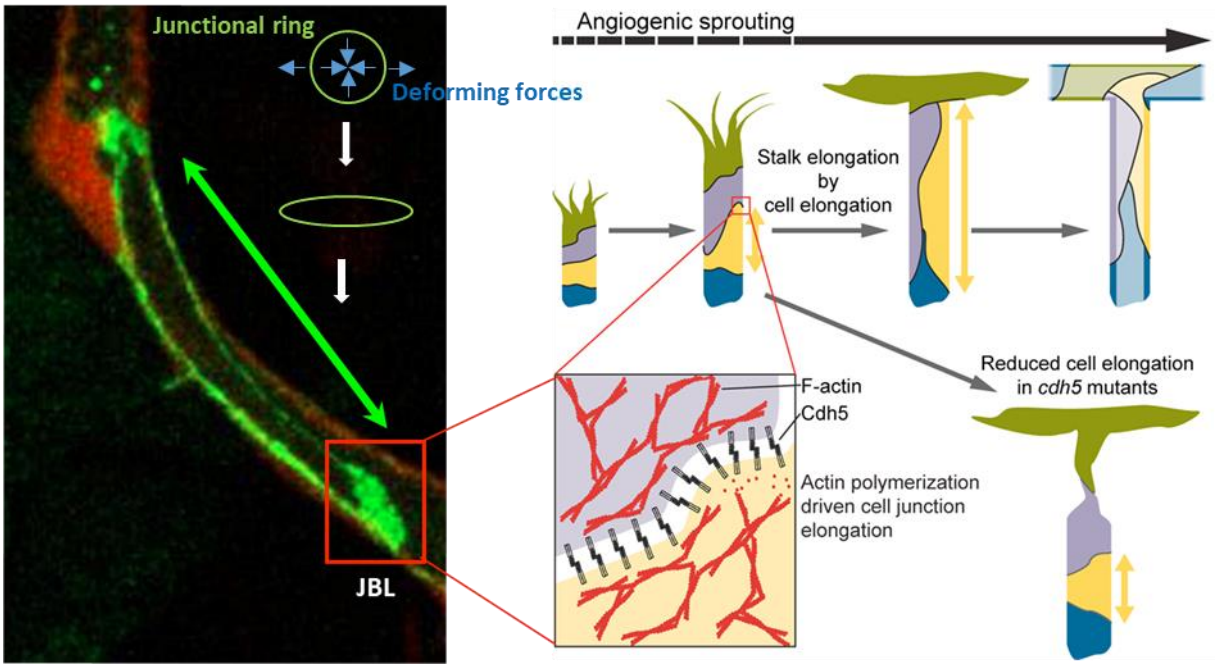

Figure I-VIII. Schematic overview of the model concerning the role of Cdh5 in angiogenesis. Sprouting of ISVs and their anastomosis into the DLAV is followed by cell elongation and cellular rearrangement into a multicellular blood vessel. In absence of Cdh5, cell elongation and remodelling does not take place, due to the inability of actin polymerisation that uses Cdh5 as an anchor point, to exert its deforming force onto the adherens junction. The left panel shows a close-up of a junction-based lamellipodium (JBL) at the distal end of Cdh5 junctional ring at the border between two endothelial cells. Adapted from Sauteur et al., 2014.

Analysis of junctional rings in the DLAV in more detail, using the Cdh5 tension sensor line (cf. 1.2.2.) to visualise Cdh5, revealed that in unicellular vessels the junctions were not uniform. Junctions were significantly thicker at the medial region than at the lateral side (Figure I-VIII, red frame on the left panel) coinciding with the direction of endothelial cell movement. Time lapse imaging of adherens junctions showed that these junctional thickenings were highly dynamic and behaved like lamellipodial protrusions, hence their name junction-based lamellipodia (JBL). Spatio-temporal analyses of JBLs as well as tight junctions allowed the description of how ECs move along each other by a, to actin-linked, Cdh5-based mechanism (Figure I-IX). In this model, actin polymerisation first forms a protrusion at the distal end of the junction which is followed by the establishment of a new junction at the anterior edge of the protrusion. Subsequently, the proximal junction is then pulled towards the anterior junction, leading to an elongation of the junctional ring. This mechanism allows endothelial cells to move along each other, change their shape and attain a multicellular configuration (Paatero et al., 2018).

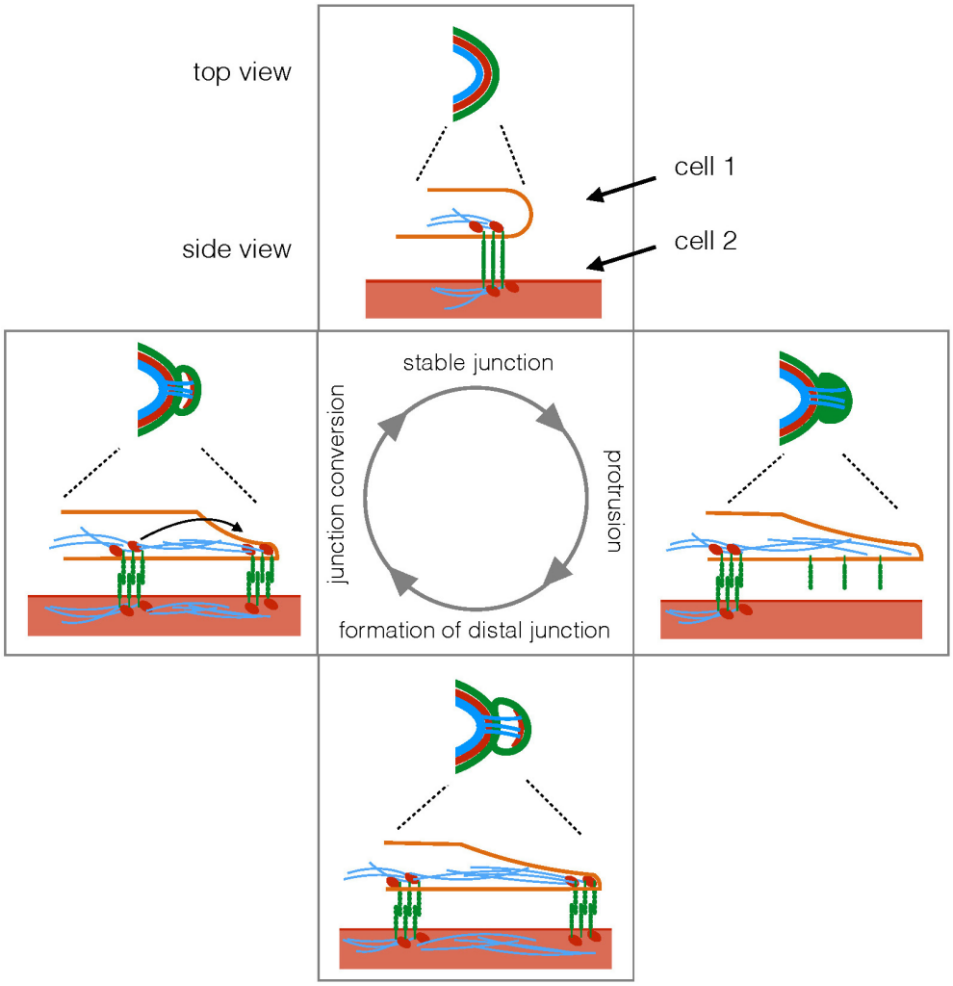

Figure I-VIII. Model of JBL-based endothelial cell movement. In order to allow EC movements whilst maintain the vascular barrier and vessel integrity, actin protrusions emanate distally form the existing junction and is followed by Cdh5 and ZO1 (component of tight junctions) accumulation at the new end of the protrusion, visible as JBLs. Finally, the proximal junction is pulled towards the distal end of the JBL and the cycle can start again. Cdh5 is visualised in green, ZO1 in red and F-actin in blue. Taken from Paatero et al., 2018.

1.3 Control of small GTPase activity in endothelial cells by Rasip1 and Radil

Cdh5 as the glue between endothelial cells and as a mechano-transducer of forces via its connection to the actin cytoskeleton, makes this protein indispensable for proper EC rearrangements without causing leakiness of the blood vessel. Actin polymerisation itself, as main contributor to force exertion via Cdh5, is also subjected to further regulation. F-actin can be polymerised (induced by e.g. ARP2/3 and formins), disassembled (by e.g. gelsolin and profilin) and contracted (by myosin), which are controlled by small GTPases. Small GTPases are a family of hydrolase enzymes that can bind and hydrolyse guanosine triphosphate (GTP). They are activated by guanine nucleotide exchange factors (GEFs) that exchange GDP for GTP. Deactivation takes place by the opposite process executed by GTPase activating proteins (GAPs). Via this system, small GTPases can be switched on and off, which makes them valuable regulators of various processes in the cell, including growth, cellular differentiation, cell movement and lipid vesicle transport (Cherfils and Zeghouf, 2013).

Examples of small GTPases are RhoA (Ras homolog family member A) that induces acto-myosin contraction and remodelling of junctions (cf. 1.2.2.), Rac1 (Ras-related C3 botulinum toxin substrate 1) that induces F-actin polymerisation and linearization of Cdh5 (cf. 1.2.2.) or Cdc42 (Cell division cycle 42) another important organiser of the cytoskeleton. In addition, inhibition of Rac1 leads to longer duration of JBLs (less dynamic) and consequently to a reduction in speed of junction elongation during DLAV anastomosis (Paatero et al., 2018). Activation of both Cdc42 and Rac1 are required for lumen formation in 3D collagen matrix assays (Iruela-Arispe and Davis, 2009). All these small GTPases belong to the Ras superfamily, the best documented family of small GTPases (Figure I-IX). However, not much is known about the regulation of small GTPases in endothelial cells yet. The only known EC specific regulating protein that controls members of the Ras superfamily is Rasip1 (Xu et al., 2011; Wilson et al., 2013).

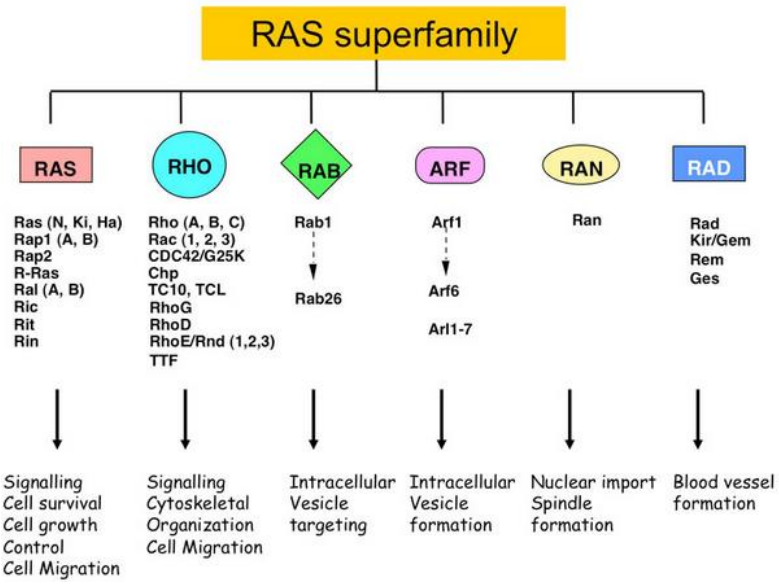

Figure I-IX. Ras superfamily of small GTPases. Taken from Khan, 2009.

1.3.1. Regulation of endothelial cell stability and lumen formation by Rasip1

Rasip1 was identified in a screen for potential effectors of Ras proteins (Mitin et al., 2004). A yeast two-hybrid system was performed using a Gal4-DNA-binding-domain-Ras-fusion protein as a bait and a human skeletal muscle cDNA library as the source of interacting proteins. Sequence analyses of the clones found five clones containing partial cDNA sequences that did not match to genes encoding for Ras effectors known at that time. These five clones represented cDNA that belonged to the same protein, but sequence comparison to the GenBank nucleotide databank did not match with an annotated gene. Since this protein was found as a Ras effector, it was named Rain (Ras interacting). Rain's protein sequence contained a Ras-associating domain homologous to other Ras effectors, where the GTP-loaded form of Ras could bind, and a dilute domain that can bind to class V myosins, important for vesicular transport (Mitin et al., 2004). The NCBI registered the annotation under the name Ras-intereacting protein 1 (Rasip1).

In a microarray screen that transcriptionally profiled embryonic aortal ECs, Rasip1 was identified as a potential regulator of blood vessel development (Xu et al., 2009). Expression analysis by *in situ* hybridisation on mouse embryos showed that Rasip1 was initially expressed within the embryonic vascular plexus, but after mouse embryonic day E10.5 in growing blood vessels and postnatal in mature endothelium. Interestingly, Rasip1 expression was absent in vascularless Vegfr2 mutant mouse embryos and knock down by siRNA prevents angiogenesis of ECs in wound-healing assays. This was the first evidence that Rasip1 is required in the endothelium of embryonic vasculature (Xu et al., 2009).

Other binding partners of Rasip1 were found by affinity purification and mass spectrometry using expression of FLAG-tagged Rasip1in endothelial cell lines (Xu et al., 2011). Rasip1 was able to bind non-muscle myosin heavy-chain IIA (NMHCIIA) as well as a RhoA-specific GAP called Arhgap29. Rasip1 knock-out mice were embryonic lethal and failed to develop lumens in all blood vessels. SiRNA knock down of either Rasip1 or Arhgap29 *in vitro* showed that both individual proteins were required for lumen formation, activation of Cdc42 and Rac1, and repression of RhoA (Western blot) (Xu et al., 2011).

In order to further investigate the *in vivo* role of Rasip1, another Rasip1 knock-out mouse was generated by a different research group (Wilson et al., 2013). These mouse embryos were smaller in size, showed severe haemorrhages throughout the whole body, developed pericardial oedema and did not survive after E10.5. Vascular lumens were formed, but ultimately collapsed. In the same study, knock down of Rasip1 in zebrafish allowed blood circulation through the DA and PCV, however, the diameter of both vessels were irregular and smaller. Subsequent antibody stainings against Rasip1 showed a cytoplasmic pattern in HUVECs, but at newly forming or remodelling Cdh5-based adherens junctions, Rasip1 showed a junctional localisation. GST pull-down assays demonstrated direct physical interaction of Rasip1 with Rap1 (a Ras small GTPase known to increase EC barrier function), but not with RhoA, Rac1 and Cdc42. Indeed, knock down of Rasip1 in HUVECs phenocopied the loss of Rap1 (or its GEF Epac1) by altering junctional actin organisation and junctional remodelling (Wilson et al., 2013).

The binding partner of Rasip1, which is essential to be present for junctional localisation is Heart of Glass 1 (Heg1) (Kreuk et al., 2016). Heg1 is a transmembrane receptor essential for cardiovascular development that also binds via its cytoplasmic domain to Krit1 (or CCM1). Krit1 can bind Rap1 and associates with Cdh5 via β-catenin (Glading et al., 2007). Upon Rap1 activation, Krit1 localises at adherens junctions where it directly interacts with Heg1. Since the cytoplasmic domain of Heg1 is highly conserved, but Krit1 requires only 10% of the tail, other Heg1 interactors were searched. Lysates of Heg1-biotin-tagged expressing HUVEC (endothelial) and HeLa (cervical cancerous) cells were analysed by mass spectrometry and yielded Rasip1 as a protein binding in HUVEC cells, but not in HELA cells, confirming its endothelial specific expression. Knock down of Heg1 and activation of Rap1 did not result in junctional localisation of Rasip1 indicating that Heg1 is required for Rasip1 localisation at the junction. Further, binding affinity, measured using FLAG-tagged Rasip1 constructs for three putative Rasip1 protein domains, showed that only a third domain, called forkhead domain, is sufficient for Heg1 binding (Figure I-X) (Kreuk et al., 2016).

To investigate the role of Rasip1 at later embryonic stages than E10.5, an inducible Rasip1 knock-out line based on tamoxifen-induced Cre-loxP recombination (cf. section 1.5), was generated. This line showed that Rasip1 is essential for blood vessel formation and maintenance in the mouse embryo, but is dispensable in quiescent adult vessels (Koo et al., 2016). The inducible Rasip1 knock out line was then crossed into mouse lines that could undergo Cre-loxP inducible ablation of RhoA and Cdc42. Ablation of Cdc42 led to blockage of vascular lumen formation, whereas the absence of RhoA led to larger vessel diameters, which could be phenocopied by ROCK (target of RhoA) inhibition. Deletion of Arhgap29 allowed normal tubulogenesis although the lumen stayed narrower, confirming its deactivating function on RhoA. These observations demonstrated that Rasip1 functions upstream of Cdc42 and RhoA. Moreover, these findings show that Rasip1 promotes Cdc42 activity in order to induce lumen formation and once the lumen is open, Rasip1 suppresses actin-myosin contractility in order to expand vessel lumens during embryonic growth (Barry et al., 2016).

1.3.2. Discovery of Radil as a homologue of Rasip1

Radil was discovered as a novel human protein in a screen for genes induced by an oncogenic translocation in a paediatric sarcoma. This protein was encoded by 1075 amino acids, including a Ras associating domain (RA), a Dilute domain (DIL) and a PDZ domain at the C-terminus (Smolen et al., 2007). The PDZ, which is not present in Rasip1, is named after the initials of the first three proteins in which the PDZ was found: post synaptic density protein (PSD95), Drosophila disc large tumour suppressor (Dlg1) and Zonula occludens-1 (ZO-1). Proteins containing PDZ domains are known to play important roles in anchoring receptor proteins in the membrane to the cytoskeleton (Lee and Zheng, 2010). Immuno-precipitation using FLAG-tagged Radil (RA and DIL domain containing protein) showed that Radil preferentially binds to the small GTPase Rap1, but not to Cdc42 and Rac1. Further *in situ* hybridisation in zebrafish demonstrated a ubiquitous expression for Radil with an enrichment in the anterior part of the embryo. Knock down of Radil led to a diminished migratory capacity of neural crest (NC) cells leading to multiple defects in NC-derived lineages e.g. cartilage, pigment cells and enteric

neurons (Smolen et al., 2007). Later, RadilB was found to bind Arhgap29 in a mass spectrometry analysis (Ahmed et al., 2012).

The physiological relevance of the Rap1-Rasip1-Arhgap29 signalling pathway was investigated in more detail by measuring the endothelial barrier (by electrical cell impedance sensing) of HUVECs. Depletion of Rasip1 reduced the basal endothelial barrier function, however, to a lesser extent than depletion of Arhgap29, suggesting that Rasip1 is not the only mediator of Arhgap29. Subsequently, depletion of both Rasip1 and Radil reduced the endothelial barrier resistance to a similar level as Arhgap29 depletion, even after overexpression of Rap1 (Post et al., 2013). Upon activation of Rap1 with the Epac1-selective activator 007-AM, GFP-Arhgap29, GFP-Rasip1 and GFP Radil redistributed from the cytosol to the plasma membrane of HUVECs. Rasip1 translocalisation upon Rap1 activation was unaffected by knock down of Radil and vice versa, indicating that both proteins independently bind Rap1 through their own RA domain and translocate to the membrane independently. Arhgap29's translocation, however, was dependent on Radil, but not on Rasip1. Truncated Radil lacking its PDZ domain, could not translocate Arhgap29, indicating that upon Rap1 activation, Radil binds Arhgap29 via the PDZ domain and then translocates to the cell membrane (Post et al., 2015). Since Rasip1 does not possess a PDZ domain, its binding to Arhgap29 was most probably found in a Rasip1-Radil-Arhgap29 complex, where Arhgap29 indirectly bound to Rasip1 via Radil (cf. Xu et al., 2011). My interpretation of the available data concerning Rasip1 and Radil is summarised in figure I-XB.

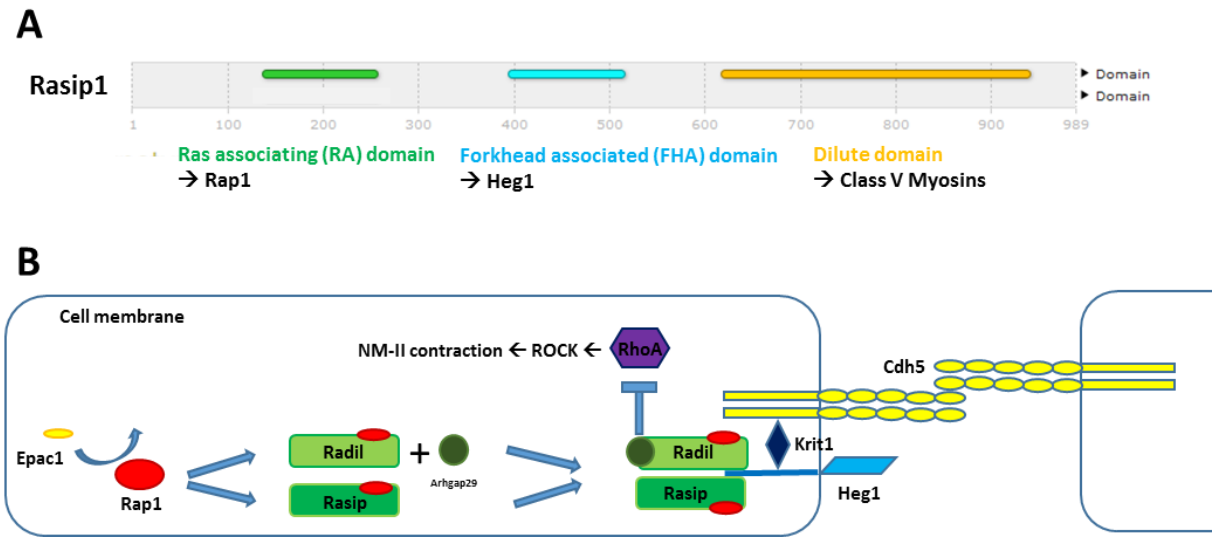

Figure I-X. Interpretation of Rasip1 protein domain functions and Rasip1/Radil working mechanism based on available literature. (**A**) Domains of Rasip1 with indicated binding partner. (**B**) Working mechanism of Rap1-Rasip1-RhoA signalling. Upon activation of Rap1 by its GEF Epac1, GTP-bound Rap1 binds Radil and Rasip1 that subsequently translocate towards the junctions. Meanwhile, Rap1-bound Radil binds the RhoA-specific GAP Arhgap29 and binds simultaneously with Rasip to the cytosolic tail of Heg1. This protein complex is linked via Krit1 (or CCM1) to β-catenin at the intracellular tail of Cdh5 and inhibits RhoA activity. RhoA is an activator of ROCK, which induces actin-myosin contraction by non-muscle myosin II (NM-II).

1.4 Introduction to BAC recombineering

Bacterial Artificial Chromosomes (BAC) have become an important tool for genomic sequencing because of their high stability and large insert size (Shizuya et al., 1992). In addition BACs are frequently used for making transgenic organisms due to the fact that in principle all regulatory sequences required for natural gene expression can be found in a single BAC (Yang et al., 1997). For my thesis, I used BAC recombineering technology in order to make an inducible Cdh5 construct as well as a photo-convertible fluorophore-tagged Cdh5 construct.

Genes in BACs can be modified based on homologous recombination via a technique called BAC recombineering (recombination-mediated genetic engineering). BAC recombineering is possible in E. coli hosts that harbour a defective λ prophage system. The genome of E. coli that are infected with the bacteriophage λ, undergoes recombination based on 50bp homology on a highly efficient rate, induced by λ-encoded genetic recombination protein machinery (Poteete, 2001). However, this λ prophage system does not harm E. coli itself when constitutively expressed on a multicopy plasmid (Zagursky and Hays, 1983). The genes encoded on the λ prophage system are Exo, which degrades the 5'-ending strand of duplex DNA, RecA, which binds to the 5'-ssDNA-overhang generated by Exo, and Bet, which promotes 3'-end assimilation in order to anneal complement single-strand DNA (Stahl et al., 1997; Court et al., 2002). The defective λ prophage system in this study does not contain RecA, but instead a gene called Gam, which inhibits another Rec protein (RecBCD) in E. coli thereby protecting linear DNA-targeting cassettes from degradation (Figure I-XI). For BAC recombineering purposes, E. coli strains are used that contain a stably integrated defective λ prophage system as described above, under control of the temperature-sensitive repressor cI857 (Lee et al., 2001).

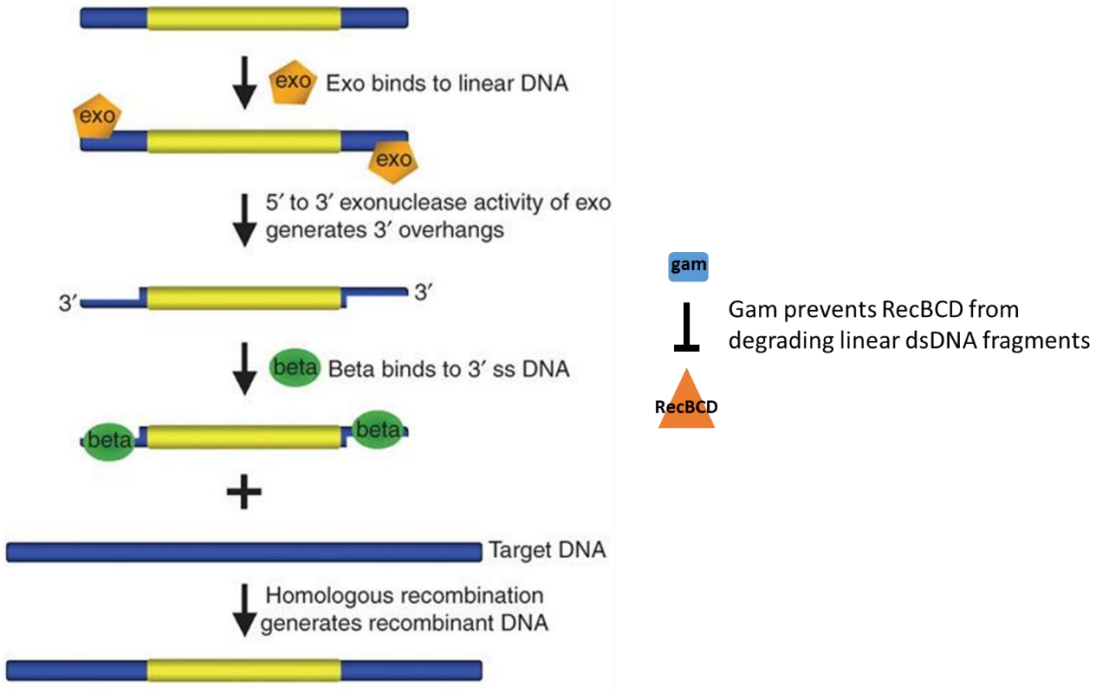

Figure I-XI. Working mechanism of the defective λ prophage system used for recombineering. Exo binds to linear DNA and has a 5′- to 3′-dsDNA exonuclease activity, which generates 3′-overhangs.

Subsequently, Beta binds to the 3'overhangs of single-stranded DNA (3′-overhangs), promotes annealing of single-stranded DNA and generates recombinant DNA via homologous recombination. Gam prevents RecBCD nuclease from degrading double-stranded linear DNA fragments. Adapted from Sharan et al., 2009.

Another important requirement for efficient genetic editing in BACs is the methods of selection for desired modification. I used the SW102 E. coli strain that contains, apart from the heat-shock inducible defective λ prophage, a galactose operon lacking the gene for galactokinase, also called galK (Warming et al., 2005). Because galK is essential for the galactose degradation pathway by phosphorylation of galactose, and since phosphorylation of deoxy-galactose (DOG) results in an E. coli toxic product, this system can be used for galK-based positive and negative selection. To this purpose, SW102 E.coli cells are grown on minimal plates that only contain galactose as carbon source. Since this strain is deficient of leucine and biotin metabolism, due to the integration location of the λ prophage system, one needs to add both biotin and leucine to the minimal plates when selecting (Warming et al., 2005).

The general BAC recombineering procedure I used, is schematically represented in figure I-XII. First, a BAC containing the gene that one wants to modify, is transformed into the SW102 E. coli. One BAC containing bacterium colony is then inoculated to gain a culture of SW102 that will be prepared for transformation by an electric pulse. Preparation include a heat-shock to induce the λ prophage system and washing to get rid of salts. In the first round, the sequence coding for galK flanked by homology arms is transformed into the bacterium. The homology arms are both identical to the two sequences in the BAC where in between the galK gene should be inserted. Only bacteria that have inserted *galK* by homologous recombination survive on minimal plates containing galactose as the only carbon source. One of the surviving colonies is subsequently inoculated, prepared for transformation and finally transformed with an insert containing the desired modification flanked with the same homology arms as the galK gene used in the first round. After the second recombination round, the bacteria are plated on minimal plates containing DOG. Only those bacteria that have exchanged their galK gene for the desired insert (those who have lost their initially inserted *galK*) can survive on DOG plates. Surviving colonies can finally be tested for having the correct modification (Warming et al., 2005).

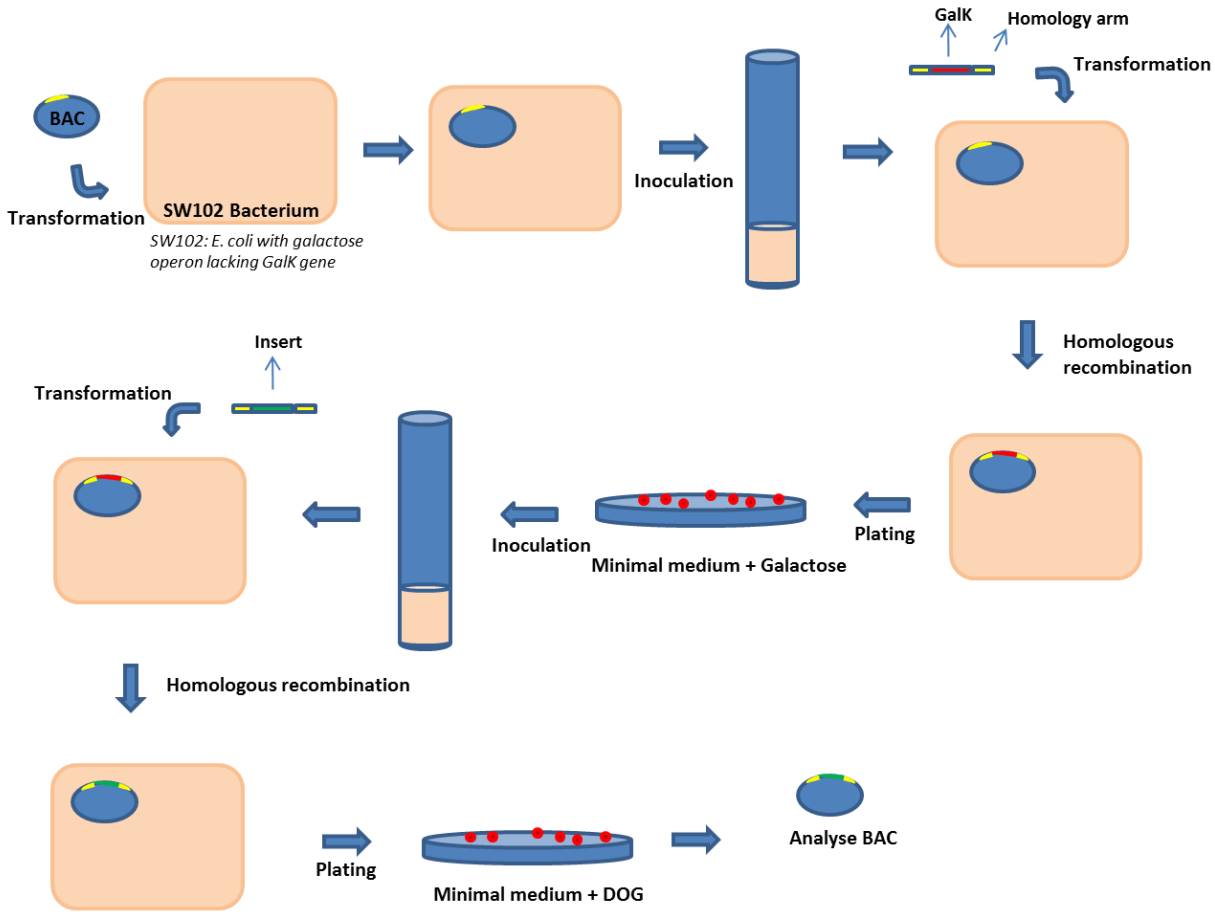

Figure I-XII. Schematic representation of BAC recombineering procedure. First a BAC containing the gene of interest is transformed into SW102. BAC containing SW102 cells are then inoculated and transformed with the galK gene (red) flanked by homology arms (yellow). The homology arms are identical to the place of the desired modification in the BAC (yellow). Selection for homologous recombination of *galK* takes place in galactose-containing minimal plates (positive selection for *galK* expression). One surviving colony is subsequently inoculated and transformed with in insert containing the genetic modification, flanked by the same homology arms as before. Transformed cells are selected on DOG containing minimal plates (negative selection for *galK* expression). Surviving colonies can be analysed for desired modification.

1.5 Transposon-mediated BAC transgenesis in zebrafish and Cre/loxP recombination

Microinjection of BACs into fertilised zebrafish eggs leads in 1-3% to integration of the BAC into the genome (Yang et al., 2006). Transposon-mediated insertion of genetic material can increase integration efficiency substantially. To this purpose, the Tol2 element was identified in the genome of the Medaka fish, encoding for a transposase protein, which was found to be autonomously active (Kawakami et al., 1998; Kawakami and Shima, 1999). DNA inserts can be transposed efficiently via a cut-and-paste mechanism provided that essential cis-sequences are present at both ends of Tol2 (Urasaki et al., 2006). In order to use this system for efficient BAC integration, these cis-sequences were characterised for minimal length required for Tol2 activity and were then cloned into a cassette in an outwards directed inversed orientation (*iTol2*). When this *iTol2*-cassette was subsequently introduced into a BAC and injected together with Tol2 transposase, the transposase excised the *iTol2* sites and integrated the BAC as a single copy into a random single genomic locus (Figure I-XIIIA). In general, 1 to 5 BAC copies were found in zebrafish transgenics with insertion lengths up until 66kb (Suster et al., 2009).

Cre (Causes recombination) is a bacteriophage P1-derived cyclic recombinase that catalyses the site-specific recombination between 34bp *loxP* sites (Locus of crossing over (x) from coliphage Pl). A DNA cassette between *loxP* sites in head-to-head orientation can be inverted by Cre-mediated recombination, whereas *loxP* sites in tandem orientation leads to circulation, excision and consequently loss of the cassette between the *loxP* sites (Figure I-XIIIB) (Sauer, 1987; Sauer and Henderson, 1988). Since the activity of Cre can be controlled by either expression under a heat-shock promoter or activation by tamoxifen (TAM), the Cre-loxP can be used for knock-out genes in an inducible way. TAM-inducible Cre is fused to a mutated oestrogen receptor, which only becomes activated and then translocates into the nucleus upon binding of TAM (Metzger et al., 1995).

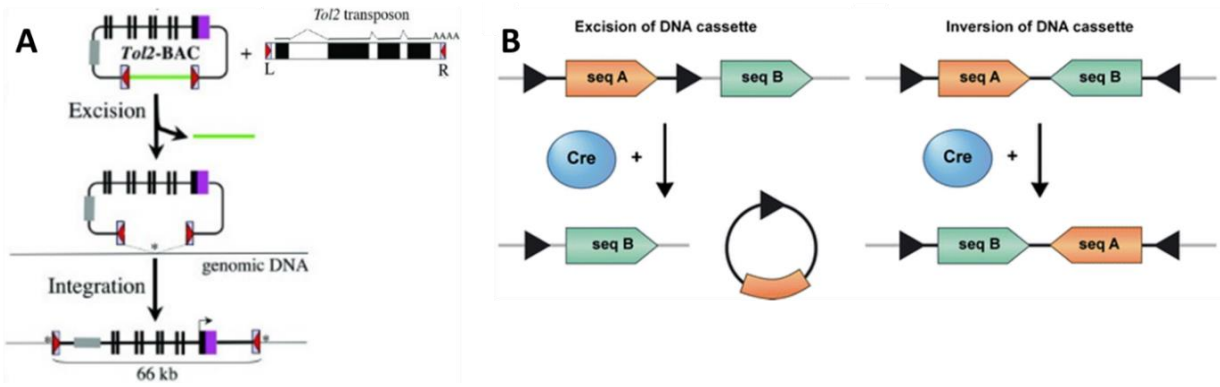

Figure I-XIII. Schematic representation of Tol2-mediated genomic insertion and Cre-loxP recombination. (**A**) When both the insert with inverted *tol2* sites and the Tol2 transposon are injected, Tol2 cuts the inverted *Tol2* (*iTol2*) sites, resulting in opening of the plasmid and loss of the region

between the excisions (green). Subsequently, Tol2 integrates the *iTol2*-flanked construct into the genome (Suster et al., 2009). (**B**) Active Cre-recombinase can recombine loxP sites. Recombination of loxP sites in tandem orientation leads to excision and loss of the construct between the loxP sites (left). Recombination of loxP sites in head-to-head orientation leads to inversion of the construct between the loxP sites (right) (Renninger et al., 2011).

1.6 Aim of this thesis

Endothelial cell interactions are key to blood vessel morphogenesis. The endothelial adhesion protein Cdh5 is essential for many aspects of this process, including anastomosis and cellular rearrangement (cf. 1.2.2. and 1.2.3.). Cdh5 as an anchor for the cytoskeleton is important for EC motility and removal of Cdh5 inhibits cellular rearrangement and proper lumen formation (Sauteur et al., 2014; Paatero et al., 2018). However, research on Cdh5 dispensability is restricted to the fact, that Cdh5-less embryos die around 5dpf. In addition, impaired heart development in absence of Cdh5 prevents blood circulation, which hampers phenotypical analyses of Cdh5 mutants, because observed phenotypes could be due to the absence of blood pressure, rather than the absence of Cdh5 within the endothelial cells under investigation.

In order to investigate Cdh5-based cell interactions *in vivo* at different time points during embryonic development and to gain mosaic ECs sprouts avoiding the need of transplantation experiments, the aim of this thesis is the generation of an inducible Cdh5 knock out zebrafish line. To that, I introduce in section 3.1 a system in which mosaic angiogenic sprouts, that contain cells with different Cdh5 levels, can be investigated. Via expression of inducible Cre-recombinase, the expression of *cdh5* can be stopped and the behaviour of ECs, which up until recombination developed in a wild type environment, can be analysed at any desired developmental stage.

In section 3.2, I introduce a photo-convertible fluorescence tagged Cdh5, using again the same BAC recombineering technology. The aim here is generating a tool that can examine to what extend individual neighbouring ECs contribute to the formation of JBL dynamics, thereby elucidating more about the dynamic endothelial cell behaviours during cell movement. Via photo-conversion of single cells, this tool will allow the visualisation of Cdh5 derived from two different cells within the same adherens junction by green and red light emission.

Regulation of the conformation of Cdh5 and the actin cytoskeleton is mainly controlled by small GTPases. Since the Rap1 effector Rasip1 was found to control various small GTPases, its expression is restricted to ECs and its absence leads to angiogenic phenotypes (Wilson et al., 2013), the former post-doc Dr. Charles Betz generated a Rasip1 knock out zebrafish line (UBS28) and he started with me to characterise Rasip1's knock out phenotype. Simultaneously, I found Radil as a protein whose structure highly resembled that of Rasip1, but which was not investigated in the context of angiogenesis so far. When Dr. Charles Betz left the lab, his Rasip1 project was taken over by the doctoral candidate Minkyoung Lee, whereas I continued mainly on characterising the Radil knock-out phenotype and supporting Minkyoung Lee where necessary. The first results of this side project are described in section 3.3 and form the basis for further comparative analysis with Rasip1 and the Rasip1/Radil double knock phenotype, in order to decipher how Rap1 signalling controls angiogenesis.

Chapter II
Materials & Methods

Methods adapted from Sauteur (2016) are indicated with [1]

2.1. Materials BAC recombineering

2.1.1. Buffers, media and solutions

Name	Composition
Biotin	0.2mg/ml d-biotin in ddH_2O sterile filtered stored at 4°C up until 4 months
Deoxy-galactose	20% (w/v) 2-deoxy-galactose in ddH_2O autoclaved stored at -20°C
DNA loading buffer (10x)	30% (v/v) glycerol 20% (w/v) Orange G in ddH_2O stored at -20°C
Embryo lysis buffer	10mM Tris pH8 2mM EDTA 0.2% Triton-X
Galactose	20% (w/v) d-galactose in ddH_2O autoclaved
Gibson master mix	100µl 5x isothermal reaction buffer 2µl T5 exonuclease 6.25µl Phusion polymerase 50µl Taq DNA ligase 217µl ddH20 aliquoted into 15µl portions stored at -20°C
Glycerol	20% (w/v) glycerol in ddH_2O autoclaved
Isothermal reaction buffer 5x (Gibson cloning)	0.75g PEG-8000 1.5ml 1M Tris-HCl, pH 7.5 150µl 1M MgCl2 150µl 1M DTT 30µl 100mM dATP 30µl 100mM dTTP 30µl 100mM dCTP 30µl 100mM dGTP 300µl 50mM NAD ddH20 to 3ml aliquoted into 100µl portions stored at -20°C
LB	1% (w/v) tryptone 0.5% (w/v) yeast extract 1% (w/v) NaCl in ddH_2O autoclaved

Leucin	10mg/ml L-leucin in ddH_2O heated, cooled down and sterile filtered
Magnesium sulfate	1M $MgSO_4 \cdot 7H_2O$
M9 Medium	42mM Na_2HPO_4 22mM KH_2PO_4 18.5mM NH_4Cl 8.5mM NaCl in ddH_2O autoclaved
M63 Medium (5x)	75.5mM $(NH_4)2SO_4$ 500mM KH_2PO4 9µM $FeSO_4 \cdot 7H_2O$ in ddH_2O adjusted pH7.0 (with KOH) autoclaved
TAE (50x)	2M Tris Base 5.71% (v/v) glacial acetic acid 50mM EDTA in ddH_2O autoclaved

2.1.2. Antibiotics

Antibiotic	Stock concentration	Working concentration
Ampicillin	100 mg/ml	100 µg/ml
Chloramphenicol	34 mg/ml	12.5 µg/ml

2.1.3. E. coli bacterial strains

Name	Genotype	Source
Top10	F- *mcr*A Δ(*mrr-hsd*RMS-*mcr*BC) φ80*lac*ZΔM15 Δ*lac*X74 *rec*A1 *ara*D139 Δ(*araleu*)7697 *gal*U *gal*K *rps*L (StrR) *end*A1 *nup*G	Invitrogen
SURE	e14-(McrA-) Δ*(mcrCB-hsdSMR-mrr)171 endA1 gyrA96 thi-1 supE44 relA1 lac recB recJ sbcC umuC*::Tn*5* (Kanr) *uvrC* [F´ *proAB lac*IqZΔ*M15* Tn*10* (Tetr)].	Invitrogen
DH10B	F^- mcrA Δ(*mrr-hsd*RMS-*mcr*BC) Φ80d*lac*ZΔM15 Δ*lac*X74 *end*A1 *rec*A1 *deo*R Δ(*ara*,*leu*)7697 *ara*D139 *gal*U *gal*K *nup*G *rps*L λ^-	NEB
SW102	F- *mcr*A Δ(*mrr-hsd*RMS-*mcr*BC) Φ80d*lac*Z M15 *Δlac*X74 *deo*R *rec*A1 *end*A1 *ara*D139 Δ(*ara, leu*) 7649 *gal*U *gal*K *rsp*L *nup*G [*λcI*857 (*cro-bio*A) <> *tet*]	NCI-Frederick

2.1.4. Fish lines

Name	Allele designation	Reference
ABC	Wild type (WT)	ZIRC, Oregon
TU	Wild type (WT)	(Haffter et al., 1996)
kdrl:EGFP	s843	(Jin et al., 2005)
VE-cadherin 4bp deletion	UBS8	(Sauteur et al., 2014)
kdrl:Cre	S898	(Bertrand et al., 2010)
hs:Cre	Zdf13	(Feng et al., 2007)

2.1.5. BACs and plasmids

Name	Description	Antibiotic	Reference
$Cdh5^{BAC}$	BAC name: CH73-357K2 in vector: pTARBAC2	Chlor-amphenicol	BACPAC Resources Center
pGalK	E. Coli GalK gene used for 2 step BAC recombineering	Ampicillin	(Warming et al., 2005)
p(Itol2;β-crystellin:mKate2)	Plasmid containing 2 inverted Tol2 sites (transposon-mediated transgenesis) and eye marker	Ampicillin	Gift from Jeroen Busmann. Cloned and handed over by Etienne Schmelzer
pAttB	Intergrase-mediated site-specific transgenesis	Ampicillin	Gift from Christian Mosimann
p(loxP-Cdh5-mCherry-loxP-nls-mCherry)	*cdh5* tagged with marker, flanked by LoxP sites	Ampicillin	This study, synthesised by ATG:biosynthetics GmbH
pRFP	Red fluorescent protein	Ampicillin	Cloned by Charles Betz
p(inls-imCherry)	Plasmid containing nls-mCherry in inverted orientation	Ampicillin	This study, synthesised by ATG:biosynthetics GmbH
pmClavGR2-NT	Convertible fluorescent protein	Ampicillin	Allele Biotech

2.1.6. Oligonucleotides

Primer name	SEQUENCE
Homo GalK loxp Fo	CTTATCGATGATAAGCTGTCAAACATGAGAATTGATCCGGAACCCTTAATCCTGTTGACAATTAATCATCGGCA
Homo GalK loxp Re	CCGATGCAAGTGTGTCGCTGTCGACGGTGACCCTATAGTCGAGGGACCTATCAGCACTGTCCTGCTCCTT
Tol2_plasmid Fo1	TCTCCGCACCCGACATAGATCCCTGCTCGAGCCGGGCCCAAGTG
Tol2_plasmid Fo2	GCGTAAGCGGGGCACATTTCATTACCTCTTTCTCCGCACCCGACATAGAT
Tol2_plasmid Rev1	ATCCTTAATTAAGTCTACTATCAGCCACAGGATCAAGAGC

Tol2_plasmid Rev2	GCGGGGCATGACTATTGGCGCGCCGGATCGATCCTTA ATTAAGTCTACTA
BAC_tol2LM_foI	TACTGCGATGAGTGGCAGG
BAC_tol2LM_revI	GGGTTATTGTCTCATGAGCGG
BAC_tol2LM_foII	GGCCACCTGATCTGCAACTT
BAC_tol2LM_revII	GCACAGCTTGAAGTTGGCTT
Homo Attb loxp Fo	CTTATCGATGATAAGCTGTCAAACATGAGAATTGATCC GGAACCCTTAATGGGTGCCAGGGCGTGCCCTTGGGCTC CCCGGGCGCGTA
Homo Attb loxp Re	CCGATGCAAGTGTGTCGCTGTCGACGGTGACCCTATAG TCGAGGGACCTATACGCGCCCGGGGAGCCCAAGGGCA CGCCCTGGCACCC
Attb_homol_Fo	ACGATGAGCGCATTGTTAGA
Attb_homol_Re	CTTATCCACAACATTTTGCGC
Attb_homol_Seq	TCATACACGGTGCCTGAC
Cdh5_ex3_GalK_fo	TGATTGCCTTTGTTTATAATTATTTTGTGTGTATTTCTTT TTTCTTTTAGCCTGTTGACAATTAATCATCGGCA
Cdh5_ex3_GalK_re	GAAAGCAACATGCATCAATGGACAAGCACATGCTTGT GTTAGTCTGTTACTCAGCACTGTCCTGCTCCTT
BAC_Cdh5_ex3_Del.	TGATTGCCTTTGTTTATAATTATTTTGTGTGTATTTCTTT TTTCTTTTAGGTAACAGACTAACACAAGCATGTGCTTG TCCATTGATGCATGTTGCTTTC
BAC_ex3_fo	AAAAGTATCTTCAAACTATTAAATC
BAC_ex3_re	TCTGTGCCATTTAGTAGTTT
BAC_ex3_seq	GAACTGCTGTTTTTAAATAA
GalK_exon2_fo	CTACAAGGCATGAATTATCATACAGATATTTGTTTTGT TGTTTTCTGCAGCCTGTTGACAATTAATCATCGGCA
GalK_exon2_re	CGGATCTCTCCAAATTAAAGTGTGATCCATTTGTTTAC AAGACCGTCTACTCAGCACTGTCCTGCTCCTT
Cdh5_exon2_fo	AAGTGTATGTACTGTATGG
Cdh5_exon2_re	TATGCTAAGAACCTAAAGAATC
Cdh5_exon2_seq	CTACAAGGCATGAATTATCA
Homol._tagRFP_Fo	GGTGAAGAAGGACGAGGCAGATCGTGATCGAGATGCC GGCGTCTCTAAGGGGGAAGAAC
tagRFP_homol._Re	AGCCATAGATGTGTAATGTGTCATAGGGAATGCCGCC GGCTTTGTACAGTTCATCCATACCA
Bac_wo_cherry_fo	GCCGGCGGCATTCCCTATG
Bac_wo_cherry_re	GCCGGCATCTCGATCACGATC
Homol_UTR_fo	TTATGGAGTAGACGGCTCTGATTCGGATAGCTCCTACT GAAGTCCATGGTCATCATC
UTR_homol_Re	TATAATGTATGCTATACGAAGTTATTAAGATACATTGA TGATAGTGAGTTAATAATCATCTGATT
Bac_wo_polyA_Fo	CATCAATGTATCTTAATAACTTCG
Bac_wo_polyA_Re	TCAGTAGGAGCTATCCGAAT
RFP_pl2_fo	GGTGAAGAAGGACGAGGC
RFP_pl2_Re	AGCCATAGATGTGTAATGTGTCATA
Plasmid1_fo_RFP	ATCTCGATCACGATCTGCCT
Plasmid1_re_RFP	GGCATTCCCTATGACACATTACA
Galk_mClav_fo	TGGCCATGATGATCGAGGTGAAGAAGGACGAGGCAGA TCGTGATCGAGATCCTGTTGACAATTAATCATCGGCA

Galk_mClav_re	GATTCGGTTCCCTCATAGCCATAGATGTGTAATGTGTC ATAGGGAATGCCTCAGCACTGTCCTGCTCCTT
Homo_mClav_fo	TGGCCATGATGATCGAGGTGAAGAAGGACGAGGCAGA TCGTGATCGAGATGCCGGCGTGAGCAAGGGCGAGGAG
Homo_mClav_re	GATTCGGTTCCCTCATAGCCATAGATGTGTAATGTGTC ATAGGGAATGCCGCCGGCCTTGTACAGCTCGTCCATGC C
Pcr_mClav_fo	GACCTGCACTTTATGCCATGG
Pcr_mClav_Re	GGTTAGACCCACTGGACGA
Pcr_mClav_Seq	TGGCCATGATGATCGAGGTG
cDNA_oligo_dT	TTTTTTTTTTTTTTTTT
cDNA_mCherry_Re	CTTGTACAGCTCGTCCATGC
cDNA_RFP_Re	ATGTCCCAGTTTACTCGGCA
cDNA_PCR_Fo_I	CAGGGAAAACGACTGTTGAA
cDNA_PCR_Fo_II	ATGGAGTAGACGGCTCTG
cDNA_PCR_Re	TTGATGTTGACGTTGTAGGC
cDNA_PCR_RFP_Fo	TGCGTATCAAGGTCGTCG
cDNA_PCR_RFP_Re	TTGTCAGCCTCCTTGATTCTC
cDNA_PCR_ORF_Fo	TATTTTTAACCAAACAGAGTACACGT
cDNA_PCR_ORF_Re	AACCTCCTTGCTTCAGC
GalK_invt._Fo	TGGCTCAGCTTTATGGAGTAGACGGCTCTGATTCGGAT AGCTCCTACTGACCTGTTGACAATTAATCATCGGCA
GalK_invt._Re	CGGATCTCTCCAAATTAAAGTGTGATCCATTTGTTTAC AAGACCGTCTACTCAGCACTGTCCTGCTCCTT
Invt._constr._Fo	TGGCTCAGCTTTATGGAGTAGACGGCTCTGATTCGGAT AGCTCCTACTGAGATCTTTTTCCCTCTGC
Invt._constr._Re	CGGATCTCTCCAAATTAAAGTGTGATCCATTTGTTTAC AAGACCGTCTACATAACTTCGTATAGCATACATTATA
PCR_Invt_Fo	TAACCTGGATTATGATTTTATACAT
PCR_Invt_Re	ACAGCAAATGTAATGTTGT
PCR_Invt_Seq	TGGCTCAGCTTTATGGAGTA
Backbone – ORF_Fo	GTGTGAACGCAGCATTATG
Backbone – ORF_Re	AAGGACAACAATATCCCCATT
LoxP-I & ORF-I_Fo	TTTTATATTTGACATATGTCTGT
LoxP-I & ORF-I_Re	AGCAGGTTAACACTCTT
LoxP-I & ORF-I_seq1	CATCATTGTTTTATGTTATT
LoxP-I & ORF-I_seq2	TGCTGTTCAAGCCAAAGACA
ORF-II&RFP-PolyA_Fo	AGGTTTCAGTACAGAGAATTC
ORF-II&RFP-PolyA_Re	CAGGCGGAATGGAC
ORF-II&RFP-PolyA_sq1	CTGATGGAGGAACGCCAGAG
ORF-II&RFP-PolyA_sq2	GCTTGGCTGGGAGGCCAACA
nlsmCherry_inv_Fo	GTAAAACCTCTACAAATGTGGTA
nlsmCherry_inv_Re	GTCTGTGGAAGAAATCACA
nlsmCherry_inv_Seq	TTATGATCAGTTATCTAGAT
cDNAsynth_Cherry	CTTGTACAGCTCGTCCATGC
cDNAsynth_RFP	ATGTCCCAGTTTACTCGGCA
cDNAsynth_Gen.	TTTTTTTTTTTTTTTTT
cDNA_PCR_ORF_fo	TATTTTTAACCAAACAGAGTACACGT
cDNA_PCR_ORF_re	AACCTCCTTGCTTCAGC

cDNA_PCR_RFP_fo	ATGCGTATCAAGGTCGTCG
cDNA_PCR_RFP_re	TTGTCAGCCTCCTTGATTCTC
cDNA_PCR_foI	CAGGGAAAACGACTGTTGAA
cDNA_PCR_fo2	ATGGAGTAGACGGCTCTG
cDNA_PCR_re	TTGATGTTGACGTTGTAGGC

2.1.7. Microscopes and binoculars

Instrument	Manufacturer	Information	Objectives
SP5 Matrix	Leica	Confocal microscope, PMT, HyD	10x air; NA=0.3 40x water; NA=1.1
SP8 Bsl2	Leica	Confocal microscope, PMT, HyD	10x air; NA=0.3 40x water; NA=1.1
Leica M205 FA	Leica	Fluorescence binocular	

2.2. Methods BAC recombineering

Paragraphs 2.2.1., 2.2.2., 2.2.3. and 2.2.4. are based on and optimised from (Warming et al., 2005), protocol 3.

2.2.1. Generation of insert probes

For each modification a set of two probes to be inserted into the BAC, needs to be designed and synthesised. First, two primers around the *galK* gene, flanked at the 5' ends by 50bp-long homology arms, were generated. These homology arms corresponded exactly to the 50bp regions at both sides of the desired position in the BAC to be modified. In that case, the primers looked as follows:

Forward: 5'----------50bp_homology-------CCTGTTGACAATTAATCATCGGCA-3'

Reverse: 5'----50bp_homology_compl._strand----TCAGCACTGTCCTGCTCCTT-3'

The first probe containing the *galK* gene was synthesised by PCR using the homology arm containing primers as described above, yielding a PCR product of 1331bp. The PCR reaction was set up as described below:

Component	Final Concentration
5x Q5 Reaction buffer	1x
dNTPs	200µM
Forward primer with homology arm	0.5µM
Reverse primer with homology arm	0.5µM
GalK plasmid	1 ng
Q5 Polymerase	0.02U/µl
H_2O	to 25µl

Thermal cycling reaction	Temperature	Duration	
Initial denaturation	98°C	30sec	
Denaturation	98°C	10sec	30 cycles
Annealing	60°C	30sec	
Extension	72°C	30sec	
Final extension	72°C	2min	

Secondly, two primers around the sequence desired to be inserted at the site of modification were synthesised. In order to substitute the initially inserted *galK* (cf. 2.2.3) in the BAC, this second pair of primers should contain the exact same homology arms as the *galK* PCR primers. The PCR procedure is similar as above, in which the annealing temperature should be adapted to the DNA template binding part of the primers (NEB TM calculator is a reliable tool to this). The duration of the annealing phase needs to be prolonged in case the DNA template exceeds 1000bp (count 30sec per 1000bp).

At the end of the PCR reaction, 1µl DpnI was directly added to the reaction mix and kept on 37°C for 30min. This step is key to remove any plasmid templates (methylated) from the PCR products (not methylated) in order to avoid false positives during transformation. Finally, a PCR column clean-up (NucleoSpin® Gel and PCR Clean-up) suffices to purify both PCR products.

2.2.2. Agar minimal plates preparation

In order to obtain 20 (deoxy-)galactose-containing agar plates, 7.5g agar in 400ml H_2O was autoclaved in a 1L flask. Subsequently, 100ml 5x M63 medium and 500µl 1M $MgSO_4 \cdot 7H_2O$ were added. After cooling down to 50°C, the following products were added:

Component	Quantity
Carbon source (either A. galactose or B. deoxy-galactose and glycerol)	5ml
Biotin	2.5ml
Leucine	2.25ml
Chloramphenicol	188µl (12.5 µg/ml)

For 20 MacConkey plates, 25g MacConkey agar (Sigma-Aldrich) in 400ml H_2O was autoclaved in a 1L flask. After cooling down to 50°C, the following products were added:

Component	Quantity
Galactose	5ml
Chloramphenicol	188µl (12.5 µg/ml)

The above agar compositions were then poured into petri dishes whereupon the remaining air bubbles were eliminated with a *crème brûlée* gas burner. These plates can be stored at 4°C up until one month. Per single modification in the BAC, at least six minimal plates containing galactose, six containing deoxy-galactose and three MacConkey plates are needed.

2.2.3. BAC recombineering procedure

BAC recombineering is a technique that allows site-specific modifications (sequence insertions, point mutations, removal of sequences) of the sequence within a BAC based on homologous recombination. BAC recombineering is performed using a special bacterial strain, called SW102 E. coli, which expresses λ-prophage genes under control of a temperature-sensitive repressor that encode for homology recombination-facilitating proteins (cf. section 1.4). In addition, its galactose operon lacks the *galK* gene, which allows selecting recombinants on the introduction of *galK* in a first step on growing plates containing only galactose as a carbon source. Moreover, it allows selection against the presence of *galK* in a second recombineering step based on survival on minimal growing plates containing deoxy-galactose. My protocol works best as follows:

a. Introduction of the BAC into SW102

1) When using a BAC for the first time, it first needs to be transformed into SW102 E. coli. After purification of the BAC using NucleoBond® BAC 100 (Macherey-Nagel), 30ng BAC was transformed into electro-competent SW102 E. coli., recovered for 1 h at 32°C in standard LB and plated on LB agar plates with 12.5µg/ml chloramphenicol at 32°C.

b. Preparation of a BAC containing SW102 culture

2) BACs that are hosted by SW102 E. coli were inoculated into 5ml standard LB with chloramphenicol at 32°C overnight, the evening prior to recombineering.

3) Next morning, 500µl of the overnight culture was diluted into 25ml standard LB with chloramphenicol in a 200ml Erlenmeyer flask and placed in a shaking incubator at 32°C. The culture was grown until an OD_{600} of approximately 0.6, which usually took 3 h.

c. *Heat shock of SW102*

4) From the moment the bacteria have reached their exponential growth phase (OD 0.6), the water bath was set at 42°C. Meanwhile 12ml of the culture was transferred to a new 200ml Erlenmeyer flask, which was then placed into 42°C-heated water for exactly 15min. The remaining culture was kept at 32°C as an "un-induced" control.

5) Meanwhile, the centrifuge was switched on to reach a temperature of at most 4°C and a bucket was filled with ice floating in water, forming an ice-water slurry. A 50ml tube filled with ddH_2O was placed into the ice-cold water.

d. Preparation of salt-free SW102 culture

6) After 15 minutes, both the induced and un-induced samples were briefly cooled in the ice-water slurry and transferred into 10ml tubes with convex bottom. Subsequently, the two cultures were pelleted in the pre-cooled centrifuge at 0°C, for 5min using 4200rpm.

7) During the next step, the supernatant was discarded and the pellet was re-suspended in 1ml ice-cold ddH_2O, by gently swirling the tubes in the ice-water slurry. The culture should not be pipetted, since shear stress would damage the BAC DNA. One should preferably use tubes with convex bottom; otherwise re-suspending the cells will take ages. Finally, another 9ml ice-cold ddH_2O was added to each tube and pelleted again as in step 6.

8) Step 7 was repeated two times, but after the second washing step, the re-suspended culture was transferred to a 15ml tube with pointed bottom. This allowed an easier harvest of the cells in the next step.

9) After pelleting the now washed and salt-free cultures, the complete supernatant was removed by inverting the tubes on a paper towel. The pellet was then suspended in 50µl ddH_2O by pipetting very gently and was kept on ice until electroporation.

e. Electro-transformation of galK

10) 25µl Of each culture ware then transferred into three 1.5ml tubes: induced, un-induced and no insert control. To the induced and un-induced cells, 50-100ng homology arms containing galK PCR product (cf. section 2.2.1.) was added. The content of each tube was transferred to a 0.1cm cuvette (BioRad) and transformed by an electric pulse: 25µF, 1.75kV and 200Ω. In case the cultures explodes during electroporation, I advise to add an extra washing step next time and/or suspend the pelleted samples in 100µl.

11) Directly after electroporation, the cells were recovered into 1ml standard LB without antibiotics for 1h at 32°C in a shaking heat block (750rpm). This step allowed the cells to recover and express their antibiotic resistance genes.

f. Preparation of a transformed SW102 cells for selection

12) After the recovery period, the three samples were pelleted in a table top centrifuge (11,000rpm, 30sec) and their supernatant was removed. Subsequently, the cells were re-suspended in 1ml M9 medium, in order to remove all nutrition present in LB, but thereby supplying essential salts. Again, pipetting was done in a cautious way.

13) Washing in M9 medium as in step 12 was repeated once more. After the second washing round, the pellet was re-suspended in 1ml M9 medium. These now LB-free samples were serially diluted 1:10 and 1:100 (100µl into 1ml M9 medium, from which one dilutes 100µl in 1ml M9 medium).

g. Plating and selection of cells

14) 100µl Of the 1:10 and 1:100 dilutions of the induced, un-induced and no product control samples were then plated on minimal plates that only contain galactose as unique carbon source (cf. 2.2.2.). The plates were subsequently incubated at 32°C for 3 days.

15) When they started to become visible, a few single colonies from the induced transformed samples were picked (check controls which dilution series worked best)

and streaked on MacConkey plates with galactose and chloramphenicol. GalK will ferment lactose, thereby lowering the pH, which converts the neutral red dye present in MacConkey into pink colour. This step allowed finding pure colonies, deriving from one single cell containing the *galK* gene. An overnight incubation at 32°C sufficed.

h. Preparation of a galK containing SW102 culture for electroporation

16) The next day, a single bright pink colony was incubated overnight in 5ml LB with chloramphenicol at 32°C.

17) Steps 3 to 10 were repeated in order to obtain electro-competent SW102 cells. However, instead of transforming a Galk PCR product, the PCR product containing identical homology arms and the desired insert/modification was now used.

18) After the transformation, the cells were recovered in 200ml Erlenmeyer flasks containing 10ml standard LB without antibiotics at 32°C in a shaking incubator (150rpm). To get best chances to obtain pure BAC (by this dilution) that have lost their *galK* present during the recombination, the samples were recovered for at least 4 h.

i. Selection against galK

19) The transformed cells were then washed twice in M9 medium and plated on deoxy-galactose containing minimal plates identical to steps 12 to 14.

20) Three days later, when the colonies became visible, a dozen of single colonies were picked and incubated overnight in 5ml LB with cloramphenicol. Next day, minipreps (cf. 2.2.4.) were made and tested by PCR (cf. 2.2.8.) whether the desired modification had taken place.

2.2.4. BAC minipreps

For BAC minipreps (1-1.5mg), 5ml overnight LB culture with chloramphenicol was pelleted for 5min at 4,200rpm, the supernatant removed, and the pellet dissolved in 250ml buffer P1 (miniprep kit, Qiagen) and transferred to an Eppendorf tube. 250ml P2 buffer was added, followed by mixing by inversion and incubation for <5min at room temperature. Then 250ml of N3 buffer was added, followed by mixing and incubation on ice for 5min. The supernatant was cleared by two rounds of centrifugation at 13,200rpm for 5min in a table top centrifuge. Each time the supernatant was transferred to a new tube. DNA was precipitated by adding 750ml isopropanol, followed by mixing and incubating on ice for 10min, and centrifugation for 10min at 13,200rpm. The pellet was then air-dried for 10min and dissolved 50ml ddH_2O.

Making minipreps of recombineered BACs allowed to quickly purify BACs good enough to screen for correct recombinants by PCR. Sequencing of the PCR products was performed at Microsynth using barcode labelled tubes. Reactions mixtures were assembled as indicated on the company's website (www.microsynth.ch). Based on its outcome, one colony can be chosen and inoculated for purification by the much more laborious, nevertheless highly accurate midiprep procedure of NucleoBond® BAC 100 (Macherey-Nagel).

Only purified BACs by midiprep can be used for restriction enzyme analyses (cf. 2.2.5.) and injections into zebrafish zygotes (cf. 2.2.7.). Freshly purified BACs can be stored at 4°C for maximal 1 month. In order to store the BAC over long time, one should re-suspend a 5ml overnight culture in 20% glycerol solution, which can be maintained for years at -80°C.

2.2.5. Restriction enzyme digestion

For BAC analysis by restriction digest, 3µg of BAC midiprep was added to a restriction digest reaction containing 15µl Cutsmart buffer (NEB), 3µl restriction enzyme, filled up to 150µl ddH_2O. After a 1-hour incubation at 37°C, 500µl ethanol was added to the reaction mix and centrifuged for 20min at 4°C using 20.000rpm. Subsequently, the supernatant was removed, the pellet air-dried for 10min and resolved in 20µl ddH_2O. The cut products were separated in ethidium bromide containing gels by electrophoresis and visualised under UV light.

2.2.6. Tol2 transposase *in vitro* mRNA transcription[1]

Generally, mRNA was transcribed with Ambion kits. 1µg of NotI-linearised pCS2FA-transposase plasmid was used to transcribe mRNA with mMESSAGE mMACHINE® SP6 Transcription Kit (Ambion) according to the manufacture's protocol. The LiCl precipitated RNA was resuspended to 200ng/µl, aliquoted and stored at -80°C until usage.

2.2.7. BAC injections[1]

The injection mix consisted of:

Component	Quantity
Fresh BAC purified using NucleoBond® BAC 100	25ng/µl
Tol2 protein	20ng/µl
Phenol Red 10x	1:10
ddH_2O	fill up to 10µl

Borosilicate glass needles for injections were produced from capillaries (outer diameter 1.0mm, inner diameter 0.5mm, 10cm length; Sutter Instruments) with a needle puller (Sutter Instruments). Freshly laid eggs were mounted into the grooves of moulded agarose (1% in 1x E3) in petri dishes and covered with egg water. Glass needles were loaded with injection mixture using Micro loader tips (Eppendorf), broken at the tip with forceps and finally the

needle was connected to a pneumatic Pico Pump (SYS-PV820) from WPI. The constant pressure was set to minimum and the injection pressure was adjusted (visually, whilst injecting) to a volume of approximately 5nl. The single cell (one-cell stage) of the freshly laid eggs was then injected.

2.2.8. DNA extraction and PCR analysis

In order to check whether the BAC has completely integrated in the genome, injected embryos with red eye marker were put in 50µl embryo lysis buffer, to which 0.5µg/ml proteinase K was added. After an overnight incubation at 55°C, proteinase K was inactivated by cooking at 95°C for 10min. The samples were cooled down, briefly vortexed, whereupon 2µl was used as DNA template. PCR was executed using primers listed in section 2.1.5. as follows:

Component	Final Concentration
5x Q5 Reaction buffer	1x
dNTPs	200µM
Forward primer	0.5µM
Reverse primer	0.5µM
2µl DNA template from DNA extraction mix	-
Q5 Polymerase	0.02U/µl
ddH_2O	to 25µl

Thermal cycling reaction	Temperature	Duration	
Initial denaturation	98°C	30sec	
Denaturation	98°C	10sec	30 cycles
Annealing	depending on primers	30sec	
Extension	72°C	30sec	
Final extension	72°C	2min	

2.2.9. Imaging procedure[1]

BAC injected embryos were selected under the fluorescent binocular for presence of the red eye marker. Before mounting, embryos were anesthetised in 1x E3 containing 1x tricaine. 0.7% Low Melting Agarose (LMA) (Sigma) was dissolved in 1x E3. Before usage, the LMA was melted in the microwave and supplemented with 1x tricaine. The LMA mixture was kept at 50°C during mounting. A glass bottom dish (MatTek) was coved with LMA and allowed to cool down a bit. Life embryos were dropped with a fish pipette into the agarose drop and orientated with an eyelash-containing handle. The samples were then imaged at the SP5 Matrix confocal microscope, with either 20x or 40x magnification.

2.2.10. Preparation and transformation of electro-competent E. coli cells[1]

A fresh Top10 E.coli colony was picked to inoculate LB without salt and grown overnight at 37°C with 200rpm. The following morning, the culture was diluted 1:100 in LB without salt (without antibiotics), grown to OD600 = 0.6-0.8 and cooled down in an ice slurry. Bacteria were pelleted in a precooled centrifuge, washed once in 10% glycerol (sterile and ice cold) and re-suspended in 10% glycerol in a 100th of the initial volume. Bacterial suspension was aliquoted and used immediately or frozen in liquid nitrogen for storage at -80°C.

For transformation electro-competent cells were thawed on ice mixed with construct (20-100ng) or plasmid (<500pg) into a Gene Pulser/Micro Pulser 1mm Cuvette(Bio-Rad) and electroporated at 1.8kV with a Micro Pulser (Bio-Rad).Subsequently the cells were re-suspended in LB (without antibiotics) and incubated for 1h at 37°C. Dilutions of cells were plated on standard agar plates with appropriate antibiotics.

2.2.11. Gibson cloning procedure

The Gibson cloning method used here is based on Gibson et al., 2009:

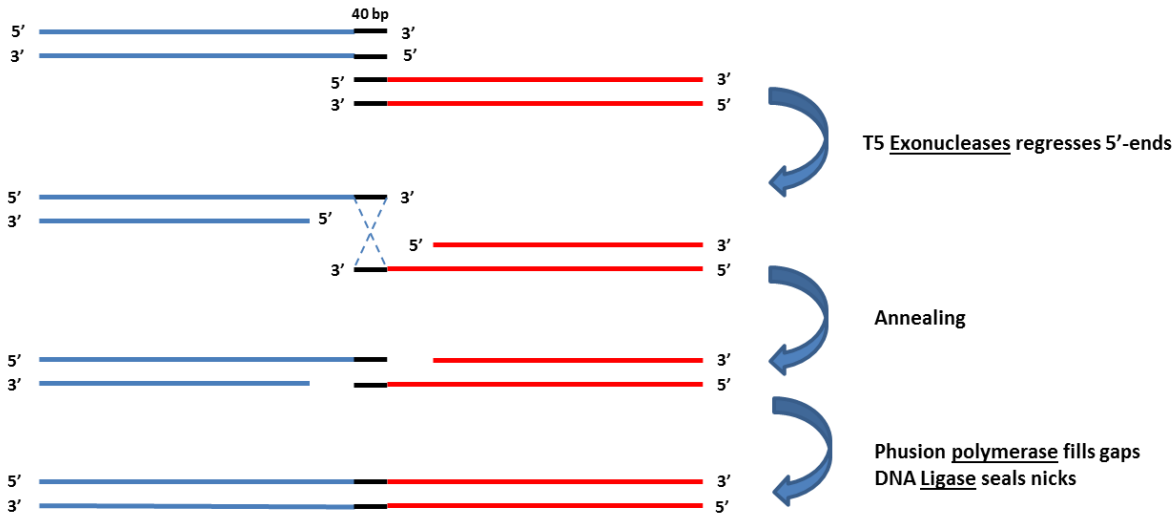

Gibson cloning allows multiple DNA fragments with overlapping homology arms to be assembled into a circular plasmid in a single-tube reaction. Pieces of DNA, either linearized plasmids or PCR products, were designed with 40bp overlaps.

First, equimolar amounts of gel-purified DNA were added together, 10-100ng per piece with a total volume of 5µl. If DNA is amplified from a plasmid, a DpnI digest on the PCR reaction should be performed. Then a 15µl aliquot of 1.33x Gibson Master Mix was thawed on ice, whereupon 5µl DNA was added to the tube and incubated at 50°C for 1h. Then, 3µl of the reaction was transformed into electric-competent Top10 E.coli cells. After transformation, the cells are recovered in LB for 1h and streaked on agar plates with appropriate antibiotic. Next, day the growing colonies can be inoculated for plasmid purification via a miniprep (NucleoSpin® Plasmid). Purified plasmids were screened by PCR and sequencing.

2.2.12. cDNA synthesis from BAC-injected embryos

In order to purify enough mRNA from BAC-injected embryos, twenty embryos were pooled in two tubes for 1. expressing red eyes and 2. not expressing red eyes. RNA was subsequently purified following the protocol of Qiagen®'s RNeasy Minikit. cDNA was synthesised using Invitrogen™ SuperScript III Reverse Transcriptase and analysed by PCR.

2.3. Materials to characterisation of RadilB and Rasip1

2.3.1. Buffers, media and solutions as far as not mentioned in 2.1.1.

Name	Composition
Alkaline Tris buffer	100mM Tris-HCl pH9.5 50mM MgCl2 100mM NaCl 0.1% Tween-20
BCIP solution (*in situ*)	50mg 5-bromo-4-chloro-3-indolyl phosphate (BCIP, Sigma) in N,N-dimethylformamide (anhydrous) stored at -20°C in the dark
Blocking solution	5% normal goat serum 1% BSA 0.1% Triton X-100 0.01% sodium azide in PBST
Blocking solution (*in situ*)	2% sheep serum 2mg/ml BSA 0.01% sodium azide 1x PBST
E3 (50x)	250mM NaCl 8.5mM KCl 16.5mM $CaCl_2$ 16.5mM $MgSO_4$ adjusted pH7.0-7.4 (with Na_2CO_3)
Hybridisation Mix (*in situ*)	5x SSC 50% deionized Formamide 50µg/ml Heparin 500µg/ml torula RNA (Sigma) adjust to pH6 (460µl 1M citric acid per 50ml solution) stored at -20°C
Labeling solution (*in situ*)	225µl NBT solution 50ml Alkaline Tris Buffer 175µl BCIP solution
Methylene blue solution	1% Methylene Blue (Sigma) ddH2O
NBT solution (*in situ*)	50mg Nitro Blue Tetrazolium (NBT, Sigma) 70% N,N-dimethylformamide ddH2O stored at -20°C in the dark
PBS (10x)	1.37M NaCl 27mM KCl 100mM Na2HPO4 18mM KH2PO4 ddH2O autoclaved
PBST	1x PBS 0.1% Tween-20

PFA (4%)	heat 500ml 1xPBS pH7.2 to 60°C (under the hood) add 40g Paraformaldehyde add 2N NaOH drop by drop until PFA dissolved cool down, adjust volume to 1l with 1x PBS filtrate stored at -20°C
PTU (50x; 2mM)	0.15% (w/v) 1-Phenyl-2-thiourea (PTU) (Sigma-Aldrich) in egg water
Stop solution (*in situ*)	1x PBS pH5.5 1mM EDTA 0.1% Tween-20
Tricaine (25x)	0.4% (w/v) Tricaine (Sigma) ddH2O adjust pH7.0 with 1M Tris HCl stored at -20°C

2.3.2. Fish lines

Name	Allele designation	Reference
ABC/TU	Wild type (WT)	ZIRC/(Haffter et al., 1996)
kdrl:EGFP	s843	(Jin et al., 2005)
kdrl:EGFPnls	UBS1	(Blum et al., 2008)
Gata1:dsRed	sd2	(Yaqoob et al., 2009)
Tension-sensor	Tg(ve-cad:ve-cadTS)	(Lagendijk et al., 2017)
RadilB mutant	sa20161	This study
Rasip1 mutant	UBS28	This study, generated by Charles Betz, maintained by Minkyoung Lee

2.3.3. Oligonucleotides

Primer name	Sequence
RadilB_mut_Fo1b	CCACAACAACCGGCTAACCAC
RadilB_mut_Re1b	ACAATGAGCCTGGGTTGCAAATAA
RadilB_mut_Re2c	TGGCCAGCACACTCTTTT
RadilB_mut_Fo2b	GCCAGGGGACCAACTATA

2.3.4. Antibodies

Primary antibody	Host	Dilution	Reference
Rasip1	Rabbit	1:500	(Wilson et al., 2013)
Cdh5	Guinea Pig	1:500	(Blum et al., 2008)
RadilB	Rabbit	1:100-500	This study

Secondary antibody	Host	Dilution	Source
Anti-Rabbit Alexa 633	Goat	1:500	Abcam
Anti-guinea pig Alexa 568	Goat	1:500	Abcam

2.4. Methods to characterisation of RadilB and Rasip1

2.4.1. Fish maintenance

Zebrafish were raised and maintained at standard conditions as described in "The Zebrafish Book" (Westerfield, 2000). Embryos were staged at 28.5°C (Kimmel et al., 1995).

2.4.2. Genotyping of RadilB mutant

Adult zebrafish were anesthetised in 1x E3 containing 1x tricaine. Paralysed fish were placed on a sterile surface and the caudal fin was spread. A razor blade was pressed vertically onto the distal part of the caudal fin and a pipette tip was used to slide along the razor blade, cutting off the fin. The DNA of the tissue sample was extracted by alkaline lysis (200µl of 50mM NaOH, 20min at 95°C. Then chilled on ice and addition of 20µl 1M Tris-HCl. Finally centrifuged at 11.000rpm for 5min. Fin clipped fish were kept individually in single cages containing egg water until genotypes were determined by PCR using the four primers of paragraph 2.3.3.:

Component	Final Concentration
10x Titanium Taq PCR buffer	1x
dNTPs	10mM
RadilB_mut_Fo1b	10µM
RadilB_mut_Re1b	10µM
RadilB_mut_Re2c	10µM
RadilB_mut_Fo2b	10µM
1µl DNA template from DNA extraction mix	-
Q5 Polymerase	20ng/µl
ddH_2O	to 25µl

Thermal cycling reaction	Temperature	Duration	
Initial denaturation	95°C	1min	
Denaturation	95°C	30sec	28 cycles
Annealing	61°C	30sec	
Final extension	68°C	3min	

Depending on the genotype, this PCR procedure can produce three different bands: 570bp (outer/control band), 400bp (wt band) and 200bp (mut band).

2.4.3. Immunohistochemistry

Embryos were transferred in 1,5ml Eppendorf tubes and fixed in 2% PFA in PBST overnight at 4°C. Next day, the samples were washed 4 times, roughly 30min each, in 1ml PBST at room temperature. Then blocking solution was added for around 4h at room temperature. At the end

of the day, the embryos were incubated in 500µl primary antibodies in blocking solution, overnight at 4°C. On the second day, the embryos were washed six times, 1h each, in 1ml PBST at room temperature. At the end of the day, the embryos were incubated in 500µl secondary antibodies in blocking solution, overnight at 4°C, kept in the dark by aluminium foil. On the third day, the embryos were washed five times, 1h each, in 1ml PBST at room temperature. The last washing step took place overnight at 4°C before imaging. Imaging was performed as described in 2.4.5.

2.4.4. *In situ* hybridisation[1]

In situ hybridisation is a technique to visualise the presence of specific mRNA by hybridising a target mRNA with a labelled antisense probe. This allows identifying the expression localisation of specific genes within fixed tissues and cells.

In this study, exon 5 of RadilA, RadilB and RadilC respectively were amplified by PCR, followed by A-tailing with Taq polymerase. Subsequently these probes were cloned into p-Gem t-easy vectors. The *in situ* hybridisation protocol was adapted from (Thisse and Thisse, 2014). DIG-labelled RNA was transcribed from linearized Radil exon 5 containing p-Gem t-easy vectors with SP6 RNA polymerase and ingredients for 2h at 37°C:

Reaction mix DIG-labeled RNA synthesis
1µg linearized plasmid
1x DIG RNA labeling mix (Roche)
1x Transcription buffer (Roche)
40U RNA polymerase (Roche)
20U RNase inhibitor (Roche)
Up to 20µl Nuclease Free H2O (Ambion)

Template DNA was then degraded by incubation with 2U TURBO DNase I (Ambion) for 15min at 37°C, and the RNA was precipitated using LiCl (protocol and reagents of Ambion mMessage mMachine transcription kits). Pre- and post-precipitation RNA were checked on Ethidium Bromide gel. RNA was frozen at -80°C until use.

Eggs were then collected right after they were laid and raised to the desired developmental stage (e.g. 30hpf), while the formation of pigments was prevented by adding PTU to the egg water. The chorions were manually removed before fixation in 4% PFA (o/n) at 4°C. The embryos were dehydrated by incubation in 100% methanol for 15min. at RT, during this process the methanol was exchanged once. Thereafter, the embryos (in methanol) were incubated at -20°C for more than 2h. The embryos were successively rehydrated in methanol dilutions (75% / 50% / 25% (v/v) Methanol and PBST, each step for 5min) and finally washed 4 times for 5min in PBST. Then, the embryos were permeabilised with Proteinase K (Roche) (10µg/ml in PBST) at RT. Depending on their developmental stage, the incubation with Proteinase K was prolonged (e.g. embryos at 28hpf for 15min, or 36hpf for 20min). Proteinase K was inhibited

by fixation of the embryos in 4% PFA for 20min at RT and subsequently washed 4 times for 5min in PBST.

The embryos (less than 100) were prehybridised in 700µl hybridisation mix for 5h. at 67°C. Then the hybridisation mix was replaced with 200µl fresh one, containing 50ng DIG-labeled RNA probe and 5% Dextran Sulfate (Merck Millipore) and the incubation was continued overnight at 67°C. The next day, the buffer was successively exchanged to 0.2x SSC. Therefore, the embryos were incubated in each of the following pre-warmed (67°C) mixes for 10 min: 100% Hybridisation mix (w/o RNA and heparin), 75% / 50% / 25% (v/v). Hybridisation mix in 2x SSC, and 2x SSC. Finally the embryos were washed twice 30min in pre-warmed 0.2x SSC at 67°C. Thereafter, the SSC was progressively replaced with PBST by incubating the embryos at RT in 75% / 50% / 25% (v/v) 0.2x SSC in PBST and finally 100% PBST 10min for each step.

After the buffer exchange to PBST, the embryos were blocked for 3-4h at RT in Blocking solution (*in situ*) and the AP-anti-DIG antibody (Roche) was applied onto the samples, diluted 1:5000 in Blocking solution (*in situ*). After overnight incubation at 4°C, the antibody was washed away by 6 times 15min PBST incubations. To prevent the formation of precipitates the samples were washed once in alkaline Tris buffer devoid of $MgCl_2$ and subsequently incubated twice for 5min in normal alkaline Tris buffer. To start the colorimetric reaction, the embryos were incubated at 37°C in freshly made labelling solution and monitored. The incubation time is around 4-5h. at 37°C. Finally, the labelling reaction was stopped by washing twice in stop solution (*in situ*). The embryos were kept in stop solution at 4°C in the dark until usage or placed in 100% Glycerol (Sigma-Aldrich) overnight at room temperature to be imaged the next day.

2.4.5. Imaging procedure[1]

Before mounting, embryos were anesthetised (not for fixed samples) in 1x E3 containing 1x tricaine and selected on a fluorescent binocular. 0.7% Low Melting Agarose (LMA) (Sigma) was dissolved in 1x E3. Before usage, the LMA was melted in the microwave and supplemented with 1x tricaine (not necessary for fixed samples). The LMA mixture was kept at 50°C during mounting. A glass bottom dish (MatTek) was coved with LMA and allowed to cool down a bit. Life embryos or tail of fixed specimen were dropped with a fish pipette into the agarose drop and orientated with an eyelash-containing handle.

The samples were then imaged at the SP5 Matrix confocal microscope, with either 20x or 40x magnification. Generally, laser intensities and detector intensities or exposure times were set to obtain single saturated pixels. For recording 3D images (stacks of focal planes) the step size in z-directions was set from 0.1µm to 1µm for objectives with magnification higher than 20x, for objectives with magnification with 10x or 20x the section thickness was set to 1µm to 4µm. For short and overnight time lapse recordings the incubation chamber of the confocal microscope was set to 28.5°C. When recording single images of live or fixed sample, the imaging was done at RT.

Chapter III

Results

3.1. Generation of an inducible Cdh5 line

The desire to examine the function of Cdh5 at different developmental stages of angiogenesis in zebrafish and to analyse EC behaviour in mosaic angiogenic sprouts with different Cdh5 levels, let to the idea to generate an inducible Cdh5 knock-out line. An inducible system, based on Cre/loxP recombination, was designed to be introduced into the zebrafish genome in the form of a bacterial artificial chromosome (BAC).

3.1.1. Design of a VE-cadherin inducible knock-out construct based on Cre-recombinase Lox technology

The initial design of a construct able to knock-out Cdh5 in an inducible manner, consisted of the Cdh5 open reading frame (ORF) flanked by *loxP* sites. The ORF includes all protein-coding exons of the endogenous *cdh5* gene and its start codon ATG is present at the beginning of exon 2. Since Cdh5 exon 1 is noncoding, it had not been included in the ORF. To stop transcription of the ORF, the SV40 polyA was placed directly after the last exon, exon 13. To visualise Cdh5 presence, a sequence encoding for the red fluorescent protein mCherry was inserted within exon 13. More precisely, between the p120-catenin and β-catenin binding sites of the translated cadherin protein. This position had been demonstrated before allowing marker fusion proteins to be expressed and translated without harming Cdh5 functionality and its design was able to rescue Cdh5 mutant phenotypes (Lagendijk et al., 2017). The ORF together with the mCherry sequence was flanked by two *loxP* sites. In the second part of the construct, the *loxP*-flanked *mCherry*-tagged *cdh5* ORF was followed by an *mCherry* sequence preceded by a nuclear localisation signal (nls) and a second SV40 polyA (Figure 1A).

In absence of Cre-recombinase, this construct expresses *cdh5* fused to mCherry. In case of Cre-recombinase activity, the *loxP* sites are recombined, resulting in the loss of the complete construct located in between. That way Cre-loxP recombination induces Cdh5 knock-out from the construct, followed by expression of *nls-mCherry* under control of the Cdh5 promoter (Figure 1A and B). Nls-mCherry serves here as in indicator to visualise those endothelial cells (ECs) in which Cre-loxP recombination has occurred.

Element	Replacement
Tol2 & marker	LoxP-I
AttB	LoxP-II
-	Exon3

Table1. Backbone modification of the Cdh5 containing BAC

To express this construct in the zebrafish in a most natural way possible, BAC recombineering technology was used. This technology allows to exchange the inducible construct for exon 2 in a BAC containing the complete zebrafish *cdh5* gene. That way, this Bac:lox-Cdh5-lox-nls-I construct was expressed under control of the endogenous Cdh5 promoter (Figure 1C). However,

in order to make the Cdh5 BAC suitable for injections and further experiments, the BAC backbone had to be modified as well (Table1). To get rid of the additional *loxP* sites present in the backbone, a construct containing inverted *tol2* sites and *β-crystalline:mKate2* eye lens marker was recombineered at the former first *loxP* location. The second *loxP* site was replaced by an *AttB* site. *Tol2* sequences serve as recognition sites for transposon-mediated integration of the BAC in the zebrafish genome. The eye marker allows efficient screening to zebrafish embryos expressing the BAC construct based on *mKate2* expression in their lens. The *AttB* sites serve for phiC31 integrase-mediated attP/attB recombination for site-directed transgenesis into single genomic *attP* landing sites (Mosimann et al., 2013). Since our Cdh5 mutant fish line (UBS8) has a null-mutation in its Cdh5 exon 3, BAC Cdh5 exon 3 was removed in order to simplify PCR screenings in which UBS8 Cdh5 mutant fish should be distinguished from BAC Cdh5 inducible mutants (Figure 1C). Backbone modifications procedures and results by BAC recombineering are depicted in Appendix-I.

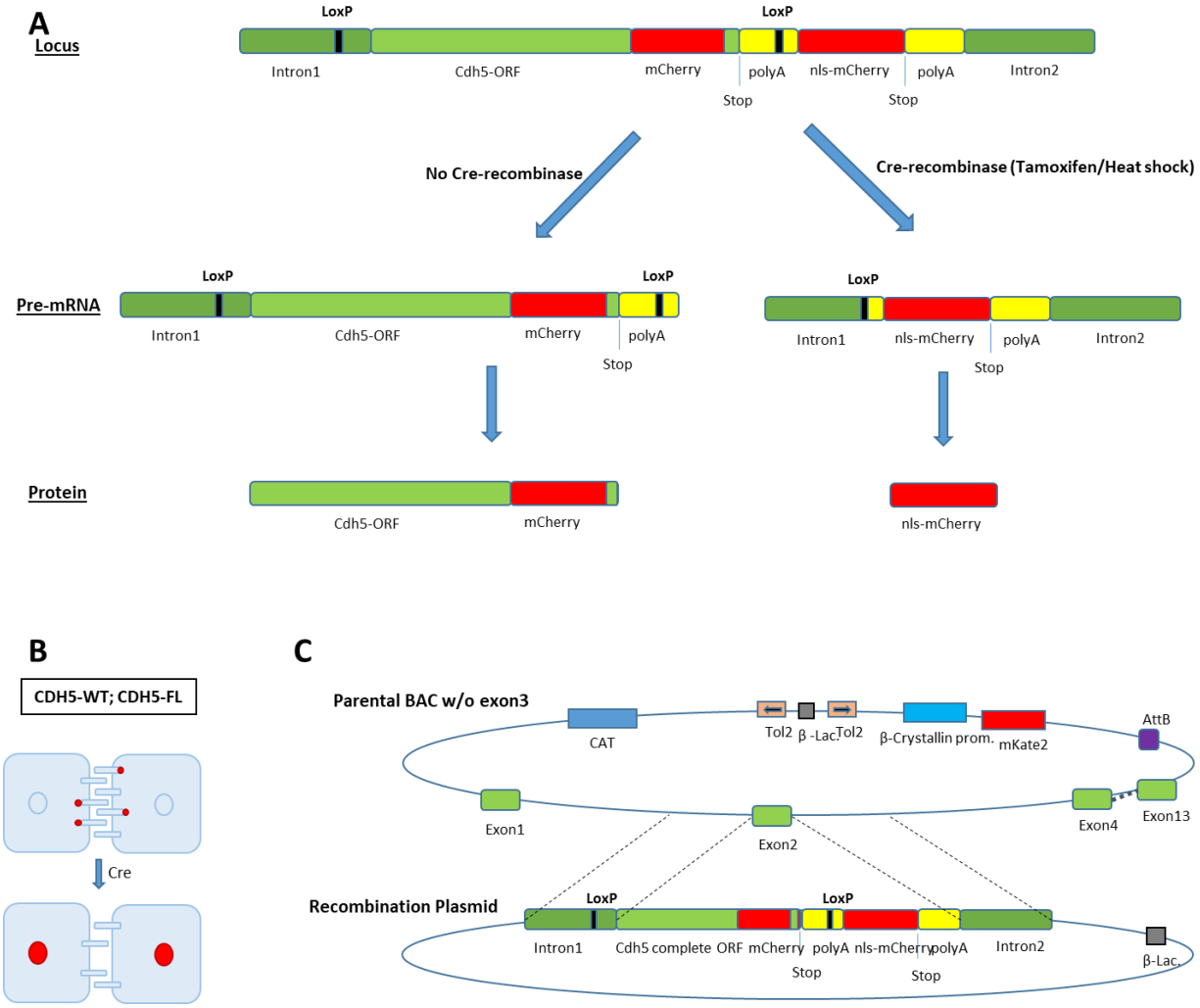

Figure 1. Design of the inducible Cdh5 recombination construct and its working mechanism. (**A**) Designed construct to be inserted into the zebrafish genome, which in absence of Cre-recombinase expresses *cdh5* tagged to *mCherry*. Cre-recombinase activity would result in deletion of the *mCherry*-tagged *cdh5* ORF and thereby activation of *nls-mCherry* expression under Cdh5 promoter control. (**B**) Endothelial cells expressing endogenous Cdh5 and the Cdh5 inducible construct. Cre-

recombinase activity stops expression of *mCherry*-tagged *cdh5* and induces EC nuclei to express *mCherry*. The latter serves as marker for LoxP recombination. (**C**) Design of the Cdh5 containing BAC with modified backbone. The backbone includes inverted *tol2* sites (integration into genome), an *mKate2* under control of *β-crystalline* promoter (eye lens marker) and an *AttB* site (site directed integration into genome). In addition, BAC Cdh5 exon 3 was removed. The recombination plasmid containing the inducible Cdh5 construct of (A) was exchanged for the BAC Cdh5 exon 2.

3.1.2. Replacement of homologous sequences and exchange of the bacterial host prevents unwanted autonomous recombination inside the construct

Prior to microinjection, the engineered Bac:lox-Cdh5-lox-nls-I was tested for correct integration of the construct. To this purpose, PCR primers were designed covering the whole inducible construct within the BAC (Figure 2A). The results from the PCR reactions proved that the region around the first *loxP* site as well as the complete ORF were present. However, reactions towards the 3' end of the construct did not result in expected product synthesis. Reaction C and E did not allow synthesis of PCR products, whereas reaction D yielded a product of 300bp instead of the expected 1400bp. Sequencing of the product D indicated that both polyA sequences within the PCR product were present, however the *loxP* and *nls-mCherry* sequences in between were missing (Figure 2A).

This result suggested that the synthesised recombination plasmid designed in Figure 1 was incomplete. When performing PCR B and D on the recombination plasmid itself (the plasmid used for the exchange of BAC exon 2), both expected products were yielded. Reaction D, however, produced the expected band of 1400bp as well the smaller 300bp product (Figure 2B). In addition, the unmodified recombination plasmid, as synthesised and obtained by ATG:biosynthetics GmbH, was sequenced, and the results were correct (data not shown). This implies that within my host Top10 E. coli population, a mixture of correct and incomplete plasmids co-existed.

Since sequencing of the small product of D showed a loss of the region starting exactly from the second *loxP* site until the last nucleotide of *nls-mCherry*, autonomous recombination between these two identical SV40 polyA sequencing had most likely occurred. Therefore, the first polyA sequence was exchanged for the endogenous Cdh5 3'UTR by Gibson cloning (cf. 2.2.11.). To this purpose, primers were designed in inverted direction around the first *mCherry*, yielding a PCR product of 8675bp. In addition, another PCR product was synthesised consisting of the Cdh5 3'UTR flanked with 40bp-long homology arms. Both PCR products were subsequently ligated to each other (Figure 2C). Since also the two *mCherry* sequences are identical, the first *mCherry* was exchanged for *tagRFP* in a similar way, in order to prevent unnecessary sequence repeats within the construct.

Despite of the removal of mCherry and SV40 homology, the newly designed construct still showed autonomous recombination. Sequencing of PCR products demonstrated the loss of the region between the two *loxP* sites (Figure 2D). Also, enzymatic digestion reaction using ScaI showed a mixture of correct and incorrect bands within one clonal Top10 E. coli stock (Figure

2F). Since exchanging one of the *loxP* sites was no option with regard to an inducible gene knock-out system, the newly designed constructed was purified and retransformed into a different host line, called SURE (Stop Unwanted Recombination Events) E. coli (Figure 2E). This host lacks components of the pathways that catalyse the rearrangement and deletion of nonstandard secondary and tertiary structures, but therefore grows much slower. Screening colonies of a re-streak from a recombination plasmid transformed SURE E. coli yielded colonies that had incorporated either the correct or the incorrect plasmid, without being mixed (Figure 2F). The correct plasmid was now purified from a SURE host and introduced into the BAC as in Figure 1C, giving rise to Bac:lox-Cdh5-lox-nls-II.

3.1.3. Introduction of Bac:lox-Cdh5-lox-nls-II into the zebrafish genome leads to *mCherry* expressing EC nuclei

In order to test whether the newly designed recombination plasmid hosted by SURE E. coli was correctly introduced into the Cdh5 BAC, XbaI digestion on purified Bac:lox-Cdh5-lox-nls-II was performed, together with the BACs at former designal stages. All expected digest products can be found in the electrophorese result (Figure 3A). Finally, the BAC was retransformed in DH10B E. coli, the usual host cells for long term BAC storage. DH10B cells do not have the heat-shock inducible genes coding for homology recombination facilitating proteins. This might reduce unwanted recombination events of the final engineered BAC, caused by potential background activities of those proteins.

Three days upon injection of the BAC into zebrafish zygotes, 80% of the survived embryos showed red eyes under the binocular. However, further screening under the confocal microscope revealed that in none of these fish Cdh5 was visible. Moreover, in 74% of the embryos with red eyes, the nuclei of endothelial cell expressed *mCherry* (Figure 3B), meaning that somehow the construct did not allow Cdh5-tagRFP synthesis and/or could not prevent *nls-mCherry* expression in absence of Cre-recombinase. To ascertain that in the genome integrated and expressed inducible construct was still intact, genomic DNA from embryos with red eyes was extracted and checked by PCR. In all examples, the Cdh5 ORF tagged with tagRFP and followed by nls-mCherry were present (Figure 3C).

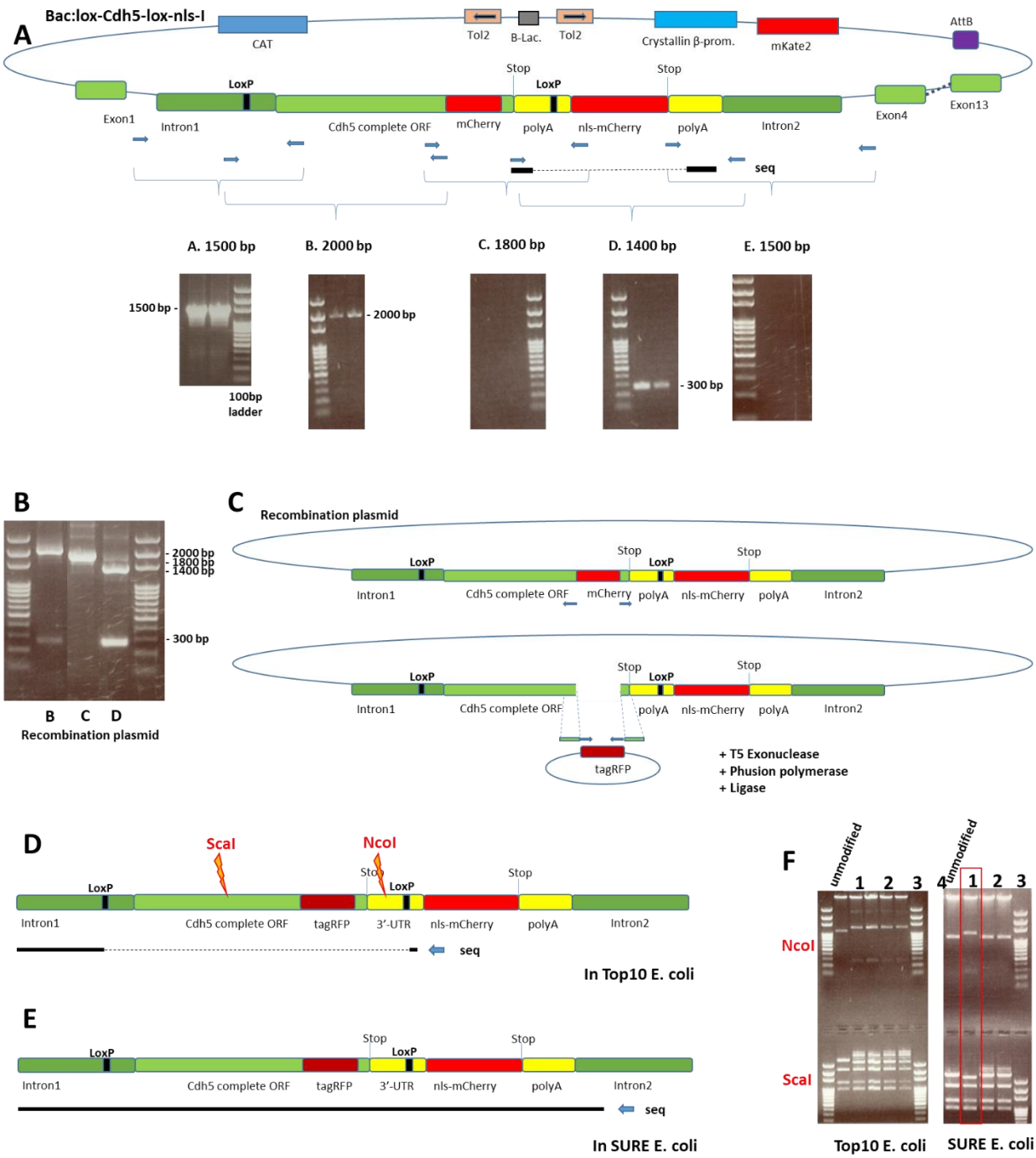

Figure 2. Exchange of homologous sequences and plasmid bacterial host to prevent unwanted autonomous recombination. (**A**) PCR results using primers covering the inducible mCherry-tagged Cdh5 construct within the BAC. Product A (1500bp) and product B (2000bp) were obtained. Products C (1800bp) and E (1500bp) were not amplified, whereas reaction D (expected to be 140bp) resulted in a smaller product of 300bp. Sequencing of product D revealed that D consists of both polyA sequences but lacked the *loxP* and *nls-mCherry* (**B**) PCR reactions performed on the recombination plasmid. Products B (2000bp) and C (1800bp) were present, however, for reaction D both the expected (1400bp) as well as a short product (300bp) similar to (A) were synthesised. (**C**) New design of the recombination plasmid in which *mCherry* was exchanged for *tagRFP* by Gibson cloning. In addition, the first polyA was exchanged for the Cdh5 endogenous 3'-UTR by the same technique (not shown in this figure). (**D**) New design of the recombination plasmid after Gibson cloning. Sequencing

of the plasmid showed that also the two *loxP* sites underwent autonomous recombination when hosted in Top 10 E.coli. (**E**) The newly designed plasmid was transformed into SURE (Stop Unwanted Recombination Events) E. coli to prevent further autonomous recombination events. (**F**) NcoI and ScaI enzymatic digestion reactions of the recombination plasmids hosted by both Top10 and SURE E.coli. Impurity of plasmids in Top10 after Gibson cloning was clearly visible. Sample 1 from the SURE host showed a pure clonal recombination plasmid after its redesign by Gibson cloning, based on the expected digestion bands (red box). The NcoI and ScaI cutting sites within the inducible construct are indicated in (D) and (E). For the gels in A, B and F a 100bp DNA ladder was used.

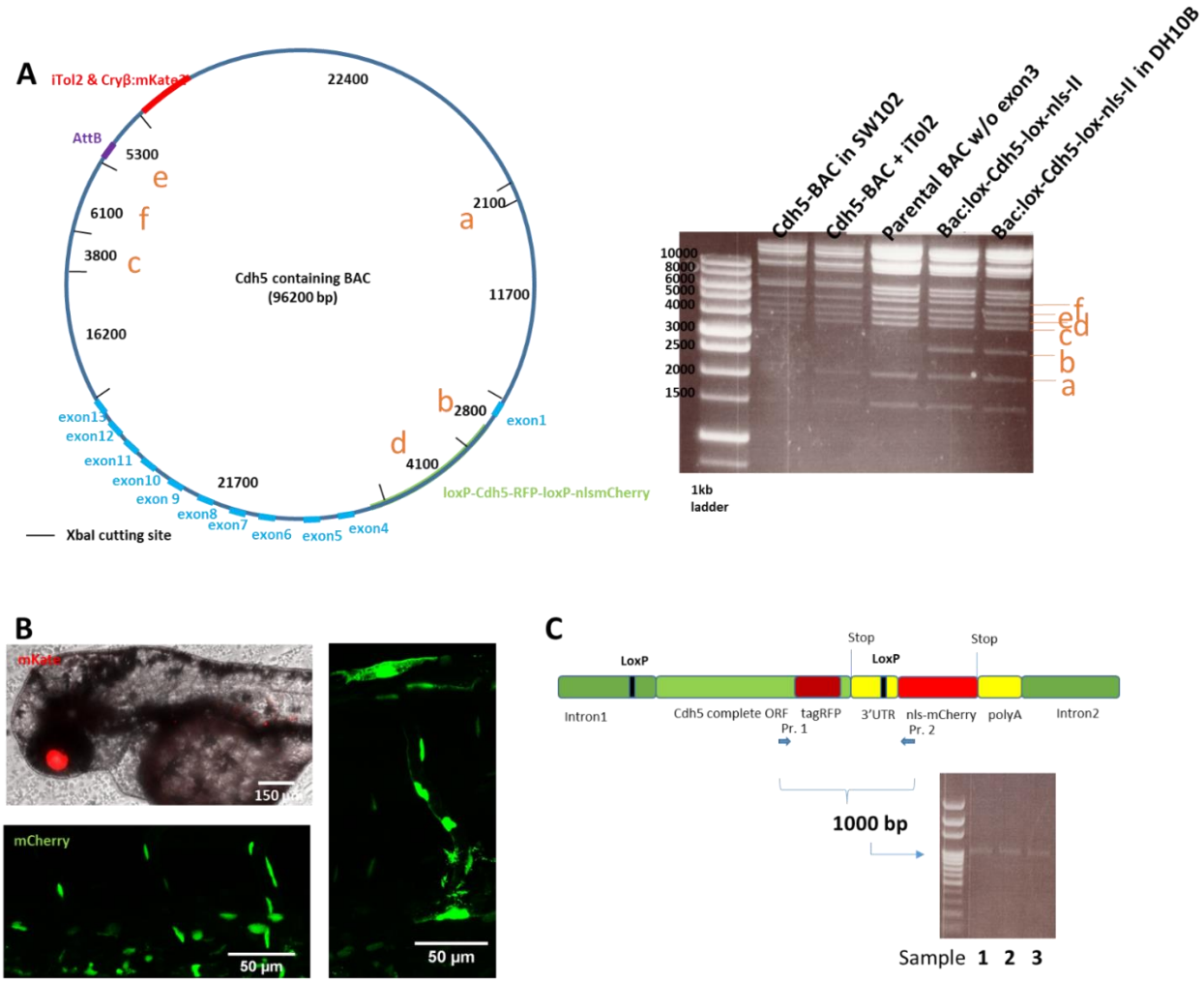

Figure 3. EC nuclei expressing *mCherry* after introduction of the inducible Cdh5 BAC into the zebrafish genome. (**A**) XbaI digestion of Bac:lox-Cdh5-lox-nls-II showing all expected cut products through the different designal stages of the BAC. The bands a to f on the gel correspond to the elements with the same letter indicated in the plasmid. A 1kb DNA ladder was used here. (**B**) Introduction of the inducible Cdh5 BAC into the zebrafish genome led to embryos with red eyes and *mCherry* (indicated here in green) expressing EC nuclei. (**C**) The inducible Cdh5 construct including the *tagRFP* and *nls-mCherry* coding sequences were present in BAC-injected zebrafish showing red eyes. PCR with the indicated primers generated a 1000bp product. For this gel a 100bp DNA ladder was used.

3.1.4. Transcriptional read-through of the Bac:lox-Cdh5-lox-nls-II construct causes expression of mCherry in ECs

A closer look at the original design of Bac:lox-Cdh5-lox-nls-II reveals that the region between the second *loxP* site and *nls* is identical to the end of intron 1. Within these intron ends a splicing acceptor sequence is present, controlling the elimination of the intron during RNA processing. Due to the fact that *nls-mCherry* was expressed in absence of cre-lox recombination, I hypothesised that the newly introduced 3'UTR did not stop transcription efficiently enough. As a consequence, transcription continued towards *mCherry*, whereupon the second exon 1 splice acceptor caused an alternative splicing event between Cdh5 exon 1 and *nls* (Figure 4A). This would lead to mRNA that only encodes for nls-mCherry, whereas our predicted mRNA should only contain a transcription of *cdh5* fused to *tagRFP*.

In order to check this hypothesis, RNA was extracted from BAC-injected embryos expressing *mKate2* in their eye lenses, as well as from BAC-injected embryos without red eyes as a control. The purified RNA served as a template for reverse transcription (RT) to synthesise cDNA, using RT primers starting at *tagRFP*, *mCherry* and polyA sequences (Figure 4B, red arrows). PCR analysis on the revealed expected product synthesis of RFP and mCherry (Figure 4B, primers indicated as blue arrows). A third triple primer pair was designed (PCR1) binding in forward direction to exon 1 and ORF exon 13/3'-UTR, and in reverse direction to *mCherry.* Since exon 1 and mCherry are located 4550bp from each other (whose PCR product would be too long to be synthesised during a 30-sec extension time), this PCR reaction should only synthesise a 1500 product between exon 13/3'-UTR. However, cDNA generated using RT primer oligo-dT (leading to synthesis of all mRNA within the zebrafish sample) also yielded a product of 700 bp, which can only be generated between the primers binding exon 1 and *mCherry*, in case of alternative (unpredicted) splicing (Figure 4B). The fact that the other PCR products expected from the desired transcription splicing are synthesised as well, points to an amplification of genomic DNA, which had not been entirely removed by DNases during cDNA synthesis procedure.

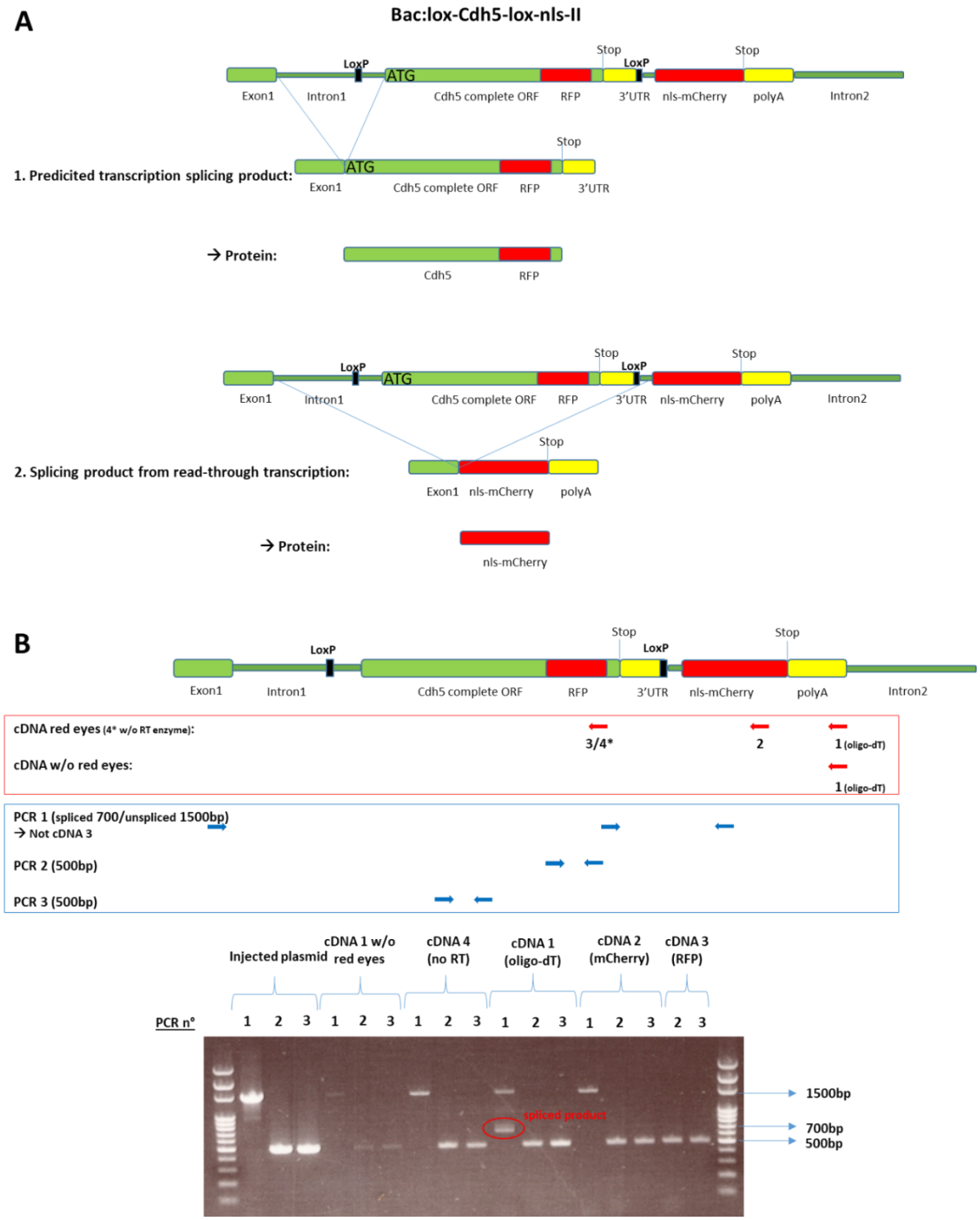

Figure 4. cDNA analysis to investigate potential alternative splicing. (**A**) Prediction of splicing products with regard to two possible splicing events during mRNA processing. In case of transcription read-through of the construct, mature mRNA encodes for nls-mCherry, whereas tagRFP-tagged Cdh5 ORF gets lost. (**B**) Primer design for reverse transcription (red arrows), followed by PCR primers (blue arrows) and electrophorese set-up in order investigate splice variants using cDNA from BAC injected embryos (with red eyes) as a template. PCR1 on oligo-dT samples could only yield a 700bp product (surrounded by red circle) in case of splicing from read-through transcription. Other PCR products were obtained either due to amplification of genomic DNA still present in the cDNA synthesis mix or, less probably, due to both splicing variant events happening at the same time. For this gel a 100bp DNA ladder was used.

3.1.5. Improved design of the inducible BAC by inversion of *nls-mCherry-polyA-loxP* ensures expression of RFP-tagged Cdh5

In order to prevent alternative splicing by read-through transcription, *nls-mCherry-polyA-loxP* part was newly designed, more precisely it was inverted. In addition, the 3'-UTR was replaced for rabbit β-globin 3'UTR, which had been shown before to efficiently terminate RNA transcription (Gil and Proudfoot, 1987). Cre recombination of two *loxP* sites oriented in the same direction, leads to excision of DNA between both sites. In this case, when a second *loxP* site is oriented in the opposite direction, recombination inverses the cassette between the *loxP* into the opposite orientation (Figure 5A). In absence of Cre-recombinase, the Cdh5 ORF including the tagRFP should be transcribed and translated. In this configuration, no other splice acceptor sites within the construct are present anymore. Flipping of the construct into opposite direction, should bring *nls-mCherry* under control of the Cdh5 promoter, which consequently should lead to *mCherry* expression in EC nuclei and no transcription of the Cdh5 ORF anymore (Figure 5A).

The *nls-mCherry-polyA-loxP* cassette in inverted orientation linked to the rabbit β-globin PolyA in normal orientation was synthesised by ATG:biosynthetics GmbH. By BAC recombineering technology, this cassette was then exchanged for the sequence of 3'-UTR up until the second loxP site in the former BAC design. Initially, BAC recombineering did not work anymore due to unstable biotin indispensable for SW102 cells to grow (appendix II). After having solved this problem, the new cassette had been introduced to Bac:lox-Cdh5-lox-nls-II to give rise to Bac:lox-Cdh5-inls-ilox and their SW102 E. coli clones were screened by PCR for having the new construct. The PCR products of correct ones were sequenced (Figure 5B). Finally, after purification of a correct Bac:lox-Cdh5-inls-ilox, it was further tested by PCR for the modified backbone elements (cf. Appendix I) and for the inducible construct similar as in Figure 2B (Figure 5C up). In addition, the new BAC was digested by XbaI, yielding all expected bands (Figure 5C down). From the moment all testing results were positive, the selected BAC was prepared for injection.

Injection of the BAC resulted in some embryos expressing red eyes (Figure 5D), whose ECs showed *tagRFP* expression at junction, e.g. in the dorsal aorta (Figure 5E). However, in certain embryos *tagRFP* expression was not exclusively restricted to junctions, but some EC nuclei seemed to express *tagRFP* as well, which I will further investigate once I have identified founder fish (Figure 5F). The presence of the complete construct in the genomes of two BAC-injected embryos were confirmed by PCR tests (Figure 5G). In order to test the functionality of the construct further, the BAC was injected into zygotes expressing Cre recombinase under control of the *kdrl* promoter. In this case, one would expect the recombination of the *loxP* sites in all ECs resulting in the inversion of the construct between the loxP sites. In this case, nls-mCherry should be expressed under control of the Cdh5 promoter, as indeed was observed in some BAC-injected *kdrl:cre;kdrl:gfp* embryos (Figure 5H).

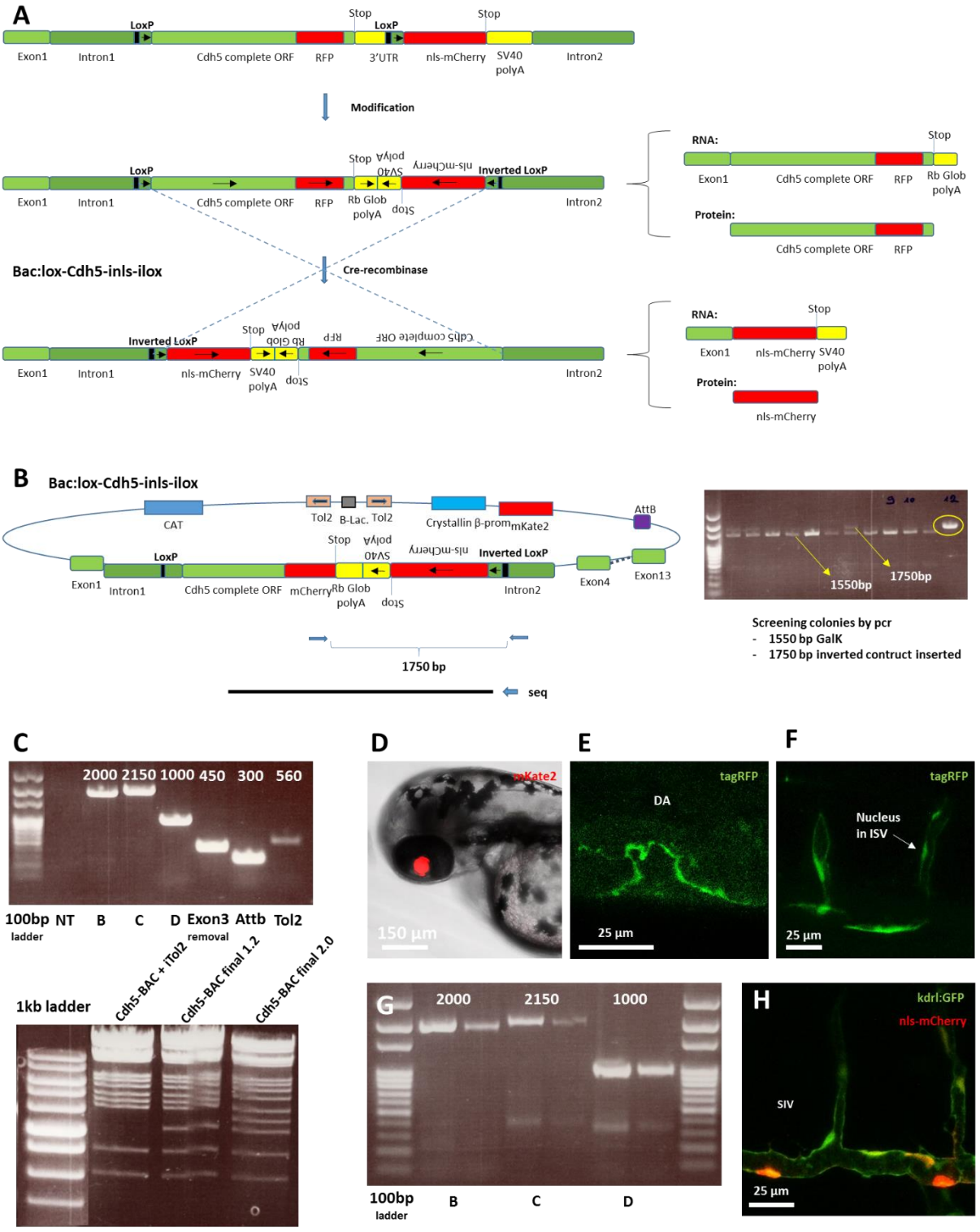

Figure 5. Redesign of the inducible BAC to prevent splicing from read-through transcription. (**A**) In the new design, *nls-mCherry-polyA-loxp* sequences were inverted. In addition, Cdh5 3'UTR has been replaced for rabbit β-globin polyA (Rb Glob PolyA). In absence of Cre recombinase activity, transcription should stop after (Rb Glob PolyA) without further possible splicing variants during mRNA processing. At the moment Cre recombinase recombines the now inverted oriented *loxP* sites, the construct between the *loxP* sites will be inverted, resulting in *nls-mCherry* expression under control of the Cdh5 promoter. (**B**) The RBpolyA- (i)SV40polyA-(i)*nls-(i)mCherry-(i)loxp* has been synthesised and exchanged for 3'UTR until the second *loxP* site by BAC

recombineering. Re-engineered clones were screened by PCR and checked by sequencing for correct integration. (**C**) Further PCR tests on the final designed purified BAC including the modified elements in the backbone (cf. Appendix I) and covering the inducible cassette identical to Figure 2B. Finally, XbaI digest showed all expected cut products. (**D**) Bac:lox-Cdh5-inls-ilox-injected embryo showing red eyes. (**E**) *TagRFP* expression in junctions within the DA of a Bac:lox-Cdh5-inls-ilox-injected embryo. (**F**) *TagRFP* expression in junctions within the ISVs of a Bac:lox-Cdh5-inls-ilox-injected embryo. Some nuclei seemed to express tagRFP (white arrow). (**G**) Genomic DNA of two BAC-injected embryos were tested by PCR similar to (C) for presence of the complete construct in their genomes, which was the case. (**H**) *Kdrl:cre;kdrl:gfp* embryos were injected with the inducible cdh5 construct as well. Cre recombination of the *loxP* sites led to the expression of *nls-mCherry* in the nuclei of endothelial cells (here in SIVs). DA: dorsal aorta; ISV: intersegmental vessel; SIV: subintestinal vessel.

3.2. Generation of a photo-convertible fluorescent protein-tagged Cdh5 line

Photo-convertible fluorescent proteins are proteins that have the capability of irreversibly switching their emission colour from green to red, when exposed to light of approximately 400nm (Hoi et al., 2010). In order to obtain a zebrafish line, in which Cdh5 can be visualised from individual neighbouring endothelial cells, a BAC construct was designed in which Cdh5 is fused to the photo-convertible fluorescent protein mClavGR2 (further indicated as mClav). To this purpose, mClav was introduced by BAC recombineering technology into the exon 13 of *cdh5*, between the p120-catenin and β-catenin binding sites of the translated cadherin protein (Figure 6A). This position has been demonstrated before allowing marker fusion proteins to be expressed and translated without harming Cdh5 functionality (Lagendijk et al., 2017). The Cdh5 parental BAC (therefore with the modified backbone, cf. Appendix IB) with the *cdh5* gene still completely intact (including exon 3), was reused for this BAC recombination procedure.

After recombineering, SW102 colonies were screened for correct BAC clones and correct ones were purified. The selected *cdh5-mClav* containing BAC was subsequently tested by XbaI digest, further PCR analyses (Figure 6B) and sequencing. From the moment one BAC was positive for all testing results, it was prepared for injection into zebrafish zygotes.

Injection of wild type zebrafish zygotes resulted in roughly 60% of the surviving embryos that showed red eyes, from whom 70% expressed *mClav*-tagged *cdh5* in endothelial cells. mClav was excited by a 488nm laser beam and indicated Cdh5's localisation in the green channel, as shown here in the subintestinal plexus of a 2dpf embryo (Figure 6C, left upper panel). mClav can be converted by 405nm laser light (20% laser intensity for 1min), which resulted in mClav light emission in the red channel after excitation by 561nm laser (Figure 6C, lower panels). In this case, the green signal decreases, which makes this tool appropriate for studying the contribution of Cdh5 from different individual ECs to the establishment of adherens junctions.

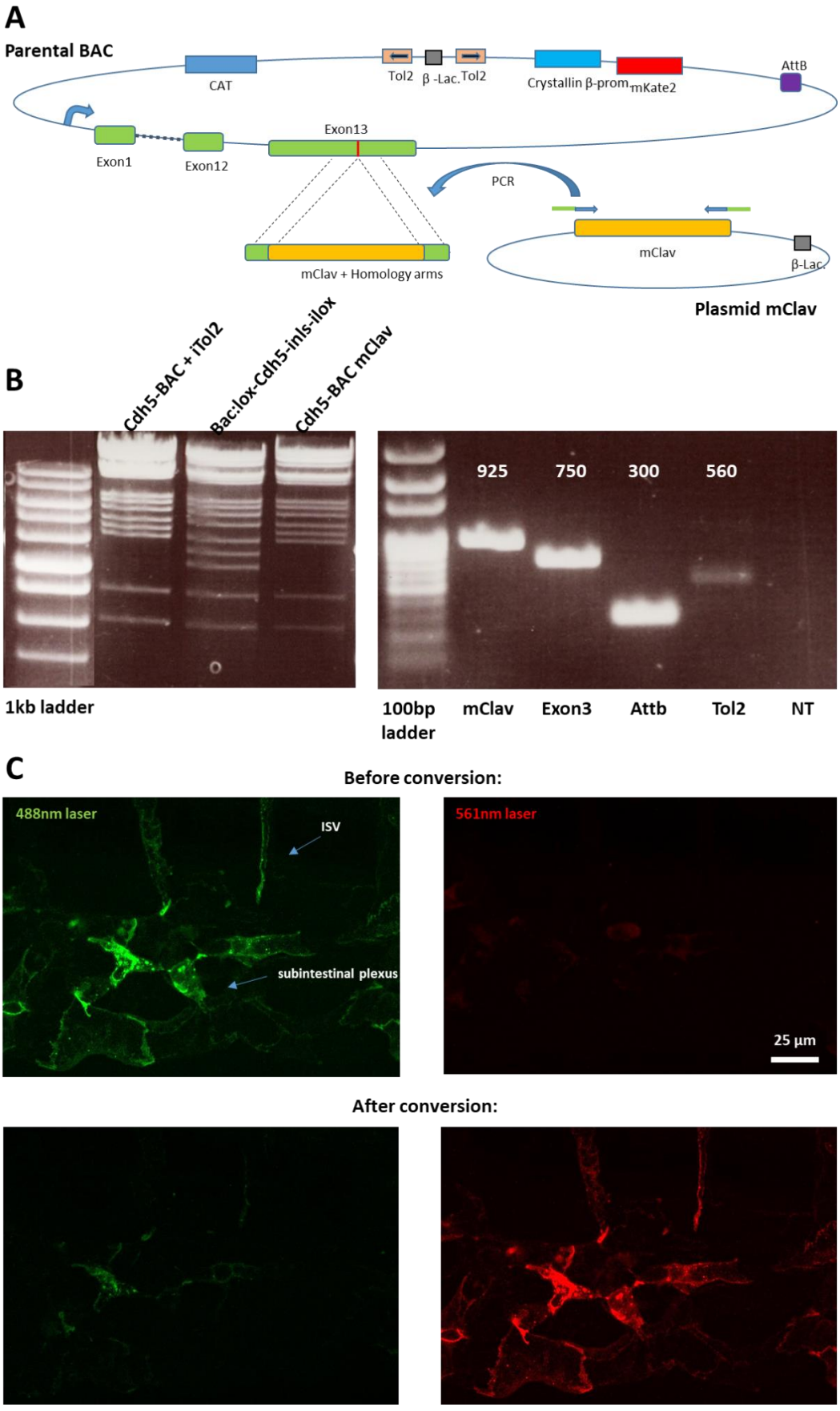

Figure 6. Design of a photo-convertible fluorescent protein-tagged Cdh5 and its expression. (**A**) Design and strategy of the Cdh5 BAC in which mClav has been introduced within

Cdh5 exon 13 by BAC recombineering technology. The Cdh5 BAC with the modified backbone has been reused from the Cdh5 inducible knock-out project (cf. Figure 1C). (**B**) Correct engineering of *mClav*-tagged *cdh5* BAC shown by XbaI digest (cf. Figure 3A) and PCR. PCR amplication products were obtained from the sequences coding for mClav (a 925bp product), Cdh5 exon 3 (750bp), AttB (300bp) and Tol2 (560bp). For the gel containing the digest, a 1kb DNA ladder was used, for the PCR analysis a 100bp ladder. (**C**) Injection of mClav-tagged Cdh5 BAC led to expression of Cdh5 marked by mClav in ECs. Initially, mClav was visualised when exited by laser of 488nm (C upper left panel). After conversion by a 405nm laser beam, the green signal decreased whereas the converted mClav became visible in the red channel excited by a 561nm laser light (C lower panels). The vessels depicted here are sub-intestinally located.

3.3. Phenotypic characterisation of RadilB during vascular morphogenesis

Since Rasip1 is known to be essential for proper Cdh5 localisation and its absence results in abnormal blood vessel development, other related proteins were searched. Radil was found to be a closely-related protein and is used in this study to understand EC behaviour *in vivo* during ISV development.

3.3.1. Amongst the three duplicated *radil* genes only *radilb* is specifically expressed in the endothelium

Protein-protein blasting of Rasip1 zebrafish protein sequence against *Danio rerio* (taxid:7955) database reference proteins (refseq_protein) of NCBI resulted in three protein suggestions sharing similar protein domains: Radil, si:ch73-281f12.4 and si:ch211-176g6.2. Since the two non-annotated proteins contain the same protein domains and a similar architecture, I call si:ch73-281f12.4 RadilB and si:ch211-176g6.2 RadilC. Although in human and mice only one *radil* gene is known, it seems that *radil* in zebrafish has undergone gene duplication events during teleost evolution. Moreover, their typical domains (ras associating domain, forkhead associated domain, dilute domain and PDZ domain) have been preserved. Only the first three mentioned protein domains are shared with Rasip1 (Figure 7A).

In zebrafish, only the annotated Radil (from now on RadilA) has been examined. Knockdown of RadilA results in multiple defects in neural crest-derived lineages such as cartilage, pigment cells, and enteric neurons (Smolen et al., 2007). However, no defects with respect to angiogenesis nor to EC homeostasis have been described yet.

Zebrafish Rasip1 shares a common ancestor with the mammalian human and mouse Rasip1, when plotting their protein sequence comparison in a phylogenetic tree (Figure 7B). Human and mouse Rasip1 are closely related given their short branch length. In contrast, the branch length of zebrafish Rasip1 indicates a farther distance to its mammalian homologue. Zebrafish RadilA, however, shows a much closer relationship with regard to its mouse and human homologue, but this is not the case for zebrafish RadilB and C. The latter share a common ancestral precedent, before their phylogenetic branches converge with the one of RadilB and mammalian Radil (Figure 7B). Most probably, genetic duplication of Radil in teleost evolution took place twice. First, between RadilA and RadilB-C, later between RadilB and RadilC.

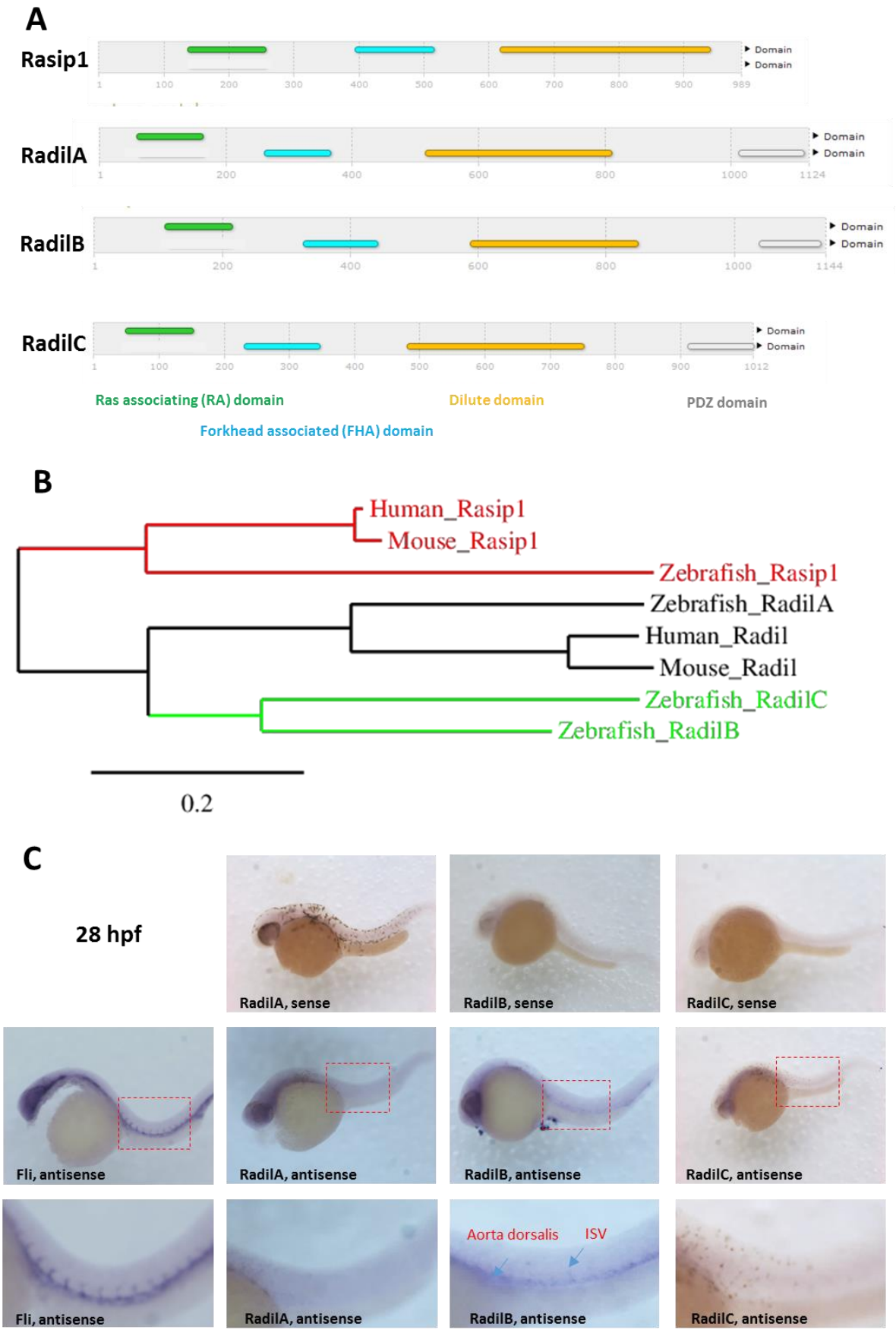

Figure 7. Gene duplication analysis for Radil in zebrafish. (**A**) Three different Radil genes are present in the zebrafish genome. All three share three common protein domains with Rasip1: Ras

associating domain (green), forkhead associated domain (blue) and the dilute domain (yellow). In addition, Radil proteins contain a PDZ domain (white). (**B**) Phylogenetic tree of Radil and Rasip1, showing their respective evolutionary relationship. Zebrafish Rasip1 has the same ancestral provenance as the mammalian mouse and human Rasip. Same is true for zebrafish RadilA. Zebrafish RadilB and C, however, are closer related to each other, but at larger distance from mouse and human Radil than zebrafish RadilA. (**C**) *In situ* hybridisation demonstrates that only *radilb* is endothelial specifically expressed. Hybridisation was performed on 28hpf fixed embryos. Only antisense probes are reversibly complement and can therefore bind to its corresponding mRNA. The probe against the endothelial specific Fli mRNA is used as positive control (left panel).

In order to find out which of the found Radils in zebrafish were of any interest to examine endothelial cell behaviour, *in situ* hybridisation on 28hpf embryos was performed. To this purpose, dig-labelled probes were made using exon 5 as a template, since this exon was longest in all three Radils. Only RadilB showed an endothelial specific expression, whereas RadilA and RadilC mRNA was ubiquitously present, although in low quantities (Figure 7C). The result of RadilA sample is in accordance with supplemental Figure 3 from Smolen et al., 2007. In mouse, *Radil* is rather ubiquitously expressed with enrichment in the lung and testis (Yue et al., 2014).

RadilB in zebrafish shows highest protein similarity with mouse Radil based on the percentage to which both protein sequences resemble. On the contrary, less resemblance is calculated for zebrafish RadilA and RadilC (Table2). All these findings together made RadilB an interesting candidate for phenotypic analysis on vascular morphogenesis.

Table 2. Protein resemblance between RadilB and its homologues in zebrafish, mouse and human

Protein	Zebrafish				Mouse		Human	
Similarities (%)	RadilA	RadilB	RadilC	Rasip1	Radil	Rasip1	Radil	Rasip1
Zebrafish RadilB	37.1%	100.0%	44.4%	33.0%	62.2%	39.0%	37.7%	38.9%

3.3.2. Null-mutation in one allele coding for RadilB does not affect angiogenesis

A zebrafish line containing a null-mutation for RadilB was ordered at ZIRC. By N-ethyl-N-eitrosourea (ENU) mutagenesis screens a mutant line was selected having a T to A point mutation close to the gene's 5'-end. This mutation converts the tyrosine-129 codon into a stop codon, leading to the loss of all functional domains (Figure 8A). Using a four primer PCR strategy, wild type, hetero- and homozygous fish can be distinguished from each other. For this genotyping procedure, two outer primers bind 600bp away from each other around the mutation. Two inner primers recognise either the wild type allele or the mutant allele, for which the wild type primer generates a 400bp product and the mutant one a 200bp PCR product (Figure 8B left panel). The effectiveness of this genotyping strategy was initially confirmed by genotyping (Figure 8B right panel).

Crossing of RadilB mutant fish to endothelial marker lines allows phenotypical analysis within the process of angiogenesis. In order to examine mutant embryos, having the exact same genetic background and laid at the same time, heterozygous mutant marker lines were incrossed. Their offspring was selected for carrying the homozygous mutation. Homozygous RadilB mutant fish are viable and fertile. In the set-up of this study, homozygous fish were crossed to heterozygous ones in order to obtain embryos with identical parental background, but carrying the RadilB mutation on either one or both alleles (Figure 8C).

Phenotypical analysis by comparison can only occur in case the heterozygous fish show no phenotype. Therefore, heterozygous marker lines were crossed with wild type fish and their offspring analysed for abnormalities in the context of angiogenesis, including collapsing ISVs, retracting ISVs, aberrant cell wall architecture and delays in development. As an example, at 50hpf no differences in blood vessel architecture nor developmental delays between heterozygous mutants and wild types were visible (Figure 8D). In addition, quantification of the incidence of angiogenic abnormalities during embryonic development from 24hpf up to 3dpf did not show significant differences between both genotypes (Figure 8E, N=21, P=0.854). Therefore, heterozygous RadilB mutants were used in this study as a control reflecting the wild type for further phenotypical analyses of RadilB.

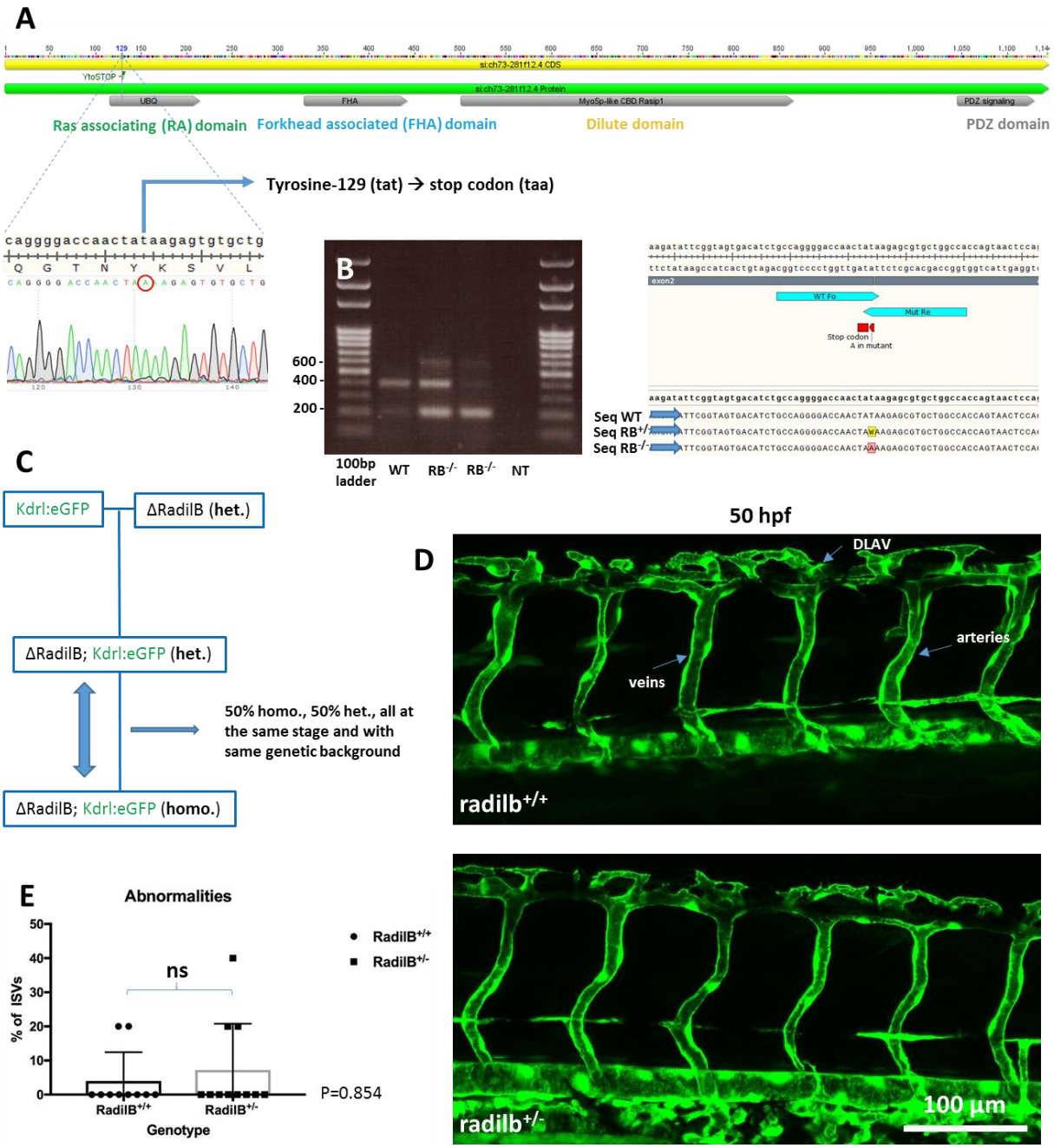

Figure 8. Characterisation of the mutation in the gene coding for RadilB. (**A**) Location of null-mutation within the RadilB protein sequence. ENU mutagenesis screens selected a T to A point mutation, resulting in the conversion of the codon for tyrosine-129 into a stop codon. This results in the loss of translation of all functional domains. (**B**) Genotyping strategy using four primers that can generate a control big product, and a smaller wild type respectively mutant band, or both. Effectiveness of the screening strategy checked by genotyping. The outer primers generate a control PCR product of 600bp, the inner primers a product of 400bp (wild type allele) or 200bp (mutant allele) respectively. (**C**) Crossing scheme for used experimental set-up. Mutants were crossed with marker line, here demonstrated for *kdrl:gfp*, to get heterozygous RadilB marker lines. Subsequent incross yielded homozygous RadilB marker lines. For the experiment set-up, heterozygous mutants were crossed with homozygous mutants to obtain 50% homo. and 50% het. offspring with same genetic background. (**D**) Heterozygous *kdrl:gfp* mutants do not show any phenotypes in blood vessel architecture and delays in vessel development at 50hpf. (**E**) Quantification of angiogenic abnormalities observed in heterozygous

kdrl:gfp mutants from 24hpf to 3dpf. Observations include collapsing ISVs, retracting ISVs, aberrant cell wall architecture and delays in development. The un-paired Mann Whitney test was used as statistical test.

3.3.3. Absence of RadilB causes intermittent lumen collapses during ISV maturation and abnormalities in blood vessel architecture at later developmental stages

Crossing of *radilb*$^{+/-}$*;kdrl:gfp* with *radilb*$^{-/-}$*;kdrl:gfp* yielded embryos from whom 50% were homozygous and 50% heterozygous. When the dorsal longitudinal anastomotic vessel (DLAV) in homozygous was being formed, the initial formed lumen within the intersegmental vessels (ISV) suddenly collapsed and reopened again (Figure 9A). This intermittent lumen collapse was observed within *radilb*$^{-/-}$ at a higher percentage (22.9% of the ISVs) than in *radilb*$^{+/-}$ embryos (10.2% of the ISVs) (Figure 9E, N=17, P=0.0284).

To better understand what exactly happened during an ISV collapse, time lapse imaging at higher magnification recorded several intermittent lumen collapses in more detail. These collapses only occured when at least two biological processes coincide: 1. the ISV undergoes an arterial to venous transition and 2. the ISV cell divides. The arterial to venous transition happened to approximately 50% of all ISVs, since initially these vessels grow as arteries (cf. 1.1.2.4.). During this transition, a secondary spout from the post cardinal vein (PCV) grows out and anastomoses with the ISV initially bound to the dorsal aorta. This phenomenon was clearly visible in Figure 9B and upon cell division of this particular vessel, the lumen collapsed. After finishing the venous formation, the lumen inflated and reopened.

Since RadilB is apparently indispensable for stable vessel lumen maintenance during arterial to venous transition, RadilB might have an influence on the amount of arterial versus venous ISVs formed during angiogenesis. However, counting of the amount of arterial versus venous ISVs at 55hpf did not show any significant differences between homozygous mutant and wild type embryos (Figure 9D, N=19, P=0.7750). 48.9% Of the wild type ISVs and 46.7% of the mutant ISVs were counted to be arterial. Thus, RadilB does not seem to have any influence on arterial versus venous cell fates.

At later stages during embryonic development, the ISVs of homozygous mutants showed an abnormal vessel wall architecture. Vessel walls of *radilb*$^{-/-}$ embryos were less smooth, rather jagged, in comparison to *radilb*$^{+/-}$. In addition, ISV show patterning problems at the place where the venous ISV had anastomosed to secondary sprouts from the PCV (Figure 9C).

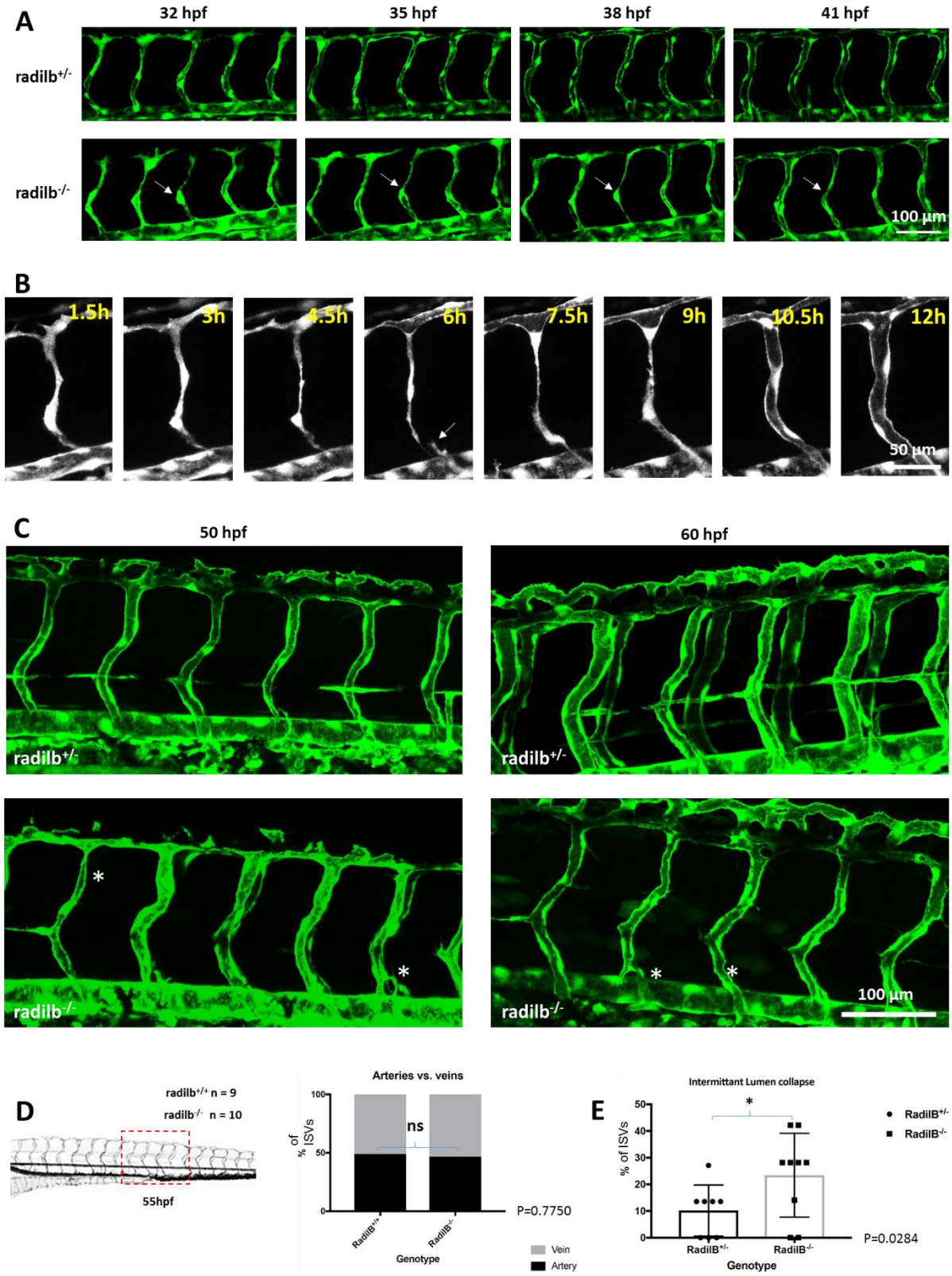

Figure 9. Intermittant lumen collapses and patterning problems in RadilB homozygous mutants. (**A**) Time-lapse imaging from 30 to 45hpf of *radilb*$^{-/-}$*;kdrl:gfp* embryos showed intermittent lumen collapses during ISV maturation. The white arrow indicates the place of cell division from the vessel that undergoes the lumen collapse (**B**) A closer look *radilb*$^{-/-}$*;kdrl:gfp* during an intermittent lumen collapse revealed that initially a lumen within the ISV had been formed, but collapsed at the moment the initial arterial vessel was transitioned into a venous vessel and simultaneously started to divide. After

cell division, the lumen opened again. The white arrow indicates the emerging venous secondary sprout. (**C**) At 50 and 60hpf the blood vessel wall architecture of *radilb*$^{-/-}$*;kdrl:gfp* embryos show abnormalities. In homozygous mutants the vessel walls are less smooth (rather jagged) and patterning problems occur where the ISV get connected to the PCV. (**D**) The amount of arterial versus venous ISVs does not differ at 55hpf between hetero- and homozygous RadilB mutants. (**E**) Quantification of the amount of intermittent lumen collapses in *radilb*$^{-/-}$ and *radilb*$^{+/-}$ embryos (N=17). The un-paired Mann Whitney test was used as statistical test.

3.3.4. RadilB mutants show arterial venous shunt formations during arterial to venous transition and reduced cell divisions during ISV outgrowth

To evaluate whether the arterial to venous transition in mutants caused problems for blood cell perfusion, *Δradilb;kdrl:gfp* mutants were crossed with a *gata1:dsRed* line, allowing visualisation of red blood cells. The onset of blood perfusion in homozygous mutant ISVs took in average place around 42hpf, whereas in heterozygous mutant perfusion started around 40hpf. Remarkably, homozygous mutants showed shunt formations at the moment venous to arterial transition occurred. Sometimes, when a venous secondary sprout anastomosed with an ISV, the ISV kept contact to the dorsal aorta, thereby enabling blood cells to move from the aorta via the shunt directly into the PCV, thereby omitting the DLAV (Figure 10A). This was observed in 28.6% of the analysed mutants ISVs. However, a closer look to heterozygotes revealed that this shunt formation also occurred (in 7.1% of the analysed ISVs), albeit less pronounced. Considering the amount of shunt incidences, no significant differences between both genotypes were observed (Figure 10C, P=0.0758). This might be partly due to a too limited sample size (N=11).

Since the absence of RadilB seemed to cause problems in vessel stability (cf. Figure 9B) and patterning during arterial to venous transition (cf. Figure 10A and 9C), I hypothesised that a reduction of ECs within the ISV might be an underlying problem. Therefore *Δradilb* mutants were crossed with a *kdrl:gfp-nls* to visualise EC cell divisions. During sprout outgrowth (24-32hpf) ECs in ISVs of homozygous RadilB mutants clearly underwent less cell divisions than in heterozygotes (Figure 10B and D, N=19, P=0.0188). In 44.6% of the analysed heterozygous ISVs, a cell division takes place, compared to 13.7% of the ISVs in homozygous mutants. Consequently, maturing ISVs in homozygous RadilB mutants must consist of less individual ECs than in those with a heterozygous background.

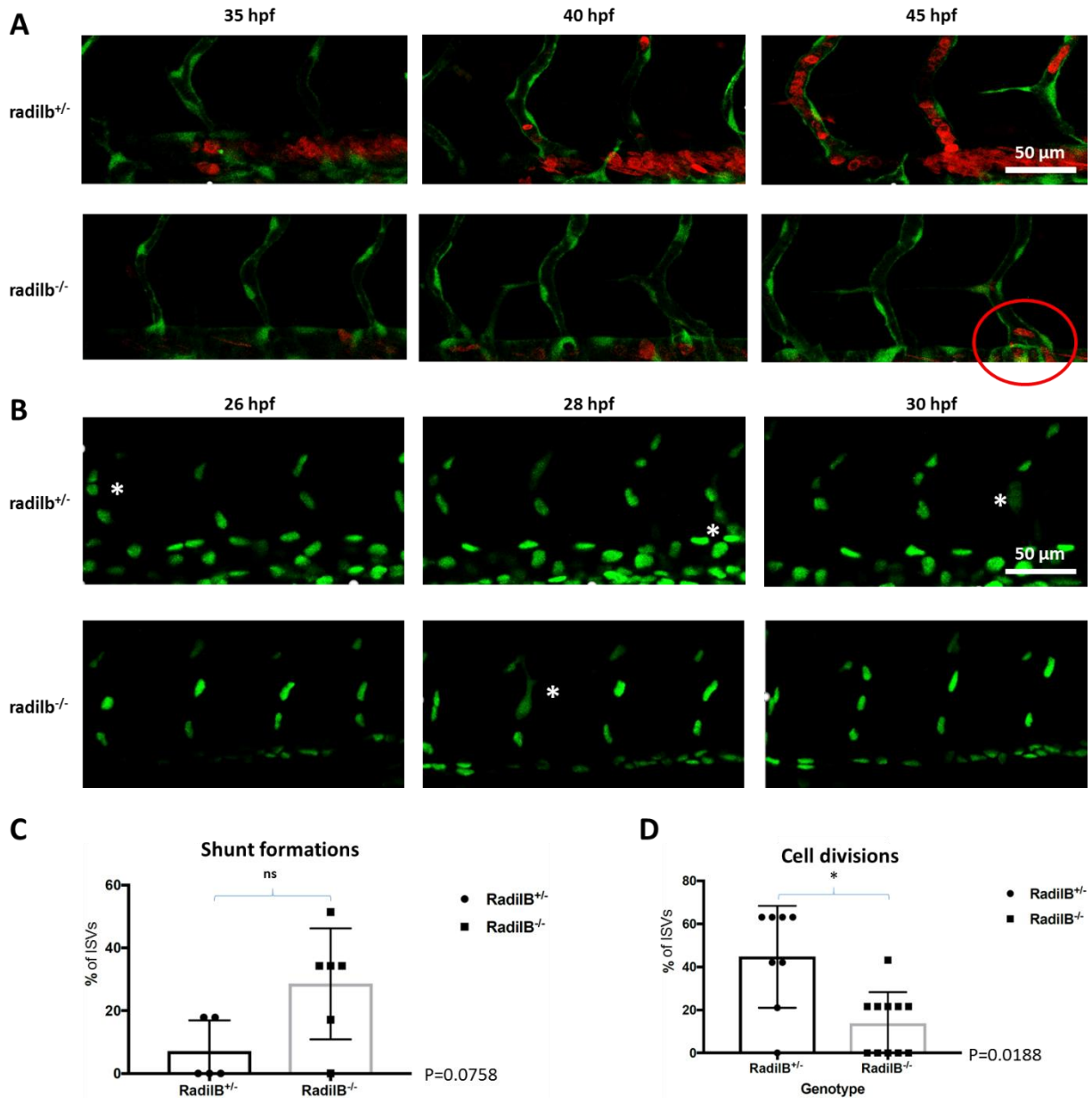

Figure 10. Arterial-venous shunt formations and reduced cell divisions in RadilB mutants. (**A**) Time-lapse images of hetero- and homozygous *Δradilb;gata1:dsRed;kdrl:gfp* showing the flow of red blood cells (red) through ECs (green). In homozygous mutants, arterial-venous shunt formations seemed to occur more frequently, although difference between hetero- and homozygotes are not significant (C). (**B**) Time-lapse images of hetero of *ΔradilB;kdrl:gfp-nls* showing cell divisions of EC nuclei (green) during ISV outgrowth. ECs in RadilB homozygous mutants underwent less cell divisions. (**C**) Quantification of the amount of cell formations in hetero- and homozygous mutants. The incidence of shunt formations showed a tendency to be higher in homozygotes, but could not be confirmed by statistical analysis (P=0.0758, N=11). (**D**) Quantification of the amount of cell divisions in hetero- and homozygous mutants. The incidence of cell division was significantly lower in homozygotes (P=0.0188, N=19). The un-paired Mann Whitney test was used as statistical test.

3.3.5. Cdh5 in RadilB mutants shows an abnormal localisation

In order to figure out the role of adherens junctions underlying the observed phenotypes in RadilB mutants, including the intermittent lumen collapses and shunt formations during arterial to venous transformation, the localisation of Rasip1 and Cdh5 in mutants was examined. Rasip1 localised in wild type embryos in continuous lines, restricted to endothelial cells (Figure 11A). At 32hpf Cdh5 was confined to Rasip1 localisation, but Rasip1 lines were also observed at locations where Cdh5 was not present (white arrows).

Concerning the localisation of RadilB itself during vascular development, I designed potential target peptides for antibody generation against RadilB. Two peptides were injected into rabbits and their generated antibodies were harvested and are still in testing phase (cf. appendix-III for the peptide design and first staining results).

Double antibody stainings against Cdh5 and Rasip1 at 32hpf-fixed mutant embryos showed first of all that the localisation of Rasip1 protein was not influenced by the absence of RadilB (Figure 11A, Rasip1 in red). However, differences between hetero- and homozygous mutants became clear at the level of Cdh5. Within the homozygous mutant ISVs, Cdh5 did not localise in a continuous way along the adherens junctions (Figure 11B, Cdh5 in green). In addition, the adherens junctions looked less enriched with Cdh5 within these cells (Figure 11B, magnification panel, see white arrows, N=8).

To visualise Cdh5 presence at later stages, the RadilB mutant line was crossed into the Cdh5 tension sensor line (Lagendijk et al., 2016), whose fluorescent Venus tag was used here as a marker for Cdh5 localisation. At 48hpf, adherens junctions showed now continuous presence of Cdh5 in both mutant lines. Some ISVs in homozygous embryos, however, had junctional lines that were detached from the dorsal aorta or PCV (Figure 11C, arrow in the middle), thereby forming ISVs that were partly unicellular. In addition, Cdh5 in homozygous mutant ISVs were localised in patches that had apparently not succeeded to align into elongated adherens junctions.

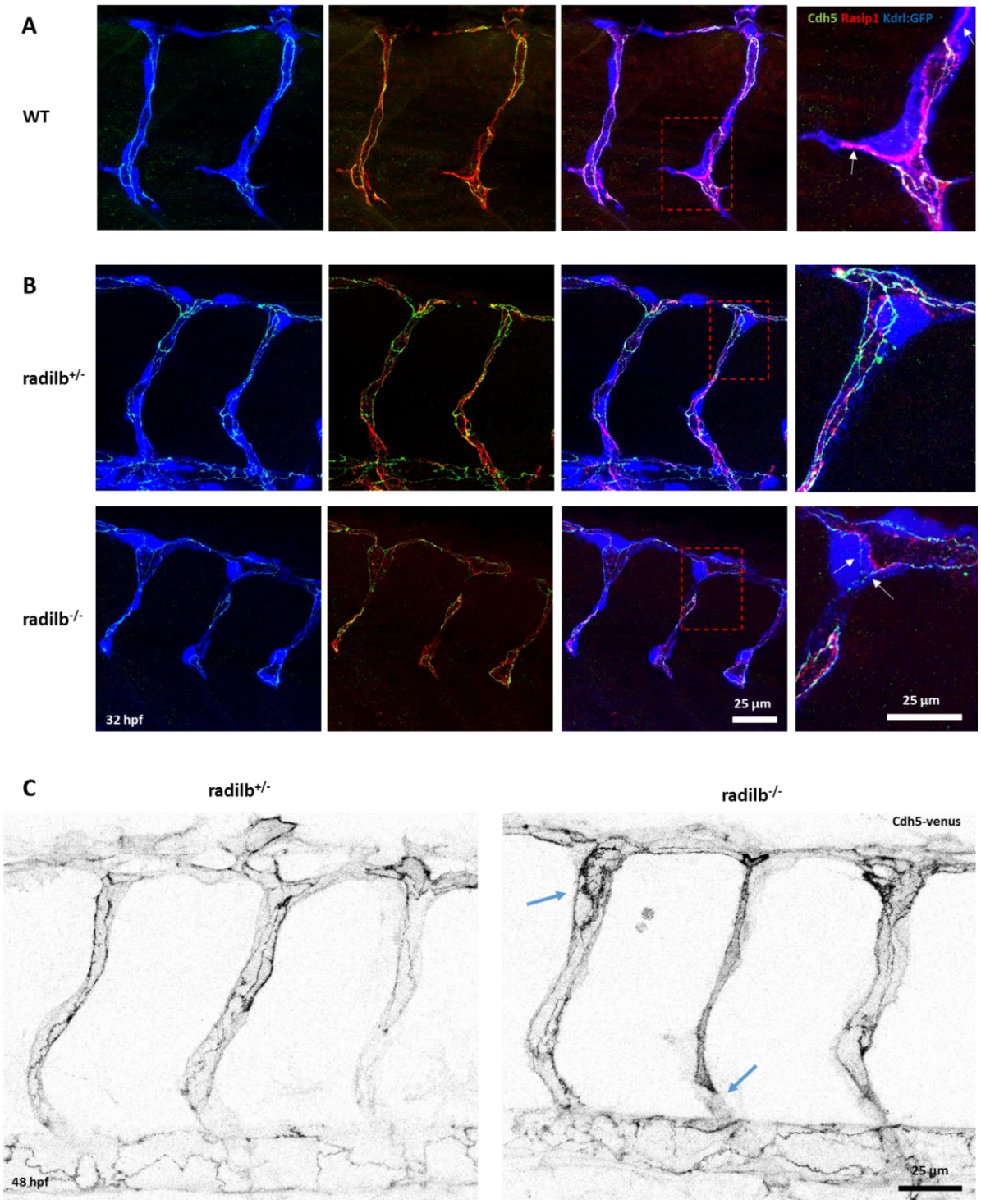

Figure 11. Aberrant junctional shapes in RadilB mutants. (**A**) In wild type, Rasip1 was localised in ECs in continuous lines, overlapping but not restricted to Cdh5 (white arrows indicate Cdh5-less Rasip1 localisation. (**B**) Antibody stainings against Rasip1 (red) and Cdh5 (green) on at 32hpf fixed embryos. Blue is endogenous expressed *kdrl:gfp*. Localisation of Rasip1 was normal in both hetero- and homozygous mutants, however, Cdh5 showed a less linearized accumulation at the adherens junctions in homozygous mutants (white arrows). Consequently, adherens junctions did not look like continuous lines. (**C**) Localisation of Cdh5 at 48hpf visualised by a venus-tagged Cdh5 marker line. Cdh5 in homozygous mutant ISVs showed sometimes a detached localisation in which parts of ISV had a unicellular configuration (arrow in the middle). In addition, unaligned patches of Cdh5 were visible within homozygous mutants as well (arrow upper left). Figure 11C was provided by Minkyoung Lee.

Chapter IV
Discussion

4.1 Generation of an inducible Cdh5 knock out line

The major focus of my thesis was to create tools that would enable us to decipher cytoskeletal junctional interactions during blood vessel morphogenesis. To this purpose, I generated an inducible Cdh5 knock out line that can be used to remove *cdh5* expression at any given time point during embryonic development, based on Cre/loxP recombination. The modifications of the Cdh5 gene were executed by BAC recombineering technology, whose design was optimised over time, based on learning by doing. Finally, the most optimal design proposed in this thesis is based on inverted *loxP* sites flanking the RFP-tagged open reading frame of Cdh5 and an nls-mCherry in opposite direction. Introduction of this design into the genome of the zebrafish led to expression of *cdh5* in Cre-less fish as well as nuclear mCherry expression in case of active Cre recombinase.

4.1.1. Optimisation of BAC recombineering

Since BAC recombineering was not performed in the lab before, the technique had to be established first. First recombination attempts seemed to be only successful in case the PCR product was clean enough and completely deprived of its template. Therefore, PCR synthesis needed to be optimised for every individual insert in order to generate one single product without any side products. In addition, proper DpnI treatment of the PCR mix was indispensable. The efficiency of generating a clean insert was more crucial than any other parameter of the technical procedure. On the contrary, the length of the insert (I used up to 7000bp) did not form any limitation for recombination to happen. BAC recombineering also requires working with freshly prepared biotin and deoxy-galactose. Both ingredients turned out be unstable when stored in solution over periods longer than four months. A lot of time was lost when all ingredients had to be tested when recombination within the BAC did not take place. In general, I optimised the complete procedure as described in section 2.2 including the generation of the insert, the preparation of different agar plates and the recombineering procedure. This thesis can therefore be used a guide for future genetic editing by BAC recombineering adapted to our lab.

4.1.2. Homologous sequences should be avoided

A big problem when hosting large constructs in E. coli are homologous sequences. Principally within the standard Top10 E.coli cells, constructs with homologous sequences undergo autonomous recombination, even sequences as small as 33bp-*loxP* sites. Avoidance of homology within the construct design is recommendable, although one could use SURE E. coli instead. However, SURE E. coli grow very slowly and cannot be used for kanamycin selection. Autonomous recombination within SW102 E. coli cannot be excluded based on my results. Since λ-prophage based recombination is based on homology, one should preferably, also within BAC hosts, limit homologous sequences to a minimum.

4.1.3. BAC recombineering is slow but allows insertion of large constructs in a controlled way

Executing one modification within a BAC will take three weeks when all steps are optimised and successful. Principally the growth speed of SW102 bacteria limits time efficiency. Another disadvantage might be some background activity of the defective λ-prophage system, which might not be completely switched off at 32°C. Especially BACs in SW102 that have been at an incubation temperature of 37°C should not be used anymore, because the λ-prophage system might have caused background mutations. A simple way to avoid this problem is the purification of the BAC from the SW102 and its retransformation into DH10B E. coli. DH10B is the standard host for BACs and does not contain a λ-prophage-based recombineering system.

The main advantage of BAC recombineering is that one can insert big inserts in a site-specific way, which cannot be done by CRISPR/Cas9 gain-of-function approaches. Each step during the DNA modification process can be controlled be negative as well as positive selection. Consequently, once a certain step does not work, one should not start from the very beginning and only needs to optimise that particular step. In addition, I chose to modify *cdh5* in the Cdh5 BAC, because that way I could keep the endogenous promoter and enhancers of *cdh5*. When introducing the Cdh5 containing BAC in the genome, the gene expressing regulation is still present and identical to the endogenous *cdh5*.

4.1.4. Transcriptional read-through might have been due to incomplete Cdh5 3'-UTR

To prevent autonomous recombination between the identical SV40-polyA tails of *cdh5* and *mCherry* within the construct, the polyA tail of *cdh5* was replaced by the Cdh5 3'-UTR. After injection of Bac:lox-Cdh5-lox-nls-II in which homologous sequences were replaced, embryos expressed mCherry in the nuclei of their ECs in absence of Cre. Because the construct was completely integrated in the genome, but its matured mRNA did not contain *cdh5-tagRFP*, I concluded that *cdh5-tagRFP* in the RNA was lost by transcriptional read-through. This observation indicated that the Cdh5 3'-UTR was not capable enough to stop transcription after the open reading frame of *cdh5*. Since the 3'-UTR of *cdh5* has not been annotated yet, the 3'-end sequence, found in the cDNA of the Cdh5 after the last coding exon, was taken. A functional terminator of transcription needs a polyadenylation signal (AAUAAA), a cleavage signal (CA) and a GU-rich sequence, so that proteins can bind the 3'-end of the RNA and add to polyA tail important for mRNA stability and localisation (Figure D-I). However, during this process of mRNA maturation, the 3'-UTR is cleaved at the cleavage signal. When generating cDNA from mRNA, one loses therefore the GU-rich sequence. Indeed, within the sequence of the 3'-UTR used in our construct, polyadenylation signals were present, but the GU-rich sequence was lacking, which could explain that the used Cdh5 3'UTR was incomplete and therefore did not stop transcription.

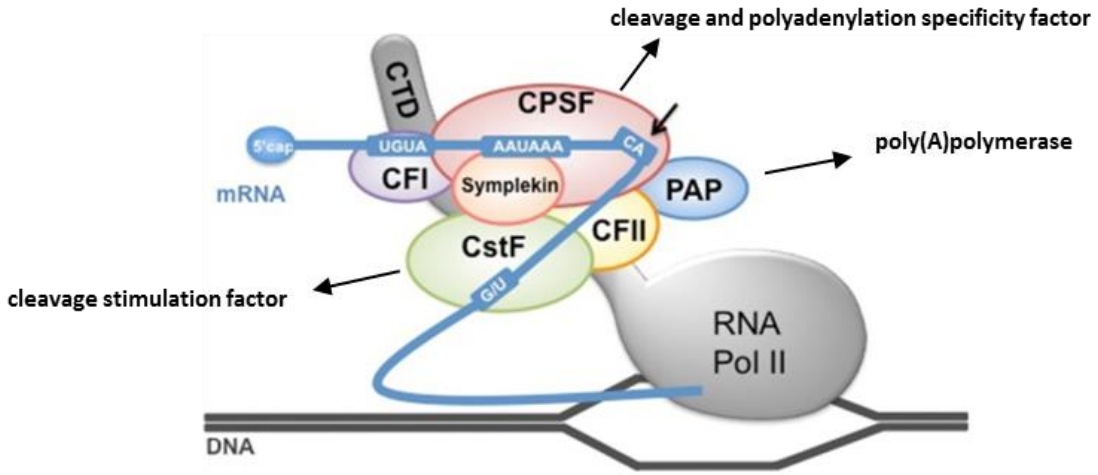

Figure D-I. The pre-mRNA 3′ processing complex. A functional terminator of transcription needs a polyadenylation signal (AAUAAA), a cleavage signal (CA) and a GU-rich sequence, so that proteins can bind the 3'-end of the RNA and add the polyA tail important for mRNA stability and localisation. The most important binding proteins include Cleavage and Polyadenylation Specific Factor (CPSF), Poly(A)polymerase (PAP) and Cleavage Stimulating Factor (CstF). Adapted from Di Giammartino and Manley, 2014.

4.1.5. Establishment of a stable inducible Cdh5 line

In order to gain a stable zebrafish line, the BAC-injected fish need to transfer the integrated BAC construct to their offspring. During the next step of this project, germline transmission has to be found by crossing out every individual BAC-injected fish to wild type fish until a founder has been found. Once the stable line has been created, Cdh5-loxP fish can be crossed to inducible Cre-driver lines, including heatshock:Cre and CreERT. The next step would be the optimisation of the Cre-based recombination by testing different heat-shock time durations or different concentrations of tamoxifen. Meanwhile, the Cdh5 BAC expressing fish should be crossed with Cdh5 mutant fish, to assure that the BAC is the only *cdh5* gene present in the genome.

4.1.6. Analysis of cytoskeletal junctional interactions during blood vessel morphogenesis

Once a stable inducible Cdh5 knock-out line has been established, experiments to analyse the cytoskeletal interactions during vessel morphogenesis can be performed. First, the dependence of ECs on Cdh5 can be observed by analysing EC behaviour during different embryonic stages. This includes time-lapse imaging of ISV sprout outgrowth and anastomosis in endothelial marker lines, when *cdh5* is removed around 24hpf or 30hpf respectively. Another important aspect would be whether removal of *cdh5* still allows cell rearrangements during the formation of unicellular tubes into multicellular tubes. During this time frame, lumen formation can be analysed as well, since heart functioning and blood flow should be established normally. The inducible knock out line will also allow analysis of Cdh5-dependent EC behaviour at later time

points beyond 50hpf: Does arterial to venous transformation still occur or do ISV stay in a unicellular configuration? Can ECs in the aorta still adapt their configuration to differences in blood pressure and shear stress?

To what extend the expression of the BAC will be mosaic, depends on the localisation of its integration in the genome as well as post-transcriptional regulation. The tension sensor line, which is also based on the Cdh5 BAC, is expressed in a non-mosaic way (Lagendijk et al., 2017). Depending on the purpose, the amount of mosaicism can manipulated by activation of Cre. Either the duration of heat-shock induction could be shortened or, in case of a CreERT line, the concentration of tamoxifen can be lowered in order to obtain more mosaicism. Generating mosaic ECs with differences of Cdh5 amounts in each individual cell would be an important tool to analyse cell-cell interaction in more detail: Would JBLs still be formed in case the neighbouring EC could not contribute to adherens junction formation? To what extend is the motility of an EC dependent on its neighbour? Within mosaic sprouts one could investigate whether cell shuffling could take place in absence between ECs with different levels of Cdh5. Can a Cdh5-less cell still take over the tip cell position when a Cdh5 expressing tip cell has been removed?

4.2 Generation of a photoconvertible fluorescent protein-tagged Cdh5 line

To examine to what extend individual neighbouring ECs contribute to the formation of JBL dynamics, I generated a photo-convertible fluorescence-tagged Cdh5 construct. In this project, the sequence encoding for mClav was introduced between the p120-catenin and β-catenin binding sites in the BAC containing *cdh5*. Introduction of this BAC construct in zebrafish, resulted in embryos expressing green mClav at the location of Cdh5 and exposure to 405nm blue light could convert the mClav signal to emission of red light.

Having established the BAC recombineering technique and having generated a Cdh5 containing BAC with *iTol2* sites and an eye marker already present in the backbone in favour of the inducible Cdh5 project, the establishment of a photoconvertible fluorescent protein-tagged Cdh5 construct could be made in one recombineering round. This demonstrates the value of the presence of a basic Cdh5 BAC with modified backbone in the lab. For further genetic editing on the *cdh5* gene in future, one could always start from this BAC, saving a lot of time.

The next step will be finding a founder that transmits the photoconvertible fluorescent protein-tagged Cdh5 to its offspring, identical to 4.1.5. Once a stable line has been established, the Cdh5 localisation of individual endothelial cells can be visualised. To that, specific ECs of interest can be exposed to blue light, converting their mClav into a red light emitting protein. Then, time lapse imaging can trace the localisation of Cdh5 and its contribution to adherens junctions with neighbouring cells whose mClav emits green light. With this tool, one could examine how JBLs are formed and to which extend a moving EC is dependent on Cdh5 presence of its neighbouring cell. This analysis will enable a description of actin-Cdh5 mobility in more detail to explain how ECs use Cdh5 to remodel and adapt to changes in growth and shear stress without losing the EC barrier.

4.3 Phenotypic characterisation of RadilB

In this side project, the *in vivo* role of RadilB underlying vascular morphogenesis was for the first time investigated. Genomic analysis showed three Radil paralogues (RadilA, -B and -C) in the zebrafish genome. Via *in situ* hybridisation for each Radil paralogue, I showed that RadilB was endothelial specifically expressed. From cell culture experiments, we know that Rasip1 is not the only Rap1 effector, but cooperates with the closely-related Radil protein that shares three of its four protein domains with Rasip1, which prompted us to initiate phenotypic vascular analyses on RadilB mutant embryos.

4.3.1. Efficiency of cellular rearrangements might be impaired in absence of RadilB

RadilB KO fish showed intermittent lumen collapses of growing ISVs that only took place in arterial ISVs that converted to venous ISVs and simultaneously divided. It was already observed before that lumens in wild type unicellular vessels collapse during cell division (Aydogan et al., 2015). An increased amount of lumen collapses suggests that within RadilB homozygous mutants the amount of unicellular ISVs might be higher than in wild type. Contrary to the initial antibody stainings against Cdh5 at 32hpf, the Cdh5-marker line at later stages indicated that Cdh5 in RadilB mutant ISVs often show a detached pattern throughout the vessel (Figure 11C), illustrating a unicellular configuration. However, more samples at different time points of the Cdh5-marker line in RadilB mutants should be imaged and analysed to claim whether RadilB homozygous embryos possess more unicellular ISVs or that the process of cellular rearrangements into multicellular vessel is delayed.

A delay in cellular rearrangement efficiency might not only explain a higher number of unicellular vessels, but might also explain the observed arterial to venous shunts, since the transforming initial arterial vessels might not be capable enough to rapidly detach itself from the DA and rearrange itself into a vein upon binding to the emerging secondary sprout.

Another reason for more unicellular vessels during ISV formation could be a consequence of the observed decrease of endothelial cell divisions in RadilB homozygous mutants. On the other hand, mice and zebrafish lacking Rasip1 form smaller dorsal aortae (Wilson et al., 2013; Koo et al 2016). I have not yet quantified abnormalities in the dorsal aorta of RadilB mutants, however, a smaller dorsal aorta will most probably supply less cells able to sprout into ISVs, resulting in more unicellular vessels.

4.3.2. RadilB does not control initiation of lumen formation but might control proper lumen expansion and rigidity

Absence of Rasip1 in mice led to either absence of lumen formation (Xu et al., 2011) or initial formation of lumens that ultimately collapsed (Wilson et al., 2013). The RadilB mutant zebrafish in this study, however, demonstrated initial lumen formation that under certain circumstances collapse and reopen again, suggesting a more prominent role for Rasip1 in lumen

formation. Further research on Cre-lox mice proposed that Rasip1 induces lumen formation via activating Cdc42 activity and from the moment the lumen has been formed, facilitates lumen expansion via suppression of actin-myosin contractility by inhibiting RhoA (Barry et al., 2016). Since only Radil can bind Arhgap29 via its PDZ domain that subsequently inhibits RhoA (Post et al., 2015), these findings suggest that Rasip1 mediates vessel morphogenesis via a Radil-dependent (via RhoA) and a Radil-independent (via Cdc42) pathway. In addition, Rap1 controls the endothelial barrier via Arhgap29, the inhibitor of RhoA (Post et al., 2013). Therefore, RadilB might not prevent lumen formation itself, but proper lumen expansion and rigidity might be disrupted due to the absence of RhoA inhibition and consequently excessive actin-myosin contractility.

Apparently, lack of RhoA control allows collapsed lumens to reopen, but generates during the maturation of blood vessels an abnormal cell wall architecture (Figure 9C). In order to decipher different roles for Rasip1 and Radil during lumen formation in more detail, one could visualise the localisation of the apical marker podocalyxin in both mutant backgrounds, since podocalyxin indicates the localisation and the onset of lumen formation. I would expect that the spatio-temporal localisation of podocalyxin would be disrupted by the absence of Rasip1, rather than RadilB.

4.3.3. Excessive actin myosin contraction on Cdh5 might hamper cellular rearrangements and cell motility

Rasip1 has been shown to be indispensable for proper Cdh5 localisation (Koo et al., 2016). Also in RadilB homozygous mutants, aberrant Cdh5 localisation patterns were observed. Since RadilB activity inhibits actin myosin contraction via RhoA and since Cdh5 serves as an anchor point for the actin cytoskeleton, the Cdh5 mislocalisation may be a consequence of excessive actin tension. In addition, too much actin myosin contraction could prevent proper cell rearrangement and EC motility induced by Cdh5 necessary for transformation into multicellular vessels and to prevent arterial to venous shunts. Whether the loss of rearrangement capacities is due to excessive cytoskeletal tension could be examined using the Cdh5 tension sensor line (Lagendijk et al., 2018) and by rescuing the phenotype using the ROCK inhibitor Y-27632 that prevents further actin myosin contraction.

4.3.4. RadilB's function is probably restricted to RhoA-inhibition

In order to decipher a RhoA-based role of RadilB, one could analyse vascular morphogenesis in Arhgap29 mutant embryos. In the zebrafish genome, two genes for Arhgap29 exist, from which *arhgap29a* expression is restricted to endothelium (Gomez et al., 2009). Comparison between the Arhrap29A phenotypes and the RadilB phenotypes will indicate whether RadilB plays either a role restricted to RhoA inhibition, or other Arhgap29- and Rasip1-independent roles. Also currently ongoing experiments on Heg1 morphants will elucidate more about to what extent Rasip1/RadilB complex formation on the one hand and Rasip1 and RadilB individually on the other hand contribute to blood vessel morphogenesis.

Another experiment that could elucidate more about whether the function of RadilB is restricted to Rasip1-RhoA pathway, would be the generation of a zebrafish line that expresses a truncated version of *radilb* that encodes for a RadilB protein lacking the PDZ domain. This line would show potential functions of RadilB independent of RhoA-inhibition via Arhgap29 as might be the case for Cdc42 activation by Rasip1. If one could show that the function of RadilB is restricted or RhoA-inhibition it could be used as a new tool for examining RhoA-induced actin-myosin contraction during angiogenesis, thereby eliminating the use of the ROCK inhibiting compound.

4.3.5. Redundancy between Rasip1 and RadilB

Future experiments should focus on comparing Rasip1 (UBS28) and RadilB phenotypes to examine the level of redundancy and therefore the importance of their cooperating system for vascular morphogenesis. An important tool will be the generated antibody against RadilB to document RadilB's presence at different stages of vascular development, which is currently in testing phase (cf. Appendix III). The phenotypic analyses of both Rasip1 and Radil will result in new insights about how EC behaviour is regulated at the level of small GTPases, enabling them to form proper blood vessels without losing their barrier function.

4.4 Acknowledgments

First of all, I want thank Prof. Dr. Markus Affolter for giving me the opportunity to start my PhD in his laboratory and giving me a lot of freedom to pursue my projects in my own manner. I really admire him for the way he treats his employees, which creates a very comfortable atmosphere, and his authentic capacity to convey his unlimited fascination for science to his direct environment as well as to a broad audience.

Secondly, I want to thank Dr. Heinz-Georg Belting for supervising my projects and triggering me each time again to get more out of myself than I initially expected was possible. His supervision has contributed a lot to developing myself into a real molecular biologist, although my former educational background was different, but above all, to becoming an intellectually much richer person then I was before. I am really grateful for that.

Thirdly, I want to thank Prof. Dr.Claudia Lengerke and Prof. Dr. Andra Banfi for being in my committee and discussing my projects in a very constructive manner.

Special thanks go to Dr. Martin Müller and Helen Mawer, because both of them contributed enormously to the organisation and maintenance of our laboratory, as well as to Cora Wiesner for correcting and supporting the content of my thesis, and Dr. Charles Betz for his supervision during my first year. In addition to Kumuthini Kulendra and Mattias Thimm for their indispensable caretaking of our zebrafish.

Then I want to thank the rest of our former and current laboratory members for the inspiring atmosphere and great discussions, including Christoph Tegtmeier, Daniel Heutschi, Dr. Dimitri Bieli, Etienne Schmelzer, Gordian Born, Gustavo Aguilar, Dr. Ilaria Alborelli, Dr. Ilkka Paatero, Dr. Loïc Sauteur, Dr. Lucien Fabre, Dr. Maria Alessandra Vigano, Dr. Maria Paraskevi Kotini, Dr. Mario Metzler, Michèle Sickmann, Milena Bauer, Minkyoung Lee, Niklas Simon, Dr. Shinya Matsuda, Dr. Stefan Harmansa and Dr. Vahap Aydogan.

I also want to thank our kitchen ladies Bernadette Bruno, Gina Evora and Karin Mauro as well as our floor manager Vaclav Mandak for all the work they performed behind the scenes, and additionally the people from our imaging core facility, including Dr. Alexia Loynton-Ferrand, Dr. Kai Schleicher and Dr. Wolf Heusermann for their competent imaging support and high quality services.

Last but not least, I want to thank my social environment, whose support provided me the basis for good performance on professional level. Dafür möchte ich gerne meinen treusten Freundinnen und Freunden danken, worunter Eugène Didier Fritz, Bettina Thommen, Anna-Sophie Hobi, Stefanie Villiger, Pauline Marion, Linda Walter, Etienne Schmelzer und Rabea Buder, sowie meine (ehemaligen) Mitbewohnerinnen Lea Altwegg, Livia Bieder, Maya Bosshard und Meret Wacker. Während der vergangenen vier Jahre haben sie alle viel für mich bedeutet und ich hoffe, dass unsere Freundschaften auch in der Zukunft bestehen bleiben. Daarnaast wil ik graag mijn vrienden uit Maastricht en omgeving bedanken, waaronder Harold Bak, Sebastiaan Augustin, Max Roosen, Annick Montulet, Maurice Houben, Joos Huys, Alex Wu, Thom Overhof en Luc Peters. Ondanks het feit dat wij al negen jaar niet meer naar dezelfde

school gaan, hebben zij toch altijd contact onderhouden, mij meerdere keren opgezocht en altijd klaargestaan wanneer ik naar Limburg kwam. Dat is zeker niet vanzelfsprekend en ik kan alleen maar hopen dat dit voor altijd zo mag blijven. Vervolgens ben ik grote dank verschuldigd aan mijn oma Tiny Schellinx-Nijs die er altijd voor heeft gezorgd dat ik toch nog een thuis had in Maastricht waarnaar ik mocht terugkomen wanneer ik maar wilde en waar het altijd gezellig was. Finalement je voudrais remercier ma copine Laetitia Driss pour sa chaleur française ainsi que pour son amitié profonde. Je tiens également à la remercier pour son soutien inconditionnel surtout pendant les derniers mois où sa présence m'a permis de ne jamais me sentir seul pendant l'écriture de ma thèse. Je ne la remercierai jamais assez pour tout cela !

Appendix

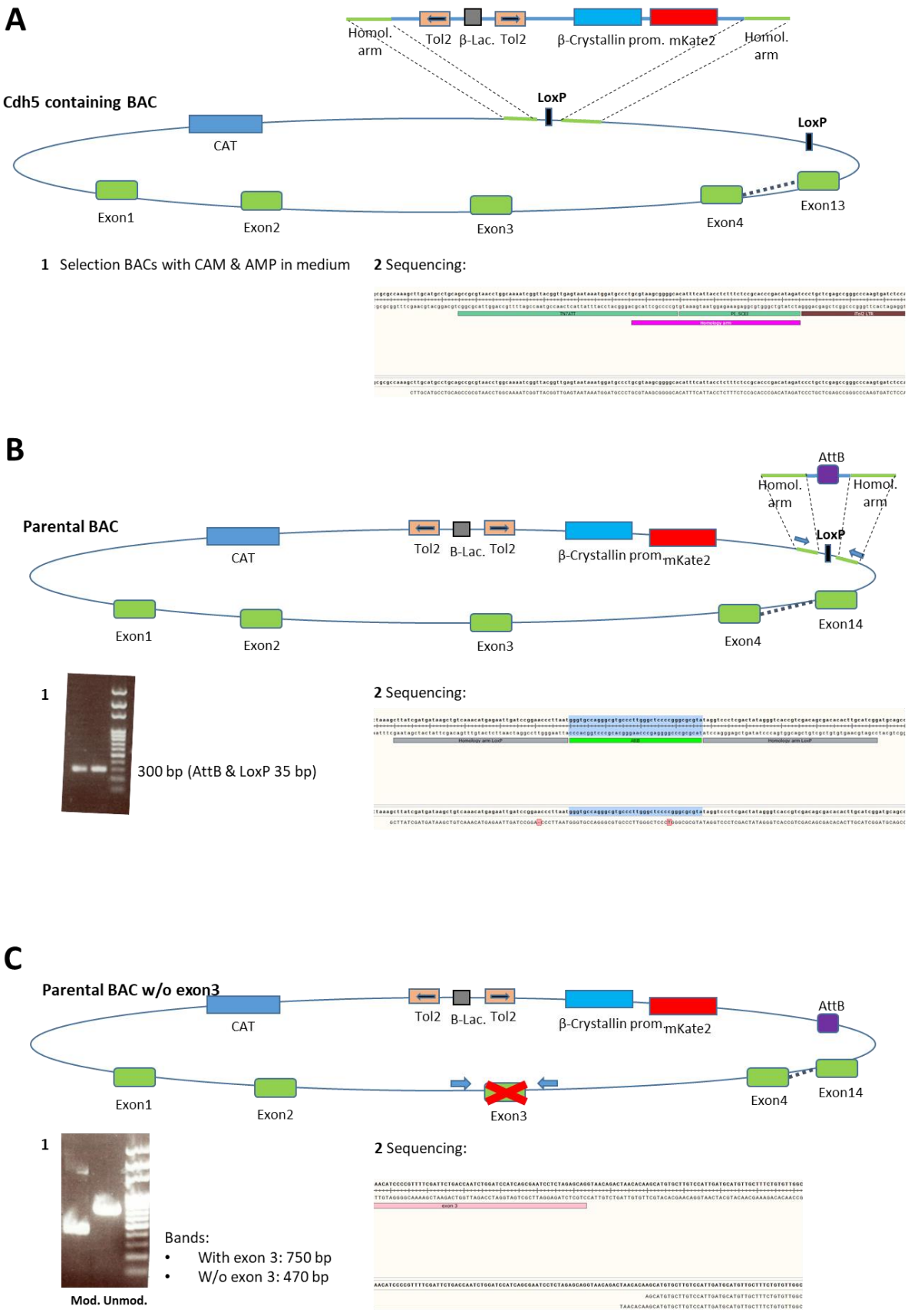

Figure A-I. Backbone modifications of the Cdh5 containing BAC in order to make it suitable for genome integration and screening for its expression. (**A**) In a first attempt to apply BAC recombineering for genomic editing, a construct containing inverted *Tol2* sites and *β-*

crystalline:mKate2 eye lens marker was exchanged for the first *loxP* site in the BAC backbone. In case of construct integration, the SW102 cells could survive on minimum plates containing ampicillin. The BAC of surviving cells was then purified and screened by PCR and correct recombination confirmed by sequencing. (**B**) Further in the backbone, a second LoxP site was present that had to be removed. This was done in a similar way as in A, thereby exchanging it for an AttB site, serving for phiC31 integrase-mediated attP/attB recombination into *attP* landing sites, present in the genome of an attP-containing zebrafish line. Recombineered BACs were screened by PCR and correct ones confirmed by sequencing. The sequencing result showed, however, a C to T point mutation in base pair 29 of the AttB site. (**C**) In order to simplify PCR screenings in which UBS8 Cdh5 mutant fish should be distinguished from BAC Cdh5 inducible mutants, BAC Cdh5 exon 3 was removed by recombineering. The removal is demonstrated by PCR and sequencing.

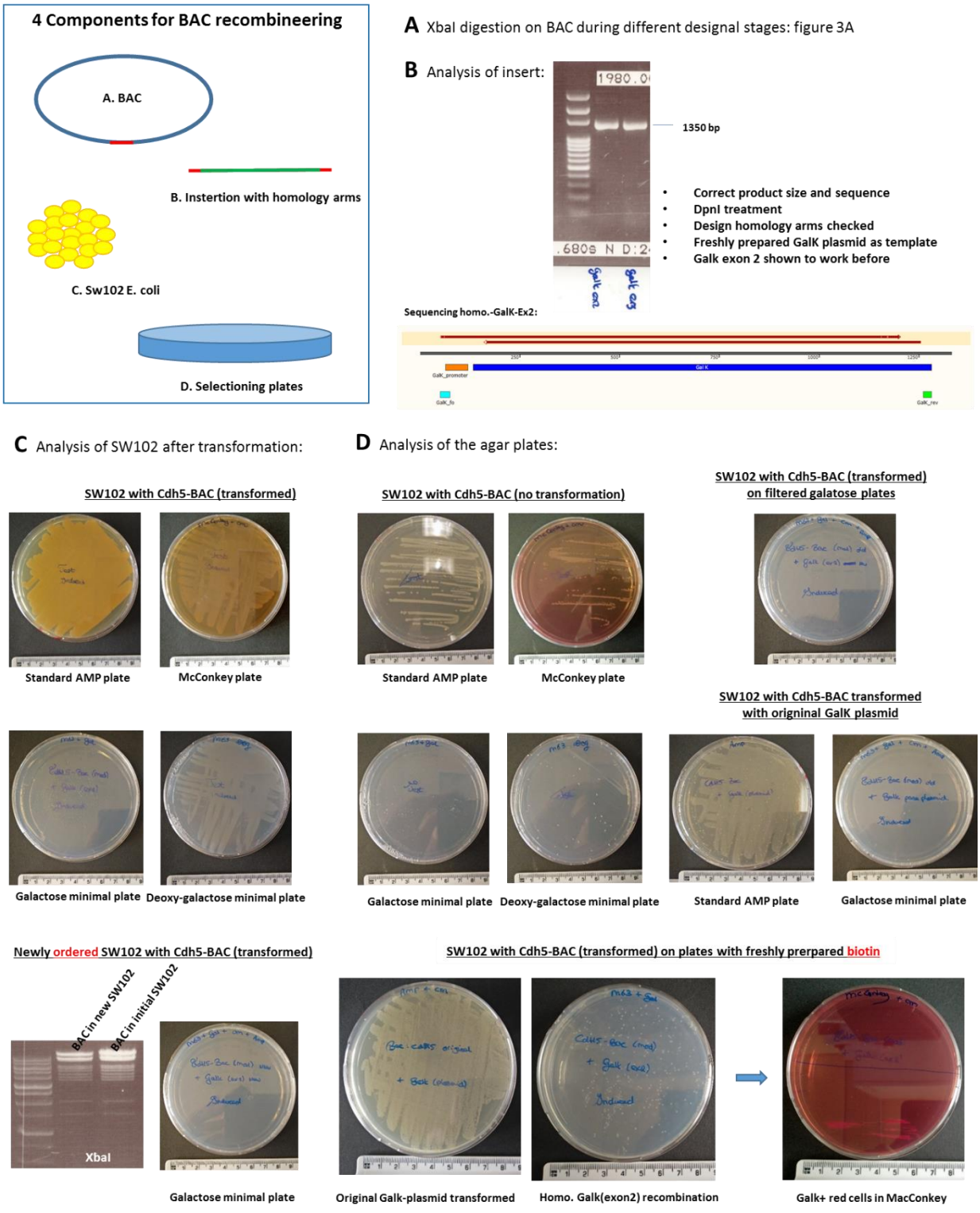

Figure A-II. Trouble shooting BAC recombineering: unstable biotin solution does not allow SW102 cell growth on minimal plates. After successfully performing BAC recombineering events over months, this technique encountered at some point some troubles: introduction of the galK gene into the BAC did not allow growth of any cells on galactose-containing minimal plates anymore. To find out which element caused a problem, the technique was divided into its four components, whereupon each component was tested individually. The tests were performed based on the exchange

of the galK gene for exon 2, since this had been demonstrated to work before (Figure 1C). (**A**) The first component is the BAC itself. To test whether the BAC was still intact, XbaI digest was performed on the BACs during their different designal stages. The results are depicted in Figure 3A. and show that the used BACs must be correct (**B**) The second component is the insert containing the desired modification of the BAC, in this case the galK gene flanked by 50bp-homology arms. PCR was performed on a freshly linearized galK plasmid and the design of its primers were rechecked. Synthesis of the insert by PCR was checked by electrophorese and sequencing. All PCR reactions were always followed by DpnI treatment to get rid of the DNA template. All results indicated that nothing was wrong with the insert. (**C**) The third component were the SW102 cells. After transformation with the galK insert, the cells could grow on standard agar plates with chloramphenicol, on MacConkey plates as well as on Deoxy-galactose-containing minimal plates indicating that the SW102 cells did not die during the procedure to make them electro-competent and/or during transformation. On minimal plates containing galactose, however, none of the cells did survive. Maybe the SW102 cells lose their recombineering efficiency over time: they were already used for multiple generations and their recombineering facilitating proteins might also cause mutations in their own genes after each generation. Therefore, a new stock of fresh SW102 cells was ordered and transformed with the Cdh5 BAC. Nevertheless, none of the new SW102 cells survived on galatose-containing minimal plates. Presumably, the cells were still working, but the plate composition was not optimal anymore. (**D**) The fourth component were the minimal plates. The plates were remade as described in paragraph 2.2.2. from freshly made solutions of all ingredients. Non-recombineered BAC-transformed SW102 E. coli were plated on standard agar, MacConkey and the two minimal plates and could survive on all of them except the galactose containing one. The latter was expected since no galK gene had been introduced yet. Given the observations that *Galk*-transformed and non-transformed SW102 could survive on deoxy-galactose containing plates, the components of the minimal plates sufficed for cell growth. The only difference between both minimal plates was the presence of either galactose or deoxy-galactose respectively. Therefore, new galactose powder was ordered and instead of autoclaving its solution, a sterile filter was used to keep the galactose as intact as possible. Still, minimal plates containing the newly prepared galactose did not allow cell growth, even when the BAC-containing cells were transformed with the original galK plasmid. Further attempts to optimise the plate's composition led to, amongst others, ordering new biotin powder from which a fresh biotin solution was made. Indeed, when the fresh bought biotin was used, galK transformed SW102 cells could survive on the galactose-containing minimal plate. Apparently, biotin does not restrict completely the survival on deoxy-galactose-containing plates. Further literature research on biotin revealed that it only stays stable in solution at 4°C up until 4 months. These requirements of biotin's stability were neither initially respected, nor reported in earlier existing BAC recombineering protocols.

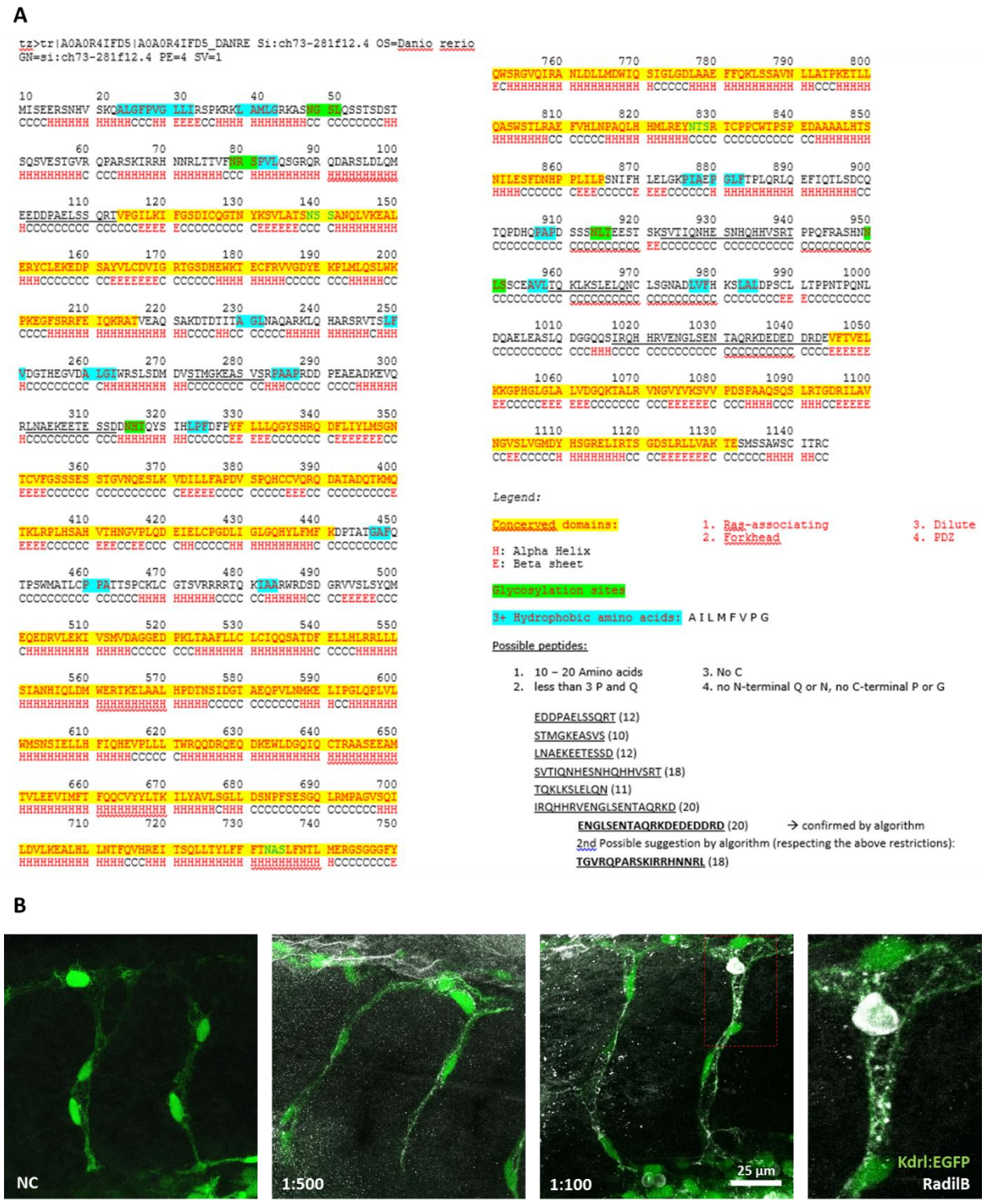

Figure A-III. Generation of an antibody against RadilB. (**A**) The protein sequence of RadilB was analysed for potential peptide candidates against which antibodies could be generated. To this purpose, alpha helices and beta sheets (indicated as H en E) are not suitable for triggering an immune response. Further, functional domains (indicated in green) were excluded since the domains are not unique to RadilB. Glycosylation site (green) as well as more than 3 hydrophobic amino acids in a row (blue) should be avoided for efficient antibody generation. Ideally, a peptide consist of 10 to 20 amino acids, contains less than 3 prolines and glutamines, no cysteines, no N-terminal glutamine or asparagine

and no C-terminal proline or glycine. When respecting the above requirements, six possible peptide candidate can be identified from RadilB's protein sequence. Two of them were found as well using an algorithm for identifying peptides by the antibody generating company (Eurogentec). Other proposed peptides from the algorithm were located partially in functional domains. The two chosen peptides were synthesised, injected into rabbit and purified by Eurogentec. (B) Preliminary results visualising the RadilB protein localisation using the generated antibody in 32hpf *kdrl:gfp* embryos. RadilB seemed to be endothelial specific and its localisation pattern showed a high similarity to the one of Rasip1 and Cdh5 (cf. Figure 11A).

References

Adams, R.H., and Alitalo, K. (2007). Molecular regulation of angiogenesis and lymphangiogenesis. Nature reviews. Molecular cell biology *8*, 464-478.

Ahmed, S.M., Thériault, B.L., Uppalapati, M., Chiu, C.W.N., Gallie, B.L., Sidhu, S.S., and Angers, S. (2012). KIF14 negatively regulates Rap1a-Radil signaling during breast cancer progression. The Journal of cell biology *199*, 951-967.

Ando, K., Fukuhara, S., Izumi, N., Nakajima, H., Fukui, H., Kelsh, R.N., and Mochizuki, N. (2016). Clarification of mural cell coverage of vascular endothelial cells by live imaging of zebrafish. Development (Cambridge, England) *143*, 1328-1339.

Aydogan, V., Lenard, A., Denes, A.S., Sauteur, L., Belting, H.-G., and Affolter, M. (2015). Endothelial cell division in angiogenic sprouts of differing cellular architecture. Biology open *4*, 1259-1269.

Barry, D.M., Koo, Y., Norden, P.R., Wylie, L.A., Xu, K., Wichaidit, C., Azizoglu, D.B., Zheng, Y., Cobb, M.H., and Davis, G.E., et al. (2016). Rasip1-Mediated Rho GTPase Signaling Regulates Blood Vessel Tubulogenesis via Nonmuscle Myosin II. Circulation research *119*, 810-826.

Bazzoni, G., and Dejana, E. (2004). Endothelial cell-to-cell junctions: molecular organization and role in vascular homeostasis. Physiological reviews *84*, 869-901.

Bertrand, J.Y., Chi, N.C., Santoso, B., Teng, S., Stainier, D.Y.R., and Traver, D. (2010). Haematopoietic stem cells derive directly from aortic endothelium during development. Nature *464*, 108-111.

Blum, Y., Belting, H.-G., Ellertsdottir, E., Herwig, L., Lüders, F., and Affolter, M. (2008). Complex cell rearrangements during intersegmental vessel sprouting and vessel fusion in the zebrafish embryo. Developmental biology *316*, 312-322.

Cattelino, A., Liebner, S., Gallini, R., Zanetti, A., Balconi, G., Corsi, A., Bianco, P., Wolburg, H., Moore, R., and Oreda, B., et al. (2003). The conditional inactivation of the beta-catenin gene in endothelial cells causes a defective vascular pattern and increased vascular fragility. The Journal of cell biology *162*, 1111-1122.

Chappell, J.C., Taylor, S.M., Ferrara, N., and Bautch, V.L. (2009). Local guidance of emerging vessel sprouts requires soluble Flt-1. Developmental cell *17*, 377-386.

Cherfils, J., and Zeghouf, M. (2013). Regulation of small GTPases by GEFs, GAPs, and GDIs. Physiological reviews *93*, 269-309.

Conway, D.E., Breckenridge, M.T., Hinde, E., Gratton, E., Chen, C.S., and Schwartz, M.A. (2013). Fluid shear stress on endothelial cells modulates mechanical tension across VE-cadherin and PECAM-1. Current biology : CB *23*, 1024-1030.

Court, D.L., Sawitzke, J.A., and Thomason, L.C. (2002). Genetic engineering using homologous recombination. Annual review of genetics *36*, 361-388.

Dejana, E., and Vestweber, D. (2013). The role of VE-cadherin in vascular morphogenesis and permeability control. Progress in molecular biology and translational science *116*, 119-144.

Di Giammartino, D.C., and Manley, J.L. (2014). New links between mRNA polyadenylation and diverse nuclear pathways. Molecules and cells *37*, 644-649.

Dorland, Y.L., and Huveneers, S. (2017). Cell-cell junctional mechanotransduction in endothelial remodeling. Cellular and molecular life sciences : CMLS *74*, 279-292.

Eichmann, A., Makinen, T., and Alitalo, K. (2005). Neural guidance molecules regulate vascular remodeling and vessel navigation. Genes & development *19*, 1013-1021.

Ellertsdóttir, E., Lenard, A., Blum, Y., Krudewig, A., Herwig, L., Affolter, M., and Belting, H.-G. (2010). Vascular morphogenesis in the zebrafish embryo. Developmental biology *341*, 56-65.

Feng, H., Langenau, D.M., Madge, J.A., Quinkertz, A., Gutierrez, A., Neuberg, D.S., Kanki, J.P., and Look, A.T. (2007). Heat-shock induction of T-cell lymphoma/leukaemia in conditional Cre/lox-regulated transgenic zebrafish. British journal of haematology *138*, 169-175.

Gerhardt, H., Golding, M., Fruttiger, M., Ruhrberg, C., Lundkvist, A., Abramsson, A., Jeltsch, M., Mitchell, C., Alitalo, K., and Shima, D., et al. (2003). VEGF guides angiogenic sprouting utilizing endothelial tip cell filopodia. The Journal of cell biology *161*, 1163-1177.

Germain, S., Monnot, C., Muller, L., and Eichmann, A. (2010). Hypoxia-driven angiogenesis: role of tip cells and extracellular matrix scaffolding. Current opinion in hematology *17*, 245-251.

Geudens, I., and Gerhardt, H. (2011). Coordinating cell behaviour during blood vessel formation. Development (Cambridge, England) *138*, 4569-4583.

Gibson, D.G., Young, L., Chuang, R.-Y., Venter, J.C., Hutchison, C.A., and Smith, H.O. (2009). Enzymatic assembly of DNA molecules up to several hundred kilobases. Nature methods *6*, 343-345.

Gil, A., and Proudfoot, N.J. (1987). Position-dependent sequence elements downstream of AAUAAA are required for efficient rabbit beta-globin mRNA 3' end formation. Cell *49*, 399-406.

Glading, A., Han, J., Stockton, R.A., and Ginsberg, M.H. (2007). KRIT-1/CCM1 is a Rap1 effector that regulates endothelial cell cell junctions. The Journal of cell biology *179*, 247-254.

Gomez, G.A., Veldman, M.B., Zhao, Y., Burgess, S., and Lin, S. (2009) Discovery and characterization of novel vascular and hematopoietic genes downstream of etsrp in zebrafish. PLoS One. 4(3):e4994.

Haffter, P., Granato, M., Brand, M., Mullins, M.C., Hammerschmidt, M., Kane, D.A., Odenthal, J., van Eeden, F.J., Jiang, Y.J., and Heisenberg, C.P., et al. (1996). The

identification of genes with unique and essential functions in the development of the zebrafish, Danio rerio. Development (Cambridge, England) *123*, 1-36.

Helker, C.S.M., Schuermann, A., Karpanen, T., Zeuschner, D., Belting, H.-G., Affolter, M., Schulte-Merker, S., and Herzog, W. (2013). The zebrafish common cardinal veins develop by a novel mechanism: lumen ensheathment. Development (Cambridge, England) *140*, 2776-2786.

Herbert, S.P., Huisken, J., Kim, T.N., Feldman, M.E., Houseman, B.T., Wang, R.A., Shokat, K.M., and Stainier, D.Y.R. (2009). Arterial-venous segregation by selective cell sprouting: an alternative mode of blood vessel formation. Science (New York, N.Y.) *326*, 294-298.

Herwig, L., Blum, Y., Krudewig, A., Ellertsdottir, E., Lenard, A., Belting, H.-G., and Affolter, M. (2011). Distinct cellular mechanisms of blood vessel fusion in the zebrafish embryo. Current biology : CB *21*, 1942-1948.

Hirata, K., Ishida, T., Penta, K., Rezaee, M., Yang, E., Wohlgemuth, J., and Quertermous, T. (2001). Cloning of an immunoglobulin family adhesion molecule selectively expressed by endothelial cells. The Journal of biological chemistry *276*, 16223-16231.

Hogan, B.M., Bos, F.L., Bussmann, J., Witte, M., Chi, N.C., Duckers, H.J., and Schulte-Merker, S. (2009). Ccbe1 is required for embryonic lymphangiogenesis and venous sprouting. Nature genetics *41*, 396-398.

Hogan, B.M., and Schulte-Merker, S. (2017). How to Plumb a Pisces: Understanding Vascular Development and Disease Using Zebrafish Embryos. Developmental cell *42*, 567-583.

Hoi, H., Shaner, N.C., Davidson, M.W., Cairo, C.W., Wang, J., and Campbell, R.E. (2010). A monomeric photoconvertible fluorescent protein for imaging of dynamic protein localization. Journal of molecular biology *401*, 776-791.

Iruela-Arispe, M.L., and Davis, G.E. (2009). Cellular and molecular mechanisms of vascular lumen formation. Developmental cell *16*, 222-231.

Ishida, T., Kundu, R.K., Yang, E., Hirata, K.-i., Ho, Y.-D., and Quertermous, T. (2003). Targeted disruption of endothelial cell-selective adhesion molecule inhibits angiogenic processes in vitro and in vivo. The Journal of biological chemistry *278*, 34598-34604.

Ishiyama, N., Lee, S.-H., Liu, S., Li, G.-Y., Smith, M.J., Reichardt, L.F., and Ikura, M. (2010). Dynamic and static interactions between p120 catenin and E-cadherin regulate the stability of cell-cell adhesion. Cell *141*, 117-128.

Isogai, S., Lawson, N.D., Torrealday, S., Horiguchi, M., and Weinstein, B.M. (2003). Angiogenic network formation in the developing vertebrate trunk. Development (Cambridge, England) *130*, 5281-5290.

Jakobsson, L., Franco, C.A., Bentley, K., Collins, R.T., Ponsioen, B., Aspalter, I.M., Rosewell, I., Busse, M., Thurston, G., and Medvinsky, A., et al. (2010). Endothelial cells dynamically compete for the tip cell position during angiogenic sprouting. Nature cell biology *12*, 943-953.

Jin, S.-W., Beis, D., Mitchell, T., Chen, J.-N., and Stainier, D.Y.R. (2005). Cellular and molecular analyses of vascular tube and lumen formation in zebrafish. Development (Cambridge, England) *132*, 5199-5209.

Kawakami, K., Koga, A., Hori, H., and Shima, A. (1998). Excision of the tol2 transposable element of the medaka fish, Oryzias latipes, in zebrafish, Danio rerio. Gene *225*, 17-22.

Kawakami, K., and Shima, A. (1999). Identification of the Tol2 transposase of the medaka fish Oryzias latipes that catalyzes excision of a nonautonomous Tol2 element in zebrafish Danio rerio. Gene *240*, 239-244.

Khan, N.A. (2009). Acanthamoeba. Biology and pathogenesis (Norfolk: Caister Acad. Press).

Kimmel, C.B., Ballard, W.W., Kimmel, S.R., Ullmann, B., and Schilling, T.F. (1995). Stages of embryonic development of the zebrafish. Developmental dynamics : an official publication of the American Association of Anatomists *203*, 253-310.

Klaus, A., and Birchmeier, W. (2008). Wnt signalling and its impact on development and cancer. Nature reviews. Cancer *8*, 387-398.

Koltowska, K., Lagendijk, A.K., Pichol-Thievend, C., Fischer, J.C., Francois, M., Ober, E.A., Yap, A.S., and Hogan, B.M. (2015). Vegfc Regulates Bipotential Precursor Division and Prox1 Expression to Promote Lymphatic Identity in Zebrafish. Cell reports *13*, 1828-1841.

Koo, Y., Barry, D.M., Xu, K., Tanigaki, K., Davis, G.E., Mineo, C., and Cleaver, O. (2016). Rasip1 is essential to blood vessel stability and angiogenic blood vessel growth. Angiogenesis *19*, 173-190.

Kreuk, B.-J. de, Gingras, A.R., Knight, J., Liu, J.J., Gingras, A.-C., and Ginsberg, M.H. (2016). Heart of glass anchors Rasip1 at endothelial cell-cell junctions to support vascular integrity. eLife *5*, e11394.

Lagendijk, A.K., Gomez, G.A., Baek, S., Hesselson, D., Hughes, W.E., Paterson, S., Conway, D.E., Belting, H.-G., Affolter, M., and Smith, K.A., et al. (2017). Live imaging molecular changes in junctional tension upon VE-cadherin in zebrafish. Nature communications *8*, 1402.

Le Duc, Q., Shi, Q., Blonk, I., Sonnenberg, A., Wang, N., Leckband, D., and Rooij, J. de (2010). Vinculin potentiates E-cadherin mechanosensing and is recruited to actin-anchored sites within adherens junctions in a myosin II-dependent manner. The Journal of cell biology *189*, 1107-1115.

Lee, E.C., Yu, D., Martinez de Velasco, J., Tessarollo, L., Swing, D.A., Court, D.L., Jenkins, N.A., and Copeland, N.G. (2001). A highly efficient Escherichia coli-based chromosome engineering system adapted for recombinogenic targeting and subcloning of BAC DNA. Genomics *73*, 56-65.

Lee, H.-J., and Zheng, J.J. (2010). PDZ domains and their binding partners: structure, specificity, and modification. Cell communication and signaling : CCS *8*, 8.

Lenard, A., Ellertsdottir, E., Herwig, L., Krudewig, A., Sauteur, L., Belting, H.-G., and Affolter, M. (2013). In vivo analysis reveals a highly stereotypic morphogenetic pathway of vascular anastomosis. Developmental cell *25*, 492-506.

Liu, Z., Tan, J.L., Cohen, D.M., Yang, M.T., Sniadecki, N.J., Ruiz, S.A., Nelson, C.M., and Chen, C.S. (2010). Mechanical tugging force regulates the size of cell-cell junctions. Proceedings of the National Academy of Sciences of the United States of America *107*, 9944-9949.

Mateer, S.C., Morris, L.E., Cromer, D.A., Benseñor, L.B., and Bloom, G.S. (2004). Actin filament binding by a monomeric IQGAP1 fragment with a single calponin homology domain. Cell motility and the cytoskeleton *58*, 231-241.

Metzger, D., Clifford, J., Chiba, H., and Chambon, P. (1995). Conditional site-specific recombination in mammalian cells using a ligand-dependent chimeric Cre recombinase. Proceedings of the National Academy of Sciences of the United States of America *92*, 6991-6995.

Mitin, N.Y., Ramocki, M.B., Zullo, A.J., Der, C.J., Konieczny, S.F., and Taparowsky, E.J. (2004). Identification and characterization of rain, a novel Ras-interacting protein with a unique subcellular localization. The Journal of biological chemistry *279*, 22353-22361.

Mosimann, C., Puller, A.-C., Lawson, K.L., Tschopp, P., Amsterdam, A., and Zon, L.I. (2013). Site-directed zebrafish transgenesis into single landing sites with the phiC31 integrase system. Developmental dynamics : an official publication of the American Association of Anatomists *242*, 949-963.

Paatero, I., Sauteur, L., Lee, M., Lagendijk, A.K., Heutschi, D., Wiesner, C., Guzmán, C., Bieli, D., Hogan, B.M., and Affolter, M., et al. (2018). Junction-based lamellipodia drive endothelial cell rearrangements in vivo via a VE-cadherin-F-actin based oscillatory cell-cell interaction. Nature communications *9*, 3545.

Post, A., Pannekoek, W.J., Ponsioen, B., Vliem, M.J., and Bos, J.L. (2015). Rap1 Spatially Controls ArhGAP29 To Inhibit Rho Signaling during Endothelial Barrier Regulation. Molecular and cellular biology *35*, 2495-2502.

Post, A., Pannekoek, W.-J., Ross, S.H., Verlaan, I., Brouwer, P.M., and Bos, J.L. (2013). Rasip1 mediates Rap1 regulation of Rho in endothelial barrier function through ArhGAP29. Proceedings of the National Academy of Sciences of the United States of America *110*, 11427-11432.

Poteete, A.R. (2001). What makes the bacteriophage lambda Red system useful for genetic engineering: molecular mechanism and biological function. FEMS microbiology letters *201*, 9-14.

Renninger, S.L., Schonthaler, H.B., Neuhauss, S.C.F., and Dahm, R. (2011). Investigating the genetics of visual processing, function and behaviour in zebrafish. Neurogenetics *12*, 97-116.

Rimm, D.L., Koslov, E.R., Kebriaei, P., Cianci, C.D., and Morrow, J.S. (1995). Alpha 1(E)-catenin is an actin-binding and -bundling protein mediating the attachment of F-actin to the membrane adhesion complex. Proceedings of the National Academy of Sciences of the United States of America *92*, 8813-8817.

Sauer, B. (1987). Functional expression of the cre-lox site-specific recombination system in the yeast Saccharomyces cerevisiae. Molecular and cellular biology *7*, 2087-2096.

Sauer, B., and Henderson, N. (1988). Site-specific DNA recombination in mammalian cells by the Cre recombinase of bacteriophage P1. Proceedings of the National Academy of Sciences of the United States of America *85*, 5166-5170.

Sauteur, L. (2016). In vivo analysis of junctional dynamics underlying angiogenic cell behaviors. (doctoral thesis). University of Basel. [s.n.].

Sauteur, L., Affolter, M., and Belting, H.-G. (2017). Distinct and redundant functions of Esama and VE-cadherin during vascular morphogenesis. Development (Cambridge, England) *144*, 1554-1565.

Sauteur, L., Krudewig, A., Herwig, L., Ehrenfeuchter, N., Lenard, A., Affolter, M., and Belting, H.-G. (2014). Cdh5/VE-cadherin promotes endothelial cell interface elongation via cortical actin polymerization during angiogenic sprouting. Cell reports *9*, 504-513.

Sharan, S.K., Thomason, L.C., Kuznetsov, S.G., and Court, D.L. (2009). Recombineering: a homologous recombination-based method of genetic engineering. Nature protocols *4*, 206-223.

Shizuya, H., Birren, B., Kim, U.J., Mancino, V., Slepak, T., Tachiiri, Y., and Simon, M. (1992). Cloning and stable maintenance of 300-kilobase-pair fragments of human DNA in Escherichia coli using an F-factor-based vector. Proceedings of the National Academy of Sciences of the United States of America *89*, 8794-8797.

Siekmann, A.F., Affolter, M., and Belting, H.-G. (2013). The tip cell concept 10 years after: new players tune in for a common theme. Experimental cell research *319*, 1255-1263.

Smolen, G.A., Schott, B.J., Stewart, R.A., Diederichs, S., Muir, B., Provencher, H.L., Look, A.T., Sgroi, D.C., Peterson, R.T., and Haber, D.A. (2007). A Rap GTPase interactor, RADIL, mediates migration of neural crest precursors. Genes & development *21*, 2131-2136.

Stahl, M.M., Thomason, L., Poteete, A.R., Tarkowski, T., Kuzminov, A., and Stahl, F.W. (1997). Annealing vs. invasion in phage lambda recombination. Genetics *147*, 961-977.

Strilić, B., Eglinger, J., Krieg, M., Zeeb, M., Axnick, J., Babál, P., Müller, D.J., and Lammert, E. (2010). Electrostatic cell-surface repulsion initiates lumen formation in developing blood vessels. Current biology : CB *20*, 2003-2009.

Suster, M.L., Sumiyama, K., and Kawakami, K. (2009). Transposon-mediated BAC transgenesis in zebrafish and mice. BMC genomics *10*, 477.

Szymborska, A., and Gerhardt, H. (2018). Hold Me, but Not Too Tight-Endothelial Cell-Cell Junctions in Angiogenesis. Cold Spring Harbor perspectives in biology *10*.

Taguchi, K., Ishiuchi, T., and Takeichi, M. (2011). Mechanosensitive EPLIN-dependent remodeling of adherens junctions regulates epithelial reshaping. The Journal of cell biology *194*, 643-656.

Thisse, B., and Thisse, C. (2014). In situ hybridization on whole-mount zebrafish embryos and young larvae. Methods in molecular biology (Clifton, N.J.) *1211*, 53-67.

Timmerman, I., Heemskerk, N., Kroon, J., Schaefer, A., van Rijssel, J., Hoogenboezem, M., van Unen, J., Goedhart, J., Gadella, T.W.J., and Yin, T., et al. (2015). A local VE-cadherin

and Trio-based signaling complex stabilizes endothelial junctions through Rac1. Journal of cell science *128*, 3514.

Torres-Vázquez, J., Kamei, M., and Weinstein, B.M. (2003). Molecular distinction between arteries and veins. Cell and tissue research *314*, 43-59.

Urasaki, A., Morvan, G., and Kawakami, K. (2006). Functional dissection of the Tol2 transposable element identified the minimal cis-sequence and a highly repetitive sequence in the subterminal region essential for transposition. Genetics *174*, 639-649.

Vincent, P.A., Xiao, K., Buckley, K.M., and Kowalczyk, A.P. (2004). VE-cadherin: adhesion at arm's length. American journal of physiology. Cell physiology *286*, C987-97.

Warming, S., Costantino, N., Court, D.L., Jenkins, N.A., and Copeland, N.G. (2005). Simple and highly efficient BAC recombineering using galK selection. Nucleic acids research *33*, e36.

Westerfield, M. (2000). The Zebrafish Book. A guide for the laboratory use of zebrafish (Danio rerio). 4th Ed., Univ. of Oregon Press, Eugene.

Wilson, C.W., Parker, L.H., Hall, C.J., Smyczek, T., Mak, J., Crow, A., Posthuma, G., Mazière, A. de, Sagolla, M., and Chalouni, C., et al. (2013). Rasip1 regulates vertebrate vascular endothelial junction stability through Epac1-Rap1 signaling. Blood *122*, 3678-3690.

Xu, K., Chong, D.C., Rankin, S.A., Zorn, A.M., and Cleaver, O. (2009). Rasip1 is required for endothelial cell motility, angiogenesis and vessel formation. Developmental biology *329*, 269-279.

Xu, K., Sacharidou, A., Fu, S., Chong, D.C., Skaug, B., Chen, Z.J., Davis, G.E., and Cleaver, O. (2011). Blood vessel tubulogenesis requires Rasip1 regulation of GTPase signaling. Developmental cell *20*, 526-539.

Yang, X.W., Model, P., and Heintz, N. (1997). Homologous recombination based modification in Escherichia coli and germline transmission in transgenic mice of a bacterial artificial chromosome. Nature biotechnology *15*, 859-865.

Yang, Z., Jiang, H., Chaichanasakul, T., Chachainasakul, T., Gong, S., Yang, X.W., Heintz, N., and Lin, S. (2006). Modified bacterial artificial chromosomes for zebrafish transgenesis. Methods (San Diego, Calif.) *39*, 183-188.

Yaqoob, N., Holotta, M., Prem, C., Kopp, R., and Schwerte, T. (2009). Ontogenetic development of erythropoiesis can be studied non-invasively in GATA-1:DsRed transgenic zebrafish. Comparative biochemistry and physiology. Part A, Molecular & integrative physiology *154*, 270-278.

Yue, F., Cheng, Y., Breschi, A., Vierstra, J., Wu, W., Ryba, T., Sandstrom, R., Ma, Z., Davis, C., and Pope, B.D., et al. (2014). A comparative encyclopedia of DNA elements in the mouse genome. Nature *515*, 355-364.

Zagursky, R.J., and Hays, J.B. (1983). Expression of the phage lambda recombination genes exo and bet under lacPO control on a multi-copy plasmid. Gene *23*, 277-292.

Zygmunt, T., Gay, C.M., Blondelle, J., Singh, M.K., Flaherty, K.M., Means, P.C., Herwig, L., Krudewig, A., Belting, H.-G., and Affolter, M., et al. (2011). Semaphorin-PlexinD1 signaling limits angiogenic potential via the VEGF decoy receptor sFlt1. Developmental cell *21*, 301-314.